

**SEDIMENTOLOGY AND PERMEABILITY
CHARACTERISTICS OF THE
ARROYO OJITO FORMATION
(UPPER SANTA FE GROUP)
ADJACENT TO THE SAND HILL FAULT,
ALBUQUERQUE BASIN, NEW MEXICO**

by

Dustin G. Smyth

Submitted in Partial Fulfillment
Of the Requirements for the Degree of

Master of Science in Geology

Department of Earth and Environmental Sciences
New Mexico Institute of Mining and Technology

Socorro, New Mexico

(May 2004)

ABSTRACT

Many important aquifers and reservoirs in the United States are found in faulted basins filled with poorly lithified sediments. Recent studies have shown that hydrologic behavior of faults in such environments differs from that of solid rock. The significance of fault-related sedimentation for fluid flow in normal-faulted sedimentary basins has not been addressed previously, although the physical characteristics (porosity, permeability, and lithofacies distribution) of the sediments in the hanging-wall block undoubtedly exert a strong control on fluid flow.

This study used 1:8,000 lithofacies mapping and stratigraphic section measuring to characterize the geometries and textures of lithofacies in the hanging-wall block of the Sand Hill fault, a high-angle normal fault on the western margin of the Albuquerque Basin and the Rio Grande rift. I divided the sediments of the study area into five mappable lithofacies: coarsening upward, laminated and cross-stratified sands and gravels (QToug); massive, laminated and cross-stratified sands with gravel channel deposits (QTous); interbedded silt and silty clay (QToum); massive sands (QToup); and cross-stratified sands with gravel channel deposits (QTouc). These sediments were deposited in two major depositional environments: 1) regional axial fluvial sediments comprised of

channel deposits, overbank floodplain and pond deposits and minor eolian deposits (QToug, QTous, and part of QToum); and 2) bioturbated colluvium, eolian, possibly sag pond, and fault-parallel fluvial deposits (QToup, QTouc, and part of QToum) which I interpret to collectively constitute fault-scarp-controlled sediments deposited in a syntectonic depositional wedge. This hypothesis cannot be fully tested due to limited exposure of hanging-wall sediments perpendicular to the strike of the fault.

The hydrogeologic properties of each lithofacies were assessed through a combination of field and laboratory measurements, including field permeability, grain-size distribution and sorting, and thin-section porosity. The sandy sediments in the field area all have similar high permeabilities regardless of depositional environment. This implies that mapping based on depositional environments is not always the most accurate representation of permeability characteristics; instead, lithofacies with similar grain-size distributions should have similar permeabilities, which can be grouped together as hydrogeologic units. Improved understanding of the relationship between sedimentology and permeability in poorly lithified sediments associated with normal faults will enhance fluid flow modeling of such systems. In many cases, it is not financially realistic to measure the permeabilities of every unit in an area the size of the Albuquerque Basin. My work will help researchers and consultants such as those in hydrology, water resources, environmental remediation, and the

petroleum industry make informed decisions about how to use physical descriptions of the sediments on geologic maps to determine appropriate hydrogeologic units for flow models.

ACKNOWLEDGMENTS

There are many people and organizations that made this project possible. First I wish to thank the Christina Lochman Balk fellowship, which made my graduate education possible. The National Science Foundation (grant EAR-9706482) funded much of my field research. New Mexico Tech and the New Mexico Bureau of Geology and Mineral Resources deserve thanks for graciously allowing the use of field transportation. I thank ENGEIO Incorporated for all of their support, including the use of drafting and word processing resources.

On a personal note, I would like to thank my advisor, Peter Mozley, for not giving up on me even though my non-traditional status has made this finale a long time in coming. I thank the rest of my thesis committee, Laurel Goodwin, Steve Cather and Sean Connell for all of their encouragement and guidance. I also thank Anna Busing, my undergraduate advisor, the Sedimentology Queen and my closest friend for all of the core knowledge, editing, ego boosting and encouragement that helped me to get this far. You're the best.

The biggest thanks go to my husband, Sean Wortman, for his tireless support, endless sacrifices and deepest love. I could not have done any of it without you. Lastly, I would like to thank my children, Dakota and Cheyanne, who inspire me to be a better person.

TABLE OF CONTENTS

	Page
LIST OF PLATES	v
LIST OF FIGURES	vi
LIST OF TABLES	vii
LIST OF APPENDICES	viii
INTRODUCTION	1
PREVIOUS WORK AND GEOLOGIC SETTING	4
Location	4
Rio Grande Rift	4
Santa Fe Group	5
Stratigraphy and Nomenclature	5
Lithofacies	8
Syntectonic Depositional Wedge	9
Sand Hill Fault	14
Fault Zone Permeability	16
METHODS	18
Sedimentology	18
Measured Stratigraphic Sections	19
Lithofacies Mapping	26
Permeability	28
Working Assumptions	28
Grain Size and Sorting	30
Thin Section Imaging	31
Air Minipermeametry	32
GEOLOGY	35
Lithofacies Descriptions	35
QToug	36
QTous	38
QToum	40
QToup	42
QTouc	45
Lithofacies Relationships	46
Vertical Sequences	46
Measured Stratigraphic Section A-A'	48
Measured Stratigraphic Section B-B'	49

Measured Stratigraphic Section C-C'	50
Measured Stratigraphic Section D-D'	51
Vertical Variation	52
Aerial Distribution	53
Interpretations of Depositional Environments	55
QToug	55
QTous	57
QToum	58
QToup	60
QTouc	65
Genetic Interpretations	66
Syntectonic Depositional Wedge Deposits	67
QToup and QTouc	67
Regional Fluvial Sedimentation	68
QToug	69
QTous	70
QToum	70
Discussion	71
HYDROLOGIC SIGNIFICANCE	77
Grain-size analysis	77
Porosity	82
In-situ Permeability Measurements	84
Hydrogeologic Implications	89
CONCLUSIONS	93
REFERENCES	96

LIST OF PLATES

Plate	Page
Plate I: Geologic Map (scale 1:8000)	Pocket

LIST OF FIGURES

Figure	Page
Figure 1: Location Map.....	2
Figure 2: Albuquerque Basin Cross-section	7
Figure 3: Colluvial Wedge Diagram.....	10
Figure 4: STDW and Soil Formation.....	12
Figure 5: Geologic Map	21
Figure 6: Measured Section A – A'	22
Figure 7: Measured Section B – B'	23
Figure 8: Measured Section C – C'	24
Figure 9: Measured Section D – D'	25
Figure 10: QToug	37
Figure 11: QTous	39
Figure 12: QToum	41
Figure 13: QToup	44
Figure 14: QTouc	47
Figure 15: Schematic Interpretation of Lithofacies	74
Figure 16: Grain-size Analysis; Texture.....	78
Figure 17: Grain-size Analysis; Lithofacies Map Units.....	79
Figure 18: Statistical Analysis of Thin Section Porosity	83
Figure 19: Air Minipermeability Box Plots; Lithologic Units.....	85
Figure 20: Air Minipermeability Box Plots; Map Units.....	87
Figure 21: Hydrogeologic Map	90

LIST OF TABLES

Table	Page
Table 1: Map Unit Designations.....	27
Table 2: Grain Size and Sorting, Porosity and Permeability.....	29
Table 3: Summary of Map Units and Lithofacies.....	72
Table 4: Grain Size and Sorting.....	80
Table 5: Porosity of Map Units.....	84
Table 6: Permeabilities Grouped by Grain Size and Sorting.....	86
Table 7: Permeabilities Grouped by Map Units.....	86

LIST OF APPENDICES

Appendix	Page
APPENDIX A: Paleocurrent Data	104
APPENDIX B: Grain-Size Analyses.....	115
APPENDIX C: Porosity Data	135
APPENDIX D: Air Minipermeameter Outcrop Photos.....	140
APPENDIX E: Permeability Data	145

INTRODUCTION

Until recently, little was known about the dynamics of fluid flow associated with faults in poorly lithified sediments, even though many important aquifers and reservoirs in the United States and elsewhere are situated in such sediments (Anderson *et al.*, 1988; Mifflin, 1988). Recent work has begun to demonstrate that faults in poorly lithified sediments differ hydrologically from faults in solid rock (Heynekamp *et al.*, 1999; Hong, 1999; Sigda *et al.*, 1999; Herrin, 2001; Rawling *et al.*, 2001). However, studies to date have focused on the fault zones themselves. No known previous studies have tried to determine the significance of fault-related sedimentation on fluid flow in normal-faulted sedimentary basins, although the physical characteristics (porosity, permeability, and lithofacies distribution) of the sediments in the hanging-wall block undoubtedly exert a strong control on fluid flow.

In this study I characterize the sedimentology and permeability of previously incompletely described sedimentary units of the Miocene to Pliocene Arroyo Ojito Formation, in the hanging-wall block of the Sand Hill fault, central New Mexico (Figure 1, upper Santa Fe Group; Hawley and Haase, 1992; Hawley *et al.*, 1995; Connell *et al.*, 1999). I suspect these units include sediments which may have a fault-controlled origin. This study comprised two phases: fieldwork

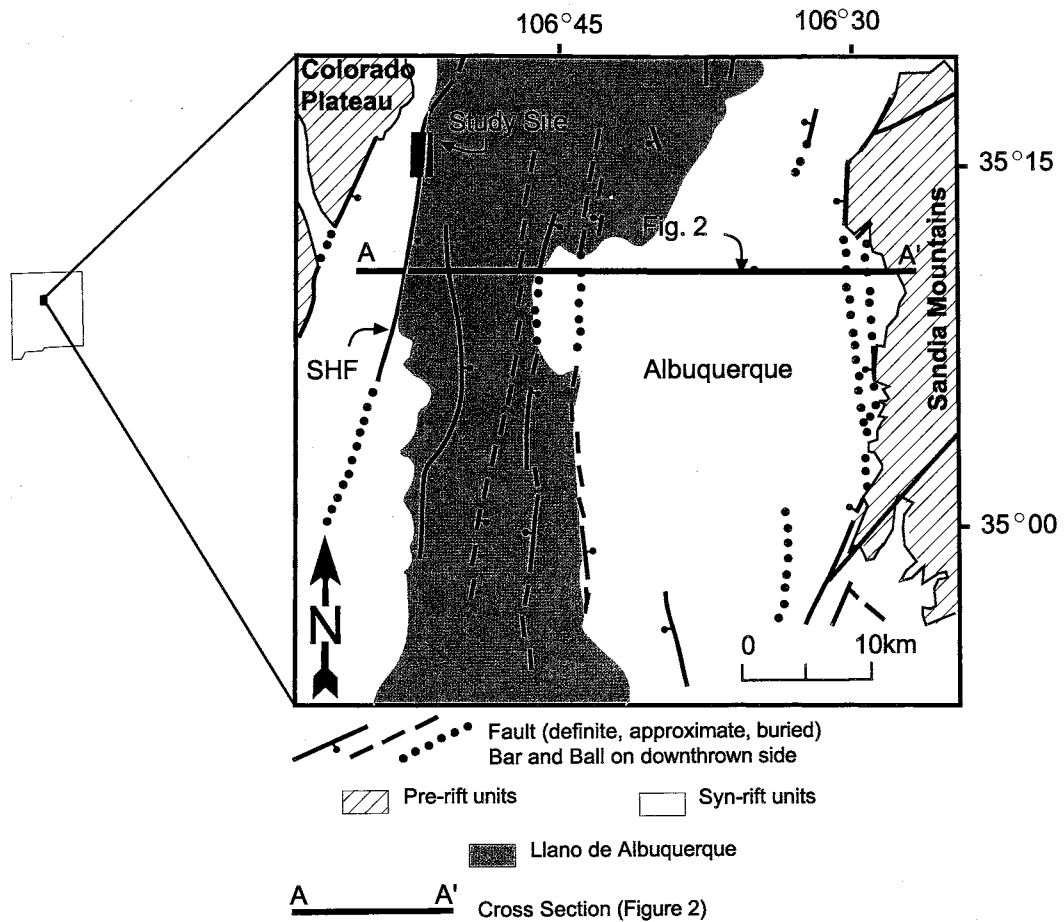


Figure 1: Location Map

Location of study site (black rectangle) with major fault traces in the Albuquerque Basin, including the Sand Hill fault (SHF). The cross section line corresponds to Figure 2. Modified from Hawley and Haase (1992).

(lithofacies mapping and detailed section measuring) to characterize the geometries and textures of lithofacies in the hanging-wall block of this high-angle normal fault zone, followed by laboratory and field measurement of the hydrogeologic properties of lithofacies identified through mapping and section measuring. The Sand Hill fault was chosen for this research for the three principle reasons listed below.

1. It is a growth fault (Heynekamp *et al.*, 1999).
2. The fault has excellent exposure created in part by preferential cementation of the fault zone (Mozley and Goodwin, 1995).
3. The bounding sediments have excellent exposures because of badlands-style topography.

My study suggests that a variety fluvial and possibly fault-related sedimentation processes produced significant volumes of sandy sediments in the study area. All of the sandy sediments have high permeabilities, regardless of the processes responsible for deposition and subsequent modification of those sediments. Results of my study will help future workers to make informed decisions regarding how to work between geologic maps and flow models, because the Sand Hill fault study area is typical of faulted sedimentary basins throughout the Basin and Range Province of the western U.S., and may be representative of normal-faulted sedimentary basins in general.

PREVIOUS WORK AND GEOLOGIC SETTING

LOCATION

The study area is located approximately 30 km northwest of Albuquerque, New Mexico and is bounded by the northern edge of the Arroyo de Las Calabacillas 7.5' quadrangle (formerly the Sky Village SE 7.5' quadrangle) in the north and the edge of the King Ranch on the Volcano Ranch 7.5' quadrangle in the south (Figure 1). The eastern border of the study area is located between the Llano de Albuquerque and the badlands of the Ceja del Rio Puerco. The western boundary of the study area is the Sand Hill fault.

RIO GRANDE RIFT

The Rio Grande rift extends for more than 1000 km as a series of asymmetrical grabens from Leadville, Colorado in the United States, to Chihuahua, Mexico. The rift is a region of late Cenozoic extensional deformation (Baldrige *et al.*, 1984). Large crustal blocks are separated by steeply dipping normal faults which characterize the rift. The main rift grabens have undergone vertical displacement of up to 6 km (Baldrige *et al.*, 1984).

SANTA FE GROUP

The Santa Fe Group comprises syn-rift sediments that range in thickness from less than 1000 m at the basin margins to nearly 5000 m in the central portion of the basin (Lozinsky, 1994; Hawley *et al.*, 1995). The region, in which the study area is found, contains two unconformity-bounded formations within the Santa Fe Group; the late Oligocene to middle Miocene Zia Formation (adjacent to this study area; Tedford, 1982; Hawley and Haase, 1992; Cather *et al.*, 1997) and the overlying Miocene to Pliocene Arroyo Ojito Formation (Connell *et al.*, 1999).

STRATIGRAPHY AND NOMENCLATURE

Bryan and McCann (1937) first documented the stratigraphy and structure of the Ceja del Rio Puerco area, and proposed one of the earliest stratigraphic designations of the Santa Fe Group (as the Santa Fe Formation). They divided the stratigraphy into a lower gray unit, middle red unit, and upper buff unit. The lower gray unit corresponds to the eolian Piedra Parada unit of Galusha (1966; not in the study area). The middle red unit corresponds to the fluvial Chamisa Mesa Member and red muds of the Canada Pilares Member of Galusha (1966; not in the study area). Bryan and McCann (1937) also included an upper unnamed member of the adjacent Zia Formation. This unnamed member is included in the middle red unit of Galusha (1966) and part of the Cerro Conejo

Member of the Arroyo Ojito Formation of Connell *et al.* (1999). The upper buff unit, described as alluvial fans by Bryan and McCann (1937), is the same as the tributary axial-fluvial Sierra Ladrones Formation of Cather *et al.* (1997) or the Arroyo Ojito Formation of Connell *et al.* (1999).

Previous workers have mapped the upper Santa Fe Group at a regional scale. Hawley and Haase (1992) show the upper Santa Fe Group extending from the western boundary to the eastern boundary of the Albuquerque Basin (Figure 2). Machette (1978b) named the interfingering fluvial and piedmont sediments of the upper Santa Fe Group the Sierra Ladrones Formation, and mapped this formation as far south as the northern Socorro Basin and as far north as the southern Albuquerque Basin. Other workers extended this nomenclature, based on their own observations of similar sediments, to the Belen Sub-Basin (Lozinsky and Tedford, 1991), the northern Albuquerque Basin (Hawley, 1978; Lozinsky, 1994; Hawley *et al.*, 1995), and the Santo Domingo Sub-Basin (Smith and Kuhle, 1998).

Based on field studies, Connell *et al.* (1999) proposed nomenclature changes within the Santa Fe Group and suggested assignment of deposits in the northwestern Albuquerque Basin to the Arroyo Ojito Formation (including those in my study area). In their nomenclature, the Arroyo Ojito Formation replaces the Sierra Ladrones Formation for sediments of the northwestern margin of the Albuquerque Basin and the southwestern margin of the Santo Domingo

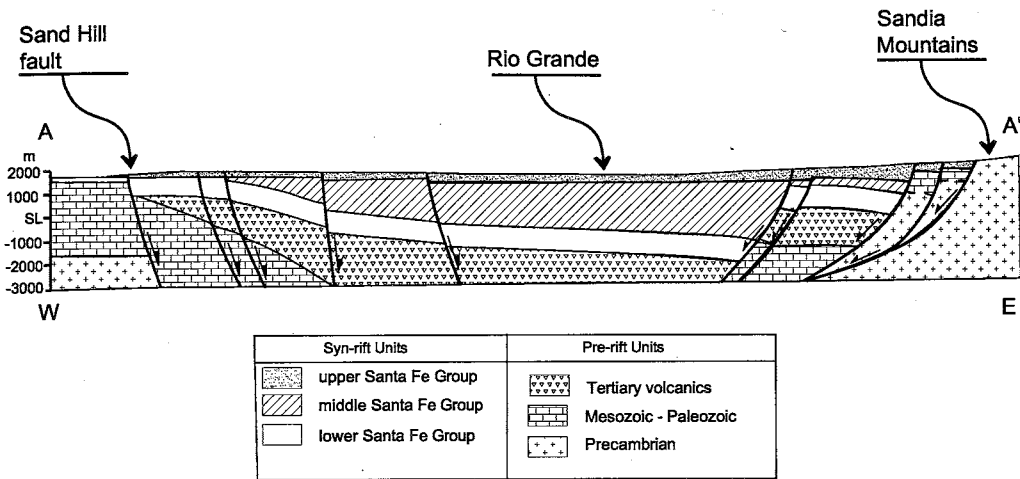


Figure 2: Albuquerque Basin Cross-section

The Sand Hill fault is on the western margin of the Albuquerque Basin.

Modified from Hawley and Haase (1992).

(Sub-) Basin. Within this formation they recognized and named the Navajo Draw Member, the Loma Barbon Member, and the Ceja Member. They also recognized and named the Pantadeleon Formation, which is poorly to moderately sorted, wedge-shaped, fault-controlled deposits of sandstone, conglomerate, and minor mudstone.

Beckner (1996) measured stratigraphic sections in the Zia Formation on the King Ranch. He concluded that the Zia Formation sediments were laterally continuous and could be easily correlated throughout his study area. He also defined the stratigraphy of the Zia Formation based on lithofacies and depositional environments. Beckner's study area, in the footwall block of the Sand Hill fault, is adjacent to mine and is assigned to the Cerro Conejo Member of the Zia Formation by Connell *et al.* (1999).

LITHOFACIES

Cather (1997) divided the upper Santa Fe Group (his Sierra Ladrone Formation) into four lithofacies based on grain size and depositional environment: conglomerate, conglomerate with sandstone, sandstone, and sandstone with mudstone. Cather *et al.* (1997) used these unit designations when mapping the Arroyo de Las Calabacillas 7.5' quadrangle at a scale of 1:24,000. Heynekamp *et al.* (1999) used mapping by Cather *et al.* (1997) to create a strip map (scale 1:6,000) of the Sand Hill fault in order to document fault

zone architecture and determine the relationship between the immediate bounding sediments and fault zone architecture.

The Arroyo Ojito Formation of the upper Santa Fe Group is dominated by fluvial deposits (Machette, 1978; Cather *et al.*, 1997; Heynekamp *et al.*, 1999). In the study area, this formation can be divided into three unconformity-bounded units: an upper cemented unit of gravel and sand; a middle unit that ranges from clay-rich beds to sand and gravel along strike; and a basal unit that has stacked fining-upward sequences (Heynekamp *et al.*, 1999). The lower portion of the basal unit of the upper Santa Fe Group is not exposed in this area (Heynekamp *et al.*, 1999).

SYNTECTONIC DEPOSITIONAL WEDGE

When surface rupture occurs through normal faulting, it creates a wedge-shaped space on the hanging-wall block (Machette, 1978; Forman *et al.*, 1991; Nelson, 1992; Amit *et al.*, 1995; Rubin *et al.*, 1999; Nelson *et al.*, 2000; McCalpin and Nelson, 2000; McCalpin, 2000; Figure 3). Material shed from the footwall block into the wedge-shaped space on the hanging-wall block is referred to as a colluvial wedge. Colluvial wedge deposits are commonly deposited in a wedge-shape configuration with the coarsest-grained and thickest portion of the deposit occurring adjacent to the fault scarp and fining and thinning away from the fault. The colluvium may bury soils developed between faulting events, creating a

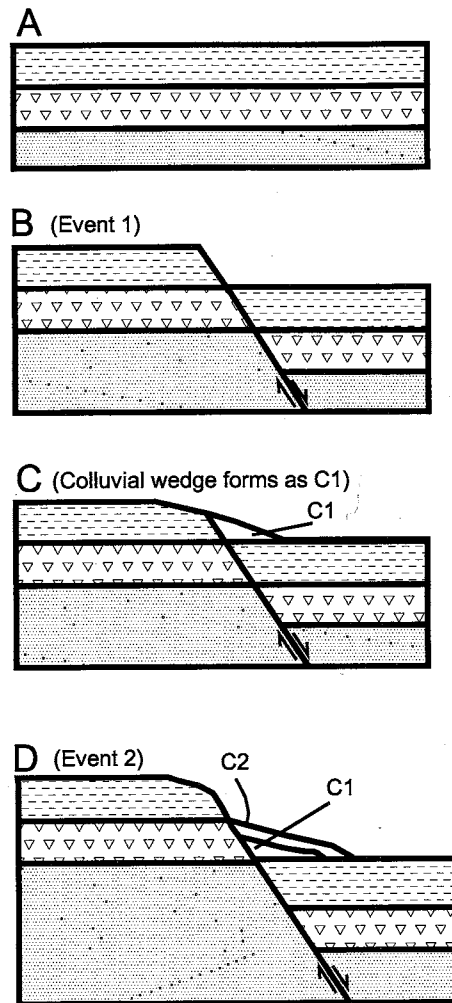


Figure 3: Colluvial Wedge Diagram

This drawing (modified from Keller and Pinter, 1996) shows the hypothetical production of a space created by normal faulting (B). A classical colluvial wedge deposit (C1) is shed into the wedge-shaped space as the footwall of the fault zone is eroded and debris falls into the space below (C). Subsequent movement on the fault (D), causes a younger deposit (C2) to form on top of C1. In addition to the colluvial wedge depicted, it is possible for this wedge-shaped space to be filled with eolian, fluvial or pond deposits (see text for further discussion).

wedge of sediment punctuated by buried soil horizons (Figure 4). The soils represent periods of landscape stability whereas the syntectonic deposits represent periods of landscape adjustment after a fault rupture event (Machette, 1978, Amit *et al.*, 1995; McCalpin, 2000).

Soil horizons on colluvial surfaces have typically been used to determine recurrence intervals and date rupture events on faults (Machette, 1978; Forman *et al.*, 1991; Nelson, 1992; Amit *et al.*, 1995; Rubin *et al.*, 1999; Nelson *et al.*, 2000; McCalpin and Nelson, 2000; McCalpin, 2000). Some researchers have used the distinctive wedge shape of fault-related colluvial deposits to locate faults by remote sensing techniques (Morey, 1998; Chow *et al.*, 2001).

Nelson (1992) presented the stratigraphy of colluvial lithofacies assemblages adjacent to normal faults in the Basin and Range Province. He describes the colluvium as an unlithified mixture of clay, silt, sand, and gravel (or rock fragments) that is poorly stratified or massive in nature. Nelson (1992) divided each colluvium cycle into a lower debris element and an upper wash element. The debris element is typically wedge shaped, thicker near the fault and thinning away from the fault. This material comes primarily from degradation of the free scarp face, and the texture of the debris reflects the type of material exposed in the fault scarp. A coarse-grained or hard-rock scarp may have

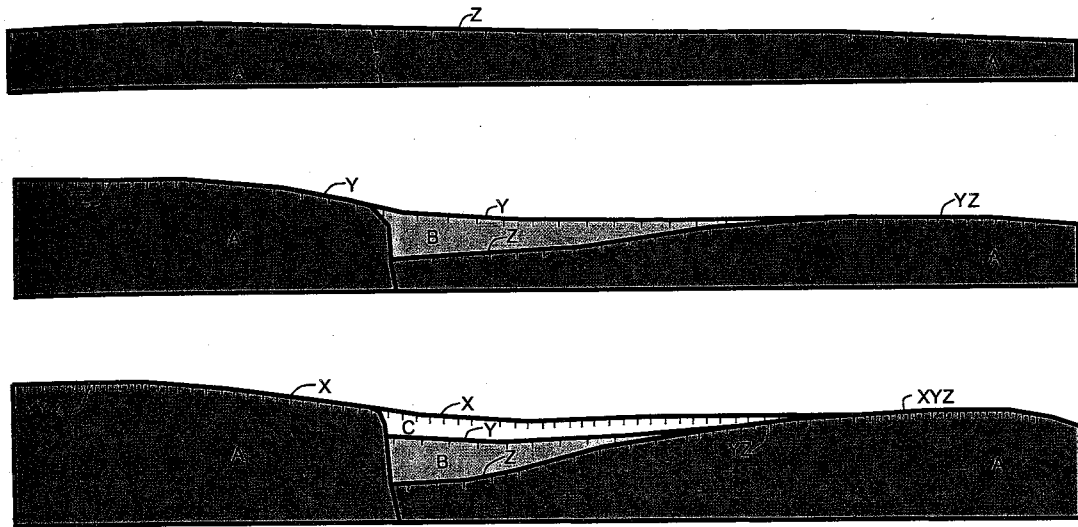


Figure 4: STDW and Soil Formation

Episodic movement on a fault, schematically illustrated above, can create successive generations of stacked STDWs (B and C). Soil-forming processes are disrupted by fault movement and the subsequent burial of surfaces under younger STDWs. This forms a sequence of stacked, soil-bounded STDWs (soils marked X, Y, and Z above). These soils coalesce away from the fault as shown at YZ and XYZ. Thus, the soil at XYZ will be the best developed and X, Y, and Z will be the least well-developed soils in the vicinity of a given fault. The spacing of tick marks along the soil surfaces shown above represents the relative degree of soil development. Modified from Machette (1978).

distinct fining-upward layers within such a debris facies whereas sediments from a fine-grained scarp may not display a fining-upward sequence.

Nelson's (1992) wash element represents movement of material away from the fault scarp in a dilute flow environment. The wash element is less wedge-shaped, extends beyond the toe of the debris element, and is laterally more extensive down-dip, thinner, and finer-grained than the debris element. He describes the wash element as non-stratified silty sand to clayey silt with pebbles or cobbles evenly distributed throughout the unit, commonly bioturbated. The wash element occurs over long periods of time where the debris element forms within a short time frame after fault rupture.

Many geologists have recognized the existence of syntectonic sedimentation in the form of colluvial wedge deposits (Machette, 1978; Forman *et al.*, 1991; Nelson, 1992; Amit *et al.*, 1995; Morey, 1998; Rubin *et al.*, 1999; Nelson *et al.*, 2000; McCalpin and Nelson, 2000; McCalpin, 2000; Chow *et al.*, 2001). Colluvium, however, is not the only type of sediment that can occur in the wedge-shaped space created on the hanging-wall block of a normal fault as a result of fault rupture. To date, only a few workers have examined the sedimentologic or hydrogeologic characteristics of fault-controlled sediments, or recognized other forms of sedimentation (e.g. fluvial, eolian, and lacustrine) that occur along the fault scarp created by normal faulting (Machette, 1978; Nelson, 1992; Connell *et al.*, 1999; Smyth and Connell, 1999). In the Albuquerque Basin,

researchers have documented fault-parallel fluvial (Connell *et al.*, 1999; Smyth and Connell, 1999) and eolian sediments (Machette, 1978) deposited in such wedge-shaped spaces.

The sediments that accumulate within the wedge-shaped space created by fault rupture are best described as a syn-tectonic depositional wedge (STDW) (Smyth and Connell, 2000). The STDW may include classic colluvium deposits (colluvial wedge; Machette, 1978; Figure 3), produced by shedding of material into the depression adjacent to the footwall block of the fault, eolian deposits (Machette, 1978), fault-parallel fluvial deposits (Connell *et al.*, 1999), and/or sag pond deposits (Forman *et al.*, 1989). The term "colluvial wedge" denotes deposition of colluvium alone into the wedge-shaped space on the hanging-wall block, whereas the term "STDW" is inclusive of all sediment deposited into the wedge-shaped space, of which colluvium is only one of many possibilities.

Syntectonic sediments associated with the Sand Hill fault are described in this project. In this study, STDW is used to refer to syntectonic sediments containing material deposited by processes like fluvial, eolian, and lacustrine deposition in addition to colluvium.

SAND HILL FAULT

The Sand Hill fault is a major north-striking high-angle normal fault along the western margin of the Albuquerque Basin and the Rio Grande rift (Figure 2).

It extends approximately 50 km (Kelley, 1977) with strikes ranging from N12°W to N23°W (Heynekamp *et al.*, 1999) within the study area. The fault accommodates dip-slip displacement in which the upper Santa Fe Group (Arroyo Ojito Formation of Connell *et al.*, 1999) has been displaced in a down-to-the-east direction (Hawley and Haase, 1992; Hawley *et al.*, 1995). The fault dips from 70°E to vertical, with slickenside striae indicating dominantly dip-slip movement with local components of sinistral or dextral strike-slip motion, depending on local fault orientation (Heynekamp *et al.*, 1999).

The maximum vertical displacement along the Sand Hill fault is approximately 600 m (Hawley *et al.*, 1995), but all the units have not been subjected to the same amount of offset. Work by Heynekamp *et al.* (1999) shows that the uppermost unit of the Arroyo Ojito Formation in the study area has only experienced approximately 10 meters of vertical offset. Based on observations of angular unconformities within sediments on the down-thrown block, Wright (1946) determined that the Sand Hill fault has experienced a history of episodic movement. The older the unit is, the greater it's minimum displacement. Because the Sand Hill fault experienced displacement during active sediment accumulation, it is considered a growth fault (Heynekamp *et al.*, 1999).

The Sand Hill fault locally juxtaposes the syn-rift deposits of the upper Arroyo Ojito Formation against the Zia Formation. Bryan and McCann (1937)

recognized and described the Sand Hill fault as a normal fault within the Santa Fe Group. They also recognized the cemented and deformed portions of the fault zone, calling them sand dikes. These features have been reinterpreted by others (Mozley and Goodwin, 1995; Heynekamp *et al.*, 1999), as portions of the Sand Hill fault zone that have been preferentially cemented and therefore, are resistant to erosion.

FAULT ZONE PERMEABILITY

Previous studies of faults have determined that faults can act as conduits, barriers, or complex barrier–conduit systems with respect to fluid flow and that permeability can evolve over time (e.g. Knipe, 1993; Caine *et al.*, 1996). Recent studies of fault–zone architecture and permeability of faulted unlithified sediments have revealed that faults in poorly lithified sediments tend to have reduced porosity and permeability relative to the adjacent parent sediments (Hong, 1999; Sigda *et al.*, 1999; Herrin, 2001; Rawling *et al.*, 2001).

Rawling *et al.* (2001) measured permeability of the Sand Hill fault in the study area and found that the deformed fault zone had permeabilities up to several orders of magnitude lower than the adjacent parent material. Rawling *et al.* (2001) reported permeabilities as high as 10^{-10} m^2 (approximately 10^2 Darcy) for sand in the protolith adjacent to the Sand Hill fault and permeabilities as low as 10^{-19} m^2 (approximately 10^{-7} Darcy) in the clay core of the fault.

Haneberg (1995) used mathematical modeling to study hydraulic gradients across faults. He found that different combinations of transmissivity contrast and recharge or discharge will create distinct head profiles. Haneberg's modeled head profiles can be used to qualitatively infer the nature of real hydrogeologic systems. Haneberg (1995) shows that hydraulic gradient ratios can be used to calculate transmissivity ratios. He states that the effectiveness of a fault to act as a pressure seal (barrier) is independent of the fault thickness and a high permeability fault will have more effect on head profiles than a low permeability fault.

METHODS

In order to address the sedimentology and permeability characteristics of the study area sediments, I implemented a two-phase plan of data collection. The first phase of data collection was to describe the sediments and delineate their relationships both laterally and vertically. This was accomplished using measured stratigraphic sections and detailed lithofacies mapping. Once the major sediment packages were identified, the second phase of data collection involved determining their hydrogeologic properties. Several methods were used, including, sieve analysis to determine particle-size distribution and sorting, thin section imaging to approximate porosity, and air minipermeametry to determine permeability. The following sections provide detailed descriptions of the methods used during the two phases of data collection.

SEDIMENTOLOGY

I did not use formal nomenclature for measured stratigraphic sections or mapping; instead I chose to use lithofacies designations for sediment packages. Unlike formal nomenclature which defines a single formal stratigraphic unit that is consistently mappable but in which different lithologies are commonly represented, a lithofacies is a stratigraphic unit based on the visual estimation of physical and chemical characteristics of the sediments (Reading and Levell,

1996), such as color, sedimentary structures, mineralogical components, and grain size.

Sediments in the southern map area are slightly more lithified and better exposed than those in the northern section. Better exposure of the southern portion of the map area led to better identification of sedimentary structures and more precise location of unit boundaries. Consequently, this area was the focus of sediment sampling and description of stratigraphic sections. Units in the northern area were identified and characterized based on similarities to the sediments in the southern area, as sedimentary structures are more difficult to observe in the northern portion of the study area.

Measured Stratigraphic Sections

Four stratigraphic sections were measured in the study area, using a Jacob's staff and Brunton compass as described by Compton (1985). Lithofacies in each section were described on a decimeter scale, based on local lithofacies changes, major bounding surfaces, and changes in the style of sedimentary structures. The purpose of the measured sections was to determine local stratigraphy and its lateral variations. These data were used to refine lithofacies units for mapping.

Soils were described using terminology primarily from Giles *et al.* (1966) and Birkeland *et al.* (1991). Stages of carbonate buildup in soil horizons were

compared visually to the sketch by Giles *et al.* (1966). Giles *et al.* (1966) presents four stages of carbonate buildup, of which Stage I has the least amount of carbonate buildup and Stage IV has the greatest amount of carbonate buildup in the soil.

I recorded paleocurrent data in the field during stratigraphic section measuring. Paleocurrent indicators are sparse in the field area due to the friable nature of the sediment units. Paleocurrent orientations were collected exclusively from channel morphology using a Brunton compass. The sediments in the area dip less than 15° and are relatively undeformed and therefore, required no structural correction (Compton, 1985).

I grouped the data into two categories, for each measured section, based on similarities of paleocurrent orientations within lithofacies units. The orientations for QToup and QTouc comprised the first group and the orientations for QTous and QToug comprised the second. I plotted these grouped data in separate rose diagrams which are presented on Figure 5, Plate 1, and in Appendix A. The mean paleocurrent orientation from each rose diagram is also displayed on the measured stratigraphic sections (Figures 6 through 9). The rose diagrams were generated using Stereopro by MWSsoftware (Walters, 1997). The analysis utilized 10° bins, and where more than five measurements were available for a given group the mean and standard deviation were also plotted. The raw data are presented in Appendix A.

Figure 5: Geologic Map

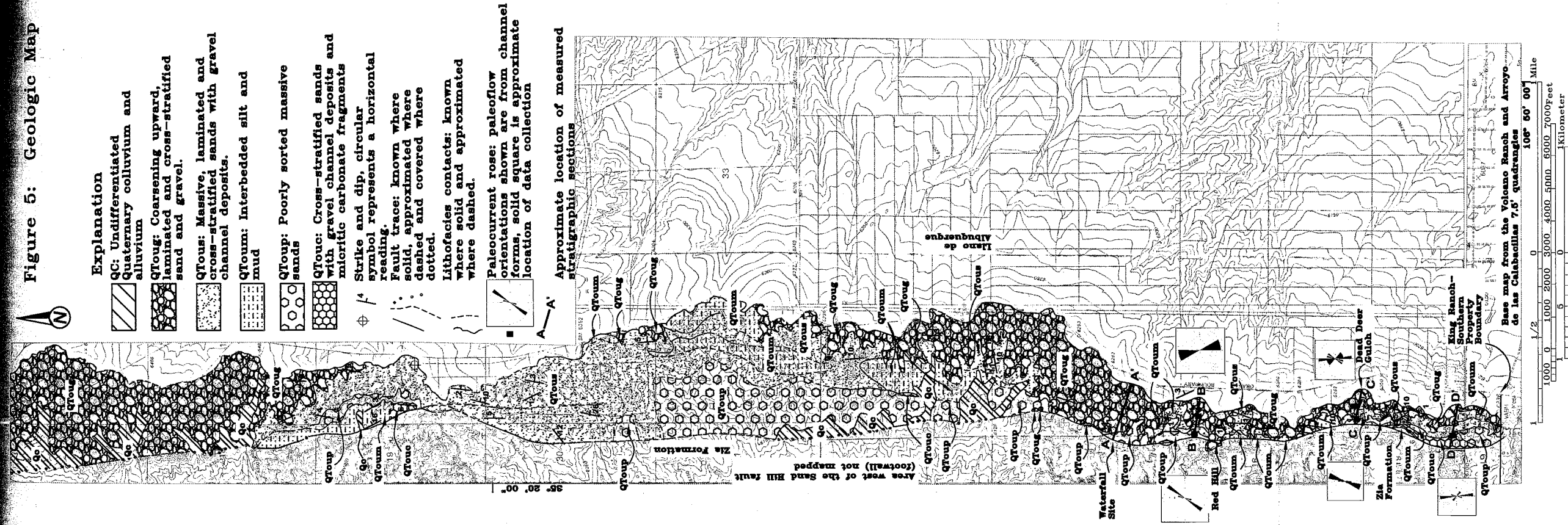
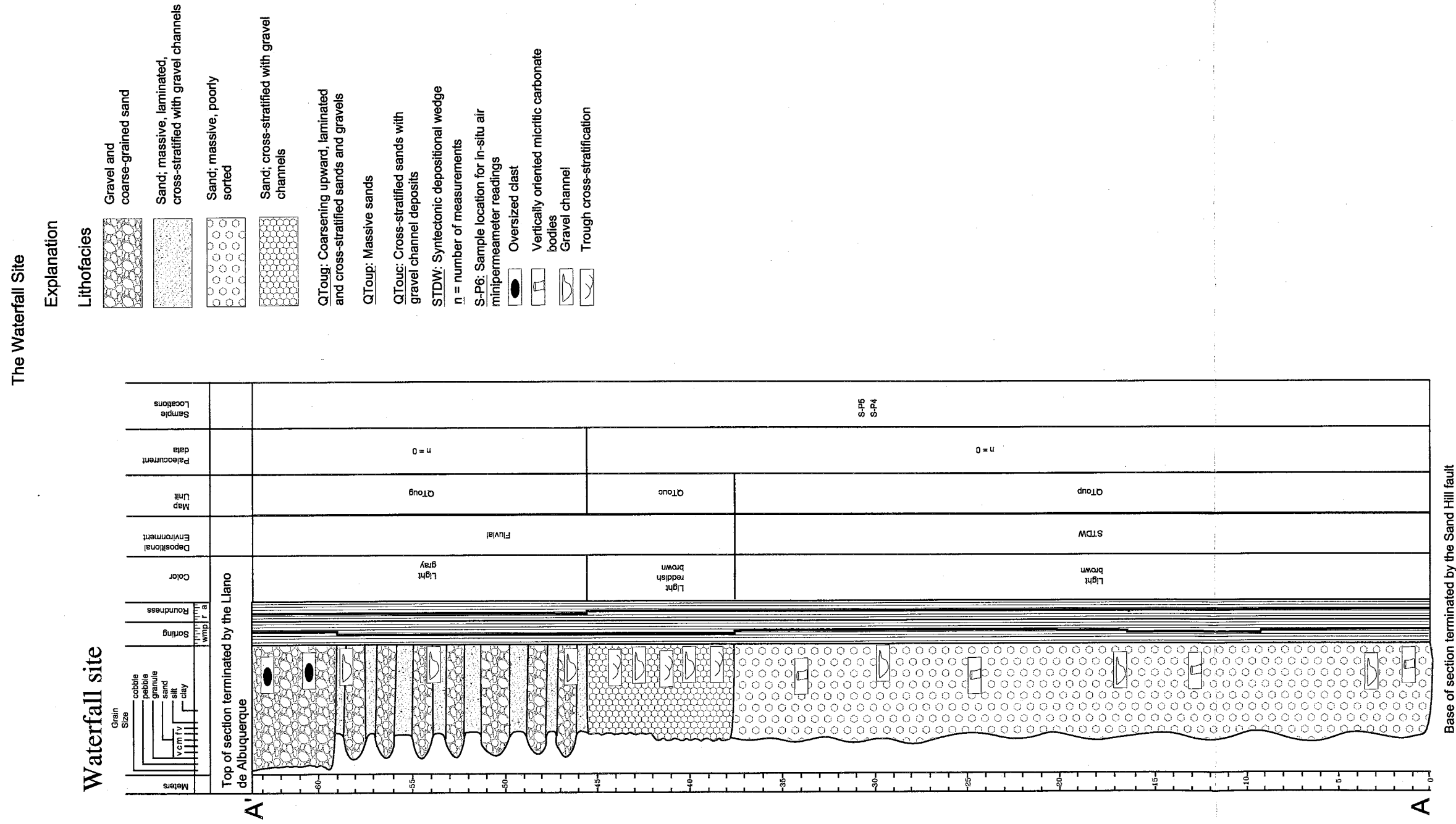


Figure 6 : Measured Stratigraphic Section A-A'



The Waterfall Site

Explanation

Lithofacies

- Gravel and coarse-grained sand
- Sand; massive, laminated, cross-stratified with gravel channels
- Sand; massive, poorly sorted
- Sand; cross-stratified with gravel channels

QTouc: Coarsening upward, laminated and cross-stratified sands and gravels

QToup: Massive sands

QTouc: Cross-stratified sands with gravel channel deposits

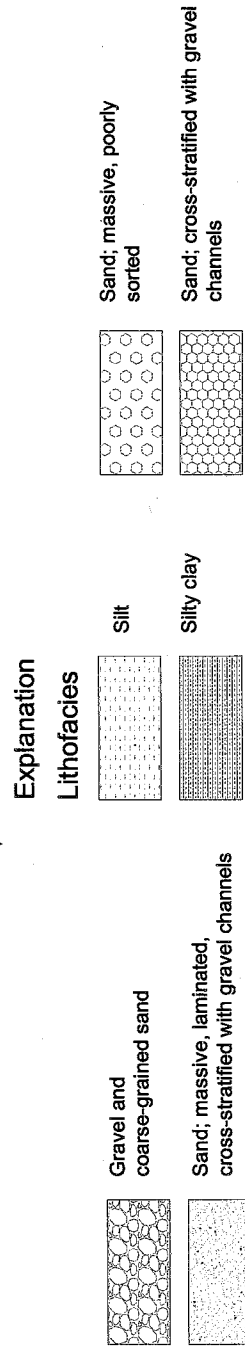
STDW: Syntectonic depositional wedge

n = number of measurements

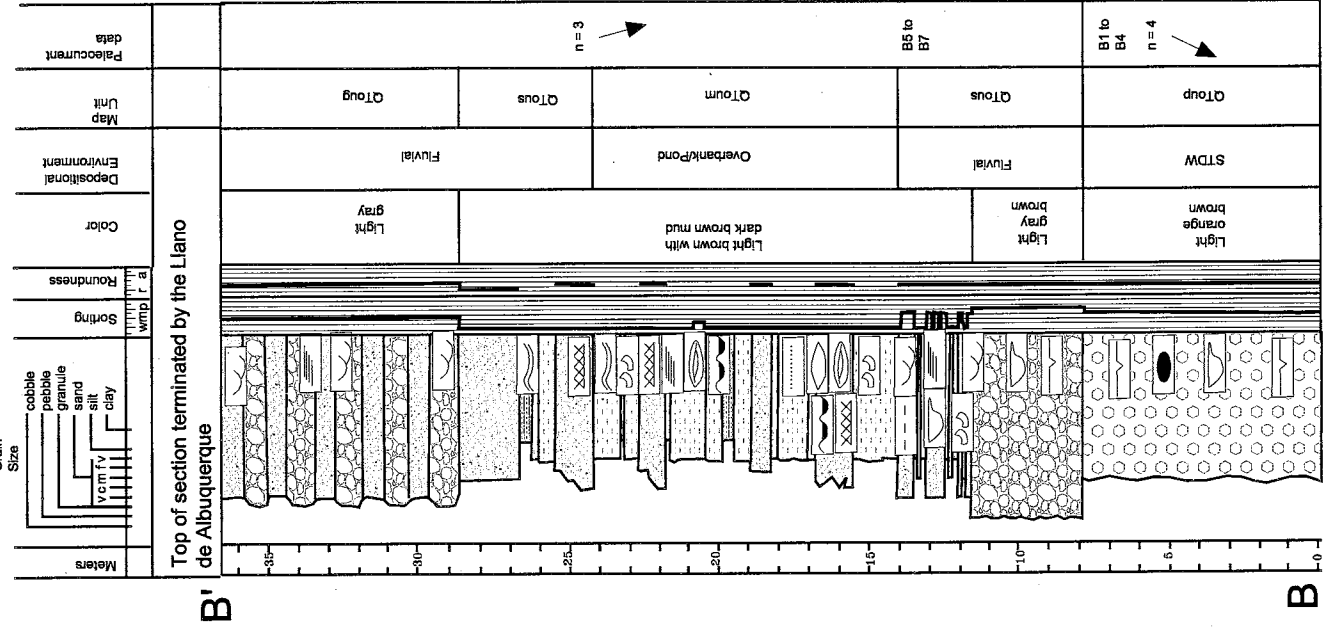
S-P6: Sample location for in-situ air minipermeameter readings

- Oversized clast
- Vertically oriented micritic carbonate bodies
- Gravel channel
- Trough cross-stratification

Figure 7 : Measured Stratigraphic Section B-B',
North of Red Hill



North of Red Hill



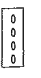

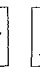




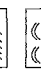


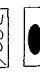
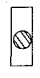

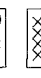






QToug: Coarsening upward, laminated and cross-stratified sands and gravels
QTous: Massive, laminated and cross-stratified sands with gravel channel deposits

QToum: Interbedded silt and silty clay
QToup: Massive sands

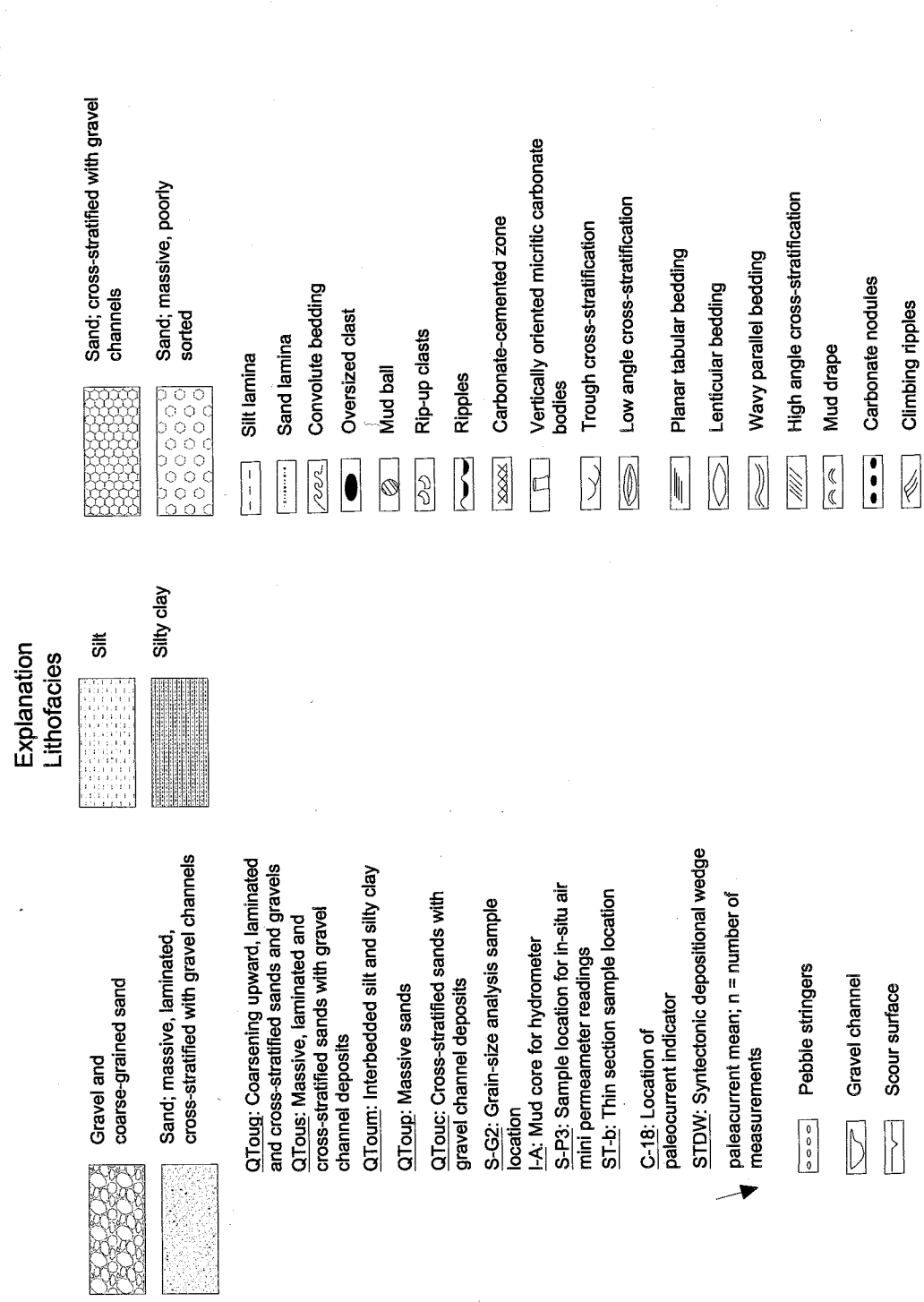
STDW: Syntectonic depositional wedge
B5: Location of paleocurrent indicator

Paleocurrent mean; n = number of measurements

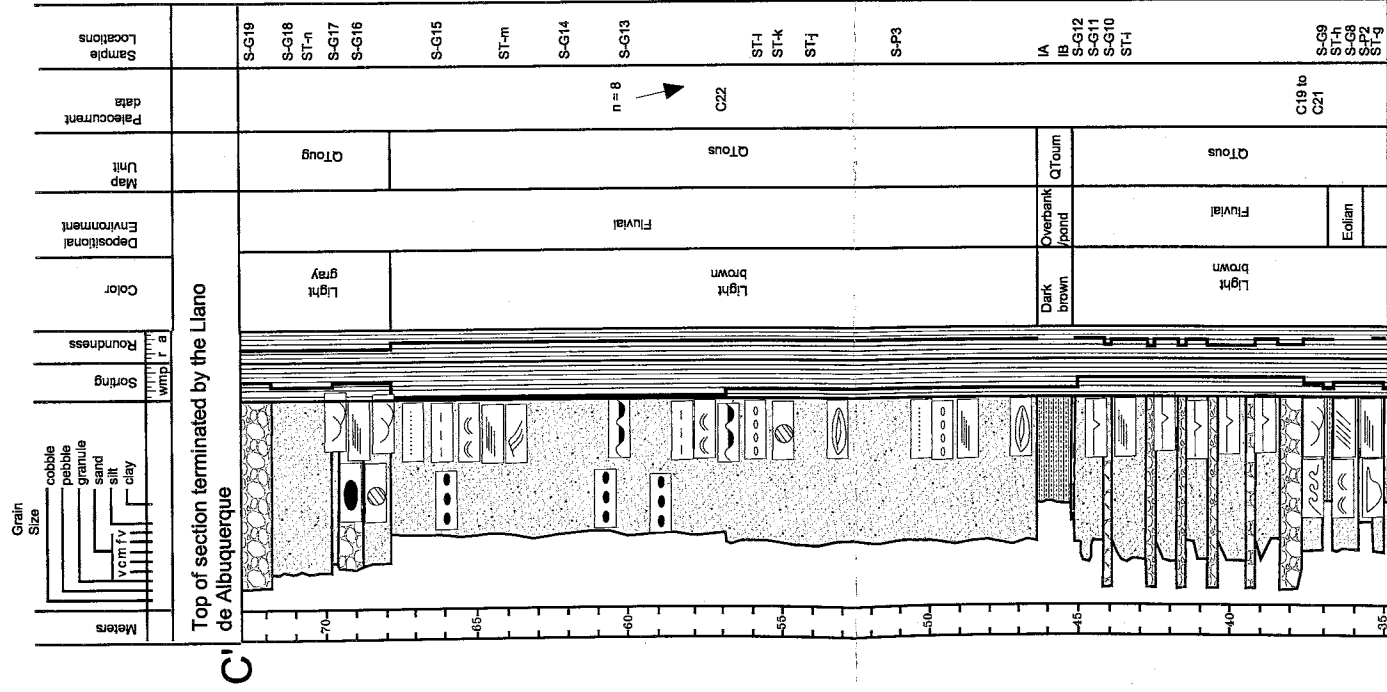
-  Silt lamina
-  Sand lamina
-  Pebble stringers
-  Gravel channel
-  Scour surface
-  Trough cross-stratification
-  Low angle cross-stratification
-  Planar tabular bedding
-  Lenticular bedding
-  Wavy parallel bedding
-  High angle cross-stratification
-  Mud drape
-  Carbonate nodules
-  Climbing ripples
-  Convolute bedding
-  Oversized clast
-  Mud ball
-  Rip-up clasts
-  Ripples
-  Carbonate-cemented zone

Base of section terminated by the Sand Hill fault

Figure 8: Measured Stratigraphic Section C-C'
Dead Deer Gulch

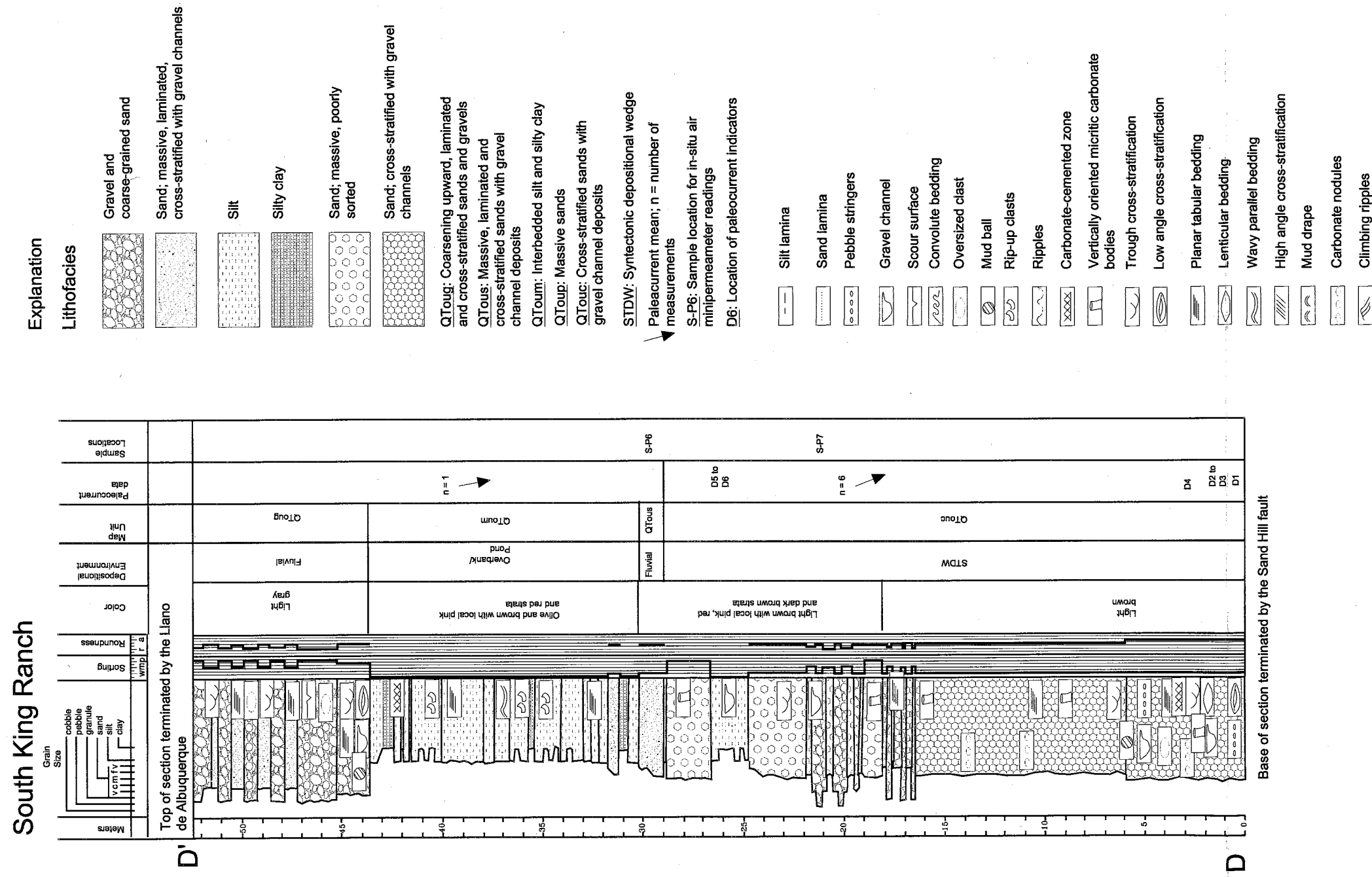


Dead Deer Gulch



See right column for continuation of stratigraphy.

Figure 9: Measured Stratigraphic Section D-D',
South King Ranch



Lithofacies Mapping

Lithofacies on the hanging-wall block of the Sand Hill fault were mapped at a scale of 1:8,000 (Plate 1; Figure 5) to permit documentation of meter-scale lateral and vertical changes in lithology. The map units were modified from Cather *et al.* (1997) and utilize the Arroyo Ojito Formation nomenclature of Connell *et al.* (1999). Cather *et al.*'s (1997) lithofacies were subdivided into smaller subunits for the purpose of this study, based on textural assemblages. The names of the map units were created by combining letters representing the age of the unit, the formal nomenclature of the unit, and the lithofacies of the unit. This naming method is based on the method described by Cather (1997). The map unit designations used in this study are presented in Table 1. The mapping facilitated interpretations of the facies architecture in the area, and therefore, allowed predictions regarding likely permeability trends.

Lithofacies mapping was conducted by observing assemblages of sedimentary structures and the texture of the lithofacies present. Where more than one lithofacies was encountered, the sediment was mapped based on which type of sediment is volumetrically dominant. Where there is little topographic relief (and hence no outcrops to analyze) lithofacies were mapped based on clast

**Table 1:
Map Unit Designations**

Map Unit	Age	Formation	Lithofacies
QToug	<u>Q</u> uaternary/ <u>T</u> ertiary	Arroyo <u>Q</u> jito Formation, <u>U</u> ndifferentiated	Coarsening-upward laminated and cross-stratified sands and <u>g</u> ravels
QTous	<u>Q</u> uaternary/ <u>T</u> ertiary	Arroyo <u>Q</u> jito Formation, <u>U</u> ndifferentiated	Massive laminated and cross-stratified <u>s</u> ands with gravel channel deposits
QToum	<u>Q</u> uaternary/ <u>T</u> ertiary	Arroyo <u>Q</u> jito Formation, <u>U</u> ndifferentiated	Interbedded silt and silty clay (<u>m</u> ud)
QToup	<u>Q</u> uaternary/ <u>T</u> ertiary	Arroyo <u>Q</u> jito Formation, <u>U</u> ndifferentiated	<u>P</u> oorly sorted massive sands
QTouc	<u>Q</u> uaternary/ <u>T</u> ertiary	Arroyo <u>Q</u> jito Formation, <u>U</u> ndifferentiated	<u>C</u> ross-stratified sands with gravel channel deposits

that and similarities in characteristics between lithofacies units and the sediment present. Consequently, lithofacies boundaries in these areas are tentative and were mapped with a dashed line.

PERMEABILITY

Working Assumptions

Grain size and sorting can help estimate the fluid flow properties of sediments. Fetter (1994) outlines four factors (revised from Masch and Denny, 1966) relating permeability to grain size and sorting, which can be used for all sediments regardless of depositional environment. These four factors, stated below, show how grain size and sorting affect permeability.

- (1) As the median grain size increases, so does permeability. This is due to larger pore openings.
- (2) Permeability decreases for a given median diameter as the standard deviation of particle size increases. The increase in standard deviation indicates an increasingly poorly sorted sample, with the finer material filling the voids between larger fragments.
- (3) As the standard deviation of particle size increases, coarser samples show a greater decrease in permeability than do fine-grained samples.

- (4) Samples with a unimodal grain-size distribution are more permeable than bimodal samples. Fine-grained material fills the void space between larger grains; therefore, this relationship is, again, a result of more poorly sorted sediments.

Table 2 shows how grain size and sorting influence porosity and permeability

Sediment Grain Size	Porosity Range (Percent)	Intrinsic Permeabilities (Darcies)
Well-sorted gravel	25-50	$10-10^3$
Well-sorted sand	25-50	$1-10^2$
Sand and gravel mixed	20-35	Not Available
Silty sands, fine sands	Not Available	$10^{-2}-1$
Glacial till (representing a poorly sorted sedimentary unit)	10-20	$10^{-3}-10^{-1}$
Silt	35-50	$10^{-3}-10^{-1}$
Clay	33-60	$10^{-6}-10^{-3}$

Revised from Fetter (1994)

In general, the table shows that the larger the grain size and the better sorted the material is, the higher the permeability. The table also shows that poorly sorted

material such as mixed sand and gravel or glacial till have lower porosities than well-sorted material, regardless of grain size.

Analyses were performed on sediment samples representing the various map units for grain-size distribution, field permeability, and porosity estimation from thin sections. Sediment samples were collected throughout the field area for grain-size analysis and thin-section porosity estimation. Certain analyses require a specific grain-size range for accuracy. Where the grain-size range was appropriate, sediments from each unit were collected for grain-size analysis, porosity measurements, and measured in the field for permeability. Where different analyses were possible on the same material, the results were compared in order to evaluate whether the different analyses methods were showing the same general hydrogeologic trends for the various lithofacies.

Grain Size and Sorting

Samples were collected for sieve analysis and hydrometer tests to determine the grain size and sorting of the different lithofacies. Coarse-grained material (sand and gravel) was sampled for sieve analysis. The sieve analysis was conducted using sieves with openings from 0.002 to 2.0 millimeters. Everything too large to pass through the 2.0-millimeter sieve is gravel-sized material. All material that passes the 0.002-millimeter sieve was considered clay-sized material. The clay-sized material and the gravel-sized material from

The sieve analysis were not sorted into smaller categories. However, two fine-grained samples were collected for hydrometer analysis. Sieve analyses were not run on the hydrometer samples; therefore, the percentage of sand-sized material in these samples was extrapolated from graphs of the grain-size distribution. Grain-size analysis was the only practical method to estimate hydrogeologic characteristics of the gravels, because the minipermeameter and thin section porosity methods described below cannot accommodate the large grain sizes of the gravel. Grain-size data are presented in Appendix B.

Thin Section Imaging

Thin section images of undisturbed sediment were used to estimate the porosity of various sediments within the field area. Coarse-grained sand from the gravel unit (QToug) and sand from various lithofacies (QTous, QTouc, and QToup) were sampled. In order to remove intact samples for thin section preparation, several steps were taken after cleaning and smoothing the outcrop. First, a 7.5-centimeter (3-inch) diameter core was drilled in the outcrop using a cordless drill. Next, the sediment outside the diameter of the core was carefully removed. Then, spray-on foam insulation was used to cover and contain the exposed core. After drying overnight, the foam-encased core was gently removed from the outcrop within its protective foam case.

Once the sediment cores had been transported to the laboratory, they were made into thin sections for imaging. The sediments sampled were non-cemented, so standard thin sections were prepared by saturating the sediment with blue epoxy. Ten photographic images were taken of each thin section along a grid to prevent sampling bias. The photographic images were imported into Scion Image (an image processing program) and then run through a series of computer programs (macros) developed by Geoffrey Rawling (New Mexico Bureau of Geology and Mineral Resources) to convert the color images to binary images in order to analyze the color differences between detritus and blue epoxy. The percentage of the blue epoxy was then used as an approximation of porosity within the unit (Appendix C).

Air Minipermeametry

The permeability of sands was measured in the field using a syringe-style air minipermeameter, which has some limitations (Davis *et al.*, 1994).

Measurement of permeability in coarse-grained sediment is problematic because the size of the tip seal is small relative to the gravel clasts. With gravel, either the clasts are bigger than the tip or the gaps between the clasts create a surface on which the tip cannot form an adequate seal. Also, it is not possible to obtain minipermeameter readings on low-permeability fine-grained or cemented material due to the limitations of the instrument. The air minipermeameter is designed to measure permeabilities in the 0.5–200 Darcy range, and optimum

sensitivity of the instrument is obtained in the 0.87–200 Darcy range (Davis *et al.*, 1994). The average permeability of silt- and clay-sized sediments studied in other areas is 10^{-1} to 10^{-6} Darcies (Fetter, 1994; Table 2).

Sampling locations were prepared by excavating several centimeters from the face of the subject outcrop, then scraping and brushing the outcrop to expose a fresh, smooth surface (Davis *et al.*, 1993; Sigda, 1995). A grid was fastened to each outcrop to facilitate the choice of multiple random sample locations (Appendix D). The grid was comprised of approximately 7.5-centimeter (3-inch) squares. The grids ranged in size from 9 squares across by 8 squares down to 20 squares across by 7 squares down. The area of intact outcrop that was suitable for taking measurements determined the external shape of the grid. The tip of the instrument was seated on the outcrop in a manner that allowed a seal to form between the instrument and the outcrop face in order to prevent erroneously high permeability readings (Davis *et al.*, 1994). The minipermeameter was field-calibrated using manufactured standards of known permeability before sampling at each outcrop (Davis *et al.*, 1994).

Outcrop surfaces in the field area are primarily north- or south-facing due to the prevalence of east-trending incised drainages carrying seasonal water from the topographically higher Llano de Albuquerque in the east to the topographically lower Rio Puerco in the west. Permeability anisotropy shows a strong correlation with the paleoflow direction in fluvial sediments (Mozley and

Davis, 1996), which is roughly from north–northwest to south–southeast in this study area (Connell *et al.*, 1999). Due to the permeability anisotropy and the primary orientation of outcrop faces, all sampling was conducted on north– or south–facing outcrops for consistency, even though the air minipermeameter used in this study does not provide directional permeability measurements.

Three measurements were collected for each grid square at each sample location. The three measurements for each square were averaged to obtain a single measurement from each collection point. The mean, median and standard deviation were calculated for each sample outcrop location.

GEOLOGY

LITHOFACIES DESCRIPTIONS

As indicated in Table 1, the sediments in my study area are divided into the five mappable lithofacies listed below.

- Coarsening-upward laminated and cross-stratified sand and gravel (QToug)
- Massive laminated and cross-stratified sand with gravel channel deposits (QTous)
- Interbedded silt and silty clay (QToum)
- Poorly to moderately sorted massive sand (QToup)
- Cross-stratified sand with gravel channel deposits (QTouc)

These units are shown on the geologic map (Figure 5; Plate I). Undifferentiated Quaternary colluvial and alluvial deposits are shown on the geologic map as Qc. These sediments are not part of this study as they are localized, thin deposits of Holocene age. The main purpose of mapping Qc was to show where Holocene deposits obscured mapping of the lithofacies units that were the focus of this

study. In the sections below, I describe the physical characteristics observed in each lithofacies unit.

QToug

QToug consists of light gray, friable to moderately indurated, coarse-grained, moderately to well-sorted sand and poorly to moderately sorted, clast-supported pebble and cobble gravel (Figure 10). The unit has approximately 70% coarse-grained sand and 30% pebbles and cobbles. QToug ranges from very thinly (1 to 3 cm) to medium bedded (10 to 30 cm).

This unit coarsens and thickens upward. The base of the unit commonly has rhythmically interbedded coarse sand and pebble and cobble beds. The top of the unit is dominated by pebble and cobble gravel beds. Decimeter- to meter-scale trough cross-stratification, planar-tabular bedding and internal laminations are common. Other sedimentary structures include oversized clasts (clasts that are larger than the general grain size, e.g. a single cobble in medium-grained sand), mud balls, scour, channel deposits, and low-angle cross-stratification.

This lithofacies is locally mildly to moderately cemented with sparry calcite. Under the Llano de Albuquerque, the top of QToug has Stage III pedogenic carbonate morphology, as defined by Birkeland *et al.* (1991). QToug



Figure 10: QToug

Coarsening upward laminated and cross-stratified sand and gravel. The light gray section at the top of this south-facing outcrop is QToug. The boundary (B) between QToug and the lower, light brown-colored QTous is unconformable. Interbedded sand and gravel and crossbeds (G) are in the overlying gray unit.

can be distinguished in the field based on its overall gray appearance and abundance of coarse-grained sediments.

QTous

The bulk of the unit consists of light brown to yellow-brown, friable, fine- to medium-grained moderately to well-sorted sand. This unit is approximately 80% sand, 15% silt and 5% clay, based on field observations. Beds are laminated to thinly bedded and appear tabular to lens-shaped.

Fining-upward sequences are observed locally. The sand is massive, laminated or cross-stratified and is commonly punctuated by decimeter- to meter-scale channel forms. The bases of the channel forms are scoured and contain coarse-grained sand or pebble to cobble gravel. The channel-form sediments are normally graded (the finest portion of the channel fill has the same grain size as the enclosing sand; Figure 11). Wavy-parallel bedding, planar-tabular bedding and high-angle cross-stratification are locally present. The high-angle cross-stratification is approximately 30° from horizontal and is approximately 0.5 to 2 meters high. Sand laminae, mudballs, mud drapes, convolute bedding, pebble stringers, silt laminae, and climbing ripples are locally present.

Cementation is rare, but consists of calcium carbonate cement where present. QTous is the most abundant lithofacies unit in the field area (Figure 5)



Figure 11: QTous

Massive, laminated and cross-stratified sands with gravel channel deposits. This south-facing outcrop shows both massive (A) and cross-bedded (B) sands with horizontal, scoured bounding surfaces (C). Soft-sediment deformation (D) at the base of the outcrop suggests possible liquefaction by a paleoearthquake. The notebook is approximately 19 centimeters long.

and can be distinguished by the dominance of fine- to medium-grained sand.

QToum

The unit is typically light to dark brown, friable silt and silty clay with local sandy silt. The unit is approximately 50% silt and 50% silty clay based on field observations. The clay and silt components are interbedded at the millimeter to decimeter scale. Where silt and silty clay are intimately interbedded, the bedding is horizontally laminated with local lens-shaped beds.

Silt and silty clay in QToum typically form decimeter- to meter-scale fining-upward sequences with sandy silt at the base grading upward to silty clay. Within fining-upward sequences, bedding is thin and the silt and silty clay are devoid of sedimentary structures (Figure 12). Centimeter- to decimeter-scale cross-stratification can be seen in the silt beds that are not with a part of the fining-upward sequences. The silty clay locally forms rippled drapes in silt layers. Mud rip-up clasts and sand laminae can be seen locally.

Bedding-parallel bands of discontinuous white micritic and horizontally elongate carbonate nodules are common in the silty clay beds. Where present, the carbonate nodule horizons occur several inches below the top of these silty clay beds. Cementation is rare, but consists of calcium carbonate where present.

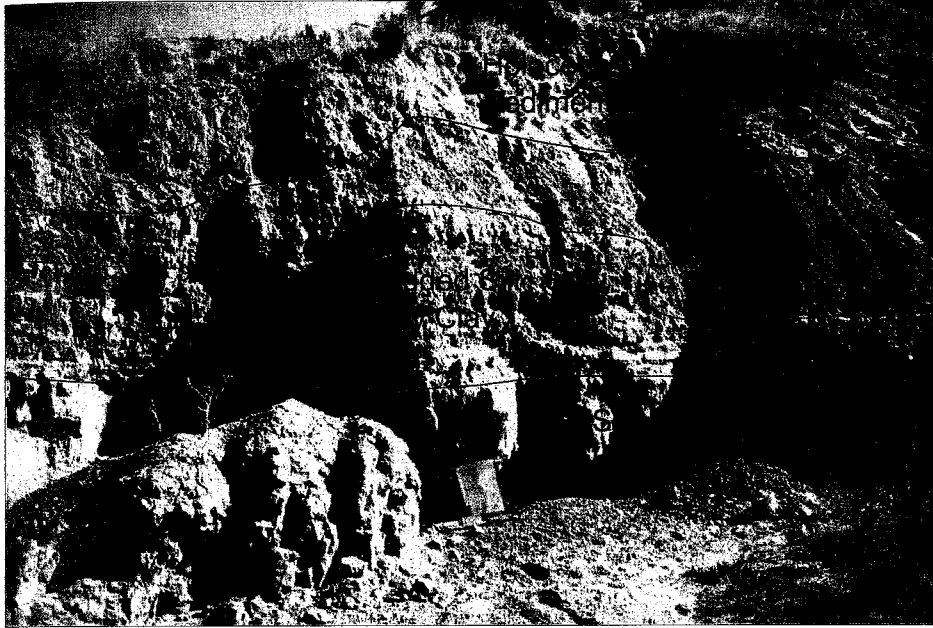


Figure 12: QToum

Interbedded silt and silty clay exposed on a southwest-facing slope.

The outcrop in this photograph shows a typical fining upward sequence within QToum. The base of this outcrop is mostly silt with fine sand. The middle section shows interbedded silt and silty clay beds. The sequence is capped by a dark brown silty clay. The map board is approximately 55 centimeters long.

Localized within some of the silty clay beds are reddish brown and greenish brown horizons. These horizons commonly occur at the top of the clay beds. The tops of the horizons have distinct boundaries whereas the lower boundaries are indistinct and gradational. The material within these colored horizons is identical to the surrounding material with the exception of the reddish and greenish colors. The characteristics of these horizons are consistent with paleosol horizons as described by Birkeland *et al.* (1991). The green hues are commonly found in a reducing environment such as standing, stagnant water and the red color is commonly found in an oxidizing environment such as a well drained environment.

QToum can be distinguished in the field by the dominance of fine-grained sediments. The unit has an overall darker look than the other units in the study area.

QToup

QToup is light brown to light yellow-brown, friable, fine- to medium-grained, poorly to moderately sorted sand with scattered matrix-supported pebbles. Based on field estimates and grain-size analysis, the unit contains <5% silt- and clay-sized particles, approximately 70% to 90% sand-sized grains and 5% to 25% pebble-sized clasts. The grain-size distribution is essentially

bimodal, with fine- to medium-grained sand as the dominant matrix material and matrix-supported pebbles as the secondary grain-size.

QToup beds range from 1 m to 37.5 m in thickness in the vicinity of the measured stratigraphic sections. The thick units do not show evidence of multiple episodes of deposition. QToup displays no internal structures of any kind; it is massive.

Cement is rare, but consists of calcium carbonate where present. Locally, there are light reddish brown horizons and white micritic carbonate horizons within the QToup unit. The tops of the horizons have distinct boundaries whereas the lower boundaries are indistinct and gradational. The material within these colored horizons is identical to the surrounding material with the exception of the reddish color or the addition of white micritic carbonate. The characteristics of these horizons are consistent with paleosol horizons described by Birkeland *et al.* (1991).

The white carbonate soil horizons are commonly Stage I but locally show Stage II development (stages defined by Gile *et al.*, 1966). I observed more paleosol horizons in QToup than any other lithofacies in the study area.

Vertically oriented micritic carbonate bodies and apparently randomly oriented micritic carbonate fragments are common in QToup (Figure 13). The carbonate bodies are cylindrical, and are typically 1.5 to 3 cm long and 1 to

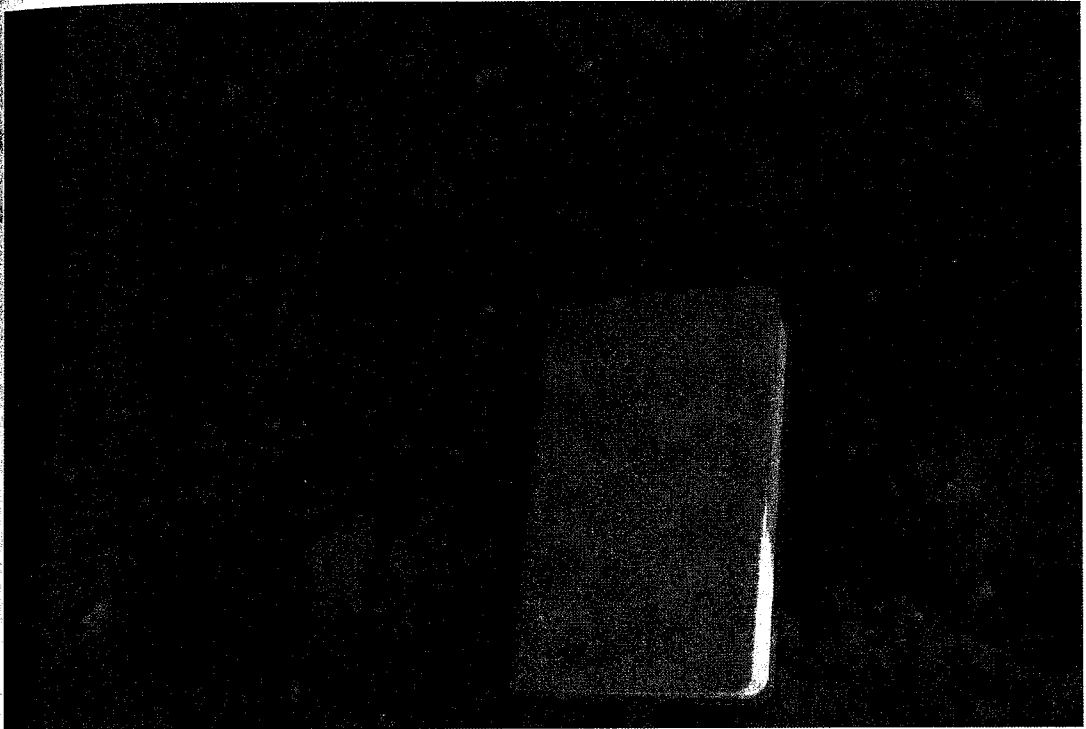


Figure 13: QToup

South-facing outcrop. This photograph shows the poorly sorted nature of QToup massive sand lithofacies. Note scattered pebble and reworked carbonate soil material. Notebook is approximately 19cm long.

1.5 cm in diameter. Neither of these carbonate features occurs in discrete horizons, but instead, they are apparently randomly scattered throughout the outcrops. The boundaries of the carbonate bodies are abrupt: the carbonate is not gradational with surrounding material.

The irregularly shaped, micritic carbonate fragments are commonly smaller than the vertically oriented carbonate bodies. The irregularly shaped micritic carbonate fragments display a variety of shapes and dimensions and are commonly subrounded to subangular. The boundaries of the carbonate fragments are abrupt. The irregular shapes and sizes and their subangular to subrounded shapes suggest that these carbonate fragments are clasts.

QToup can be distinguished in the field by its poorly sorted nature and the abundant vertically oriented carbonate bodies and scattered matrix-supported pebbles. This is the only unit with vertically oriented carbonate bodies.

QTouc

QTouc comprises light brown to yellow-brown, friable, fine- to medium-grained, moderately to well-sorted sand with apparently randomly oriented, micritic carbonate fragments. The micritic carbonate fragments are smaller than the micritic bodies in QToup but have similar physical properties. QTouc consists of approximately 75% sand, 15% clast-supported gravel and 10% silt and silty clay based on field estimates and grain-size analysis. Bedding ranges

from laminated to very thinly bedded. Fining-upward sequences are locally present. The sand is massive to locally cross-stratified with decimeter-scale trough cross-beds and scoured surfaces with decimeter- to meter-scale gravel channel deposits (Figure 14). Channel axes are sub-parallel to the Sand Hill fault (Figure 5; Plate I; Appendix A). In addition to these major characteristics, the unit locally displays planar-tabular and wavy parallel bedding, lens-shaped bedding, sand laminae, pebble stringers, mud balls and oversized clasts. Other structures are rarely seen, such as low-angle cross-stratification, convolute bedding and isolated irregular carbonate-cemented zones. Cement is rare, but consists of calcium carbonate where present. Paleosol horizons are not observed in the unit.

QTouc can be distinguished in the field by its fine- to medium-grained sand with apparently randomly oriented micritic carbonate fragments. This is the only unit other than QToup where these fragments occur, but QTouc lacks the vertically oriented carbonate bodies seen in QToup.

LITHOFACIES RELATIONSHIPS

Vertical Sequences

The stratigraphic sections (Figures 6 through 9), measured in the slightly more lithified southern portion of the study area, show the vertical relationships and stacking sequences of the map units and their subordinate lithofacies. They

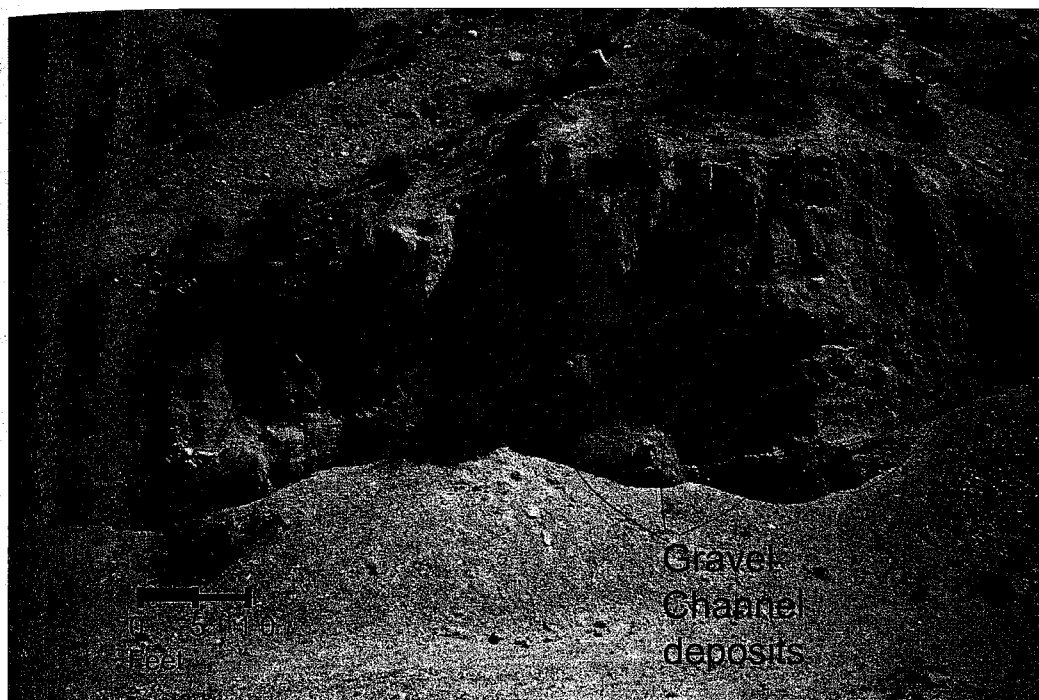


Figure 14: QTouc

This photograph shows QTouc overlain by QToup. Note the dark gray, gravel channel forms exposed on this south-facing slope. These channel forms are located near the Dead Deer Gulch stratigraphic measured section. The gravel channels are sub-parallel to the Sand Hill fault.

also show variations in unit thickness and stacking patterns along strike.

Measured Stratigraphic Section A-A'

Section A-A', at the Waterfall Site, begins at the Sand Hill fault and continues 65 meters up section, terminating at the top of the Llano de Albuquerque (Figure 6). The base of this section has 37.5 meters of QToup with isolated channel forms within lenses of QTouc. The QTouc lenses are discontinuous and no unconformity or erosional discontinuity was observed in the field. QTouc was measured directly above the QToup from 37.5 to 45.5 meters.

Even though QTouc is commonly found within QToup at a scale too small to document on the map or even the measured stratigraphic sections, the material within the normally graded channel forms shows evidence of reworked material from QToup as well as evidence of material imported from outside of QToup. Reworked QToup material, in the form of abundant apparently randomly oriented carbonate fragments, is evident within the channel form material. Conversely, the channel forms also have gravel lags at the base containing larger pebbles and cobbles than are found in the matrix-supported floating pebbles of QToup. This implies that the larger pebbles and cobbles were imported from outside of QToup.

This measured section is capped by 15 meters of QToug. This unit has rhythmically interbedded coarse sand and pebble and cobble gravel beds from

5.5 to 59 meters. The upper portion of QToug, from 59 to 65 meters, is dominated by clast-supported pebble and cobble gravel beds. No paleocurrent data were collected in this location.

Measured Stratigraphic Section B-B'

Section B-B', in the area North of Red Hill, begins at the Sand Hill fault and continues 36.5 meters up section, terminating at the top of the Llano de Albuquerque (Figure 7). The base of the section, from 0 to 8 meters, comprises QToup with isolated channels of QTouc. From 8 to 12 meters is a section of clast-supported pebble and cobble gravels. Cross-stratified sands of QTous with channels occupy the section from 12 to 14 meters. Interbedded silt and silty clay with local fine-grained sand and sandy silt beds are present from 14 to 24 meters. Even though there are local fine sand beds, there is volumetrically more silt and clay in this section, hence the classification of QToum. There is QTous from 24 to 27 meters. QToug caps the section, consisting of rhythmically interbedded coarse sands and clast-supported pebble and cobble gravel beds.

Even though much of the section is divided into different lithofacies map units, the section from 8 to 27 meters appears to consist of stacked fining-upward sequences including the lower gravel bed, QTous, and QToum. The fining-upward sequences range from 3 to 6 meters thick.

Paleocurrent data were collected in QTous and from isolated channels of QTouc within the QToup unit. Three paleocurrent orientations were measured in QTous, which yielded a mean paleocurrent orientation of northwest/southeast. Four paleocurrent orientations were measured from QTouc channels and they yielded a mean paleocurrent orientation of northwest/southwest (Figures 5 and 7; Appendix A).

Measured Stratigraphic Section C-C'

Section C-C', in the Dead Deer Gulch area, begins at the Sand Hill fault and continues 73 meters up section, terminating at the top of the Llano de Albuquerque (Figure 8). The base of this section has 25 meters of interbedded QToup and QTouc. The average QToup unit in this section is approximately 3 meters thick and the average QTouc unit is approximately 6 meters thick. Locally, QTouc consists of approximately 3 meter thick fining-upward sequences with sand at the base and silty clay at the top. There are also rhythmically bedded coarse- and fine-grained sand beds with scoured bases.

There are 20 meters of QTous above the QToup and QTouc sections. From 25 to 37 meters, QTous is primarily sand with very minor silt and gravel. From 37 to 45 meters, QTous has rhythmically interbedded sand and gravel beds with scoured bases. The average gravel bed is approximately 0.25 meters thick and the average sand bed is approximately 1 to 1.5 meters thick. QToum is

approximately 1.5 meters thick, from 45 to 46.5 meters, and appears to cap a fining-upward sequence beginning with the underlying QTous. Another section of QTous overlies QToum from 46.5 to 68 meters. This section of QTous comprises only medium- and coarse-grained sand. QToug is interbedded coarse sand and gravel in the upper 5 meters of the stratigraphic section, from 68 to 73 meters.

Paleocurrent data were collected in QTous and QTouc at this site. Eight paleocurrent orientations were measured in QTous, which yielded a mean paleocurrent orientation of northwest/southeast. Fourteen paleocurrent orientations were measured from QTouc channels and they yielded a mean paleocurrent orientation of northeast/southwest (Figures 5 and 8; Appendix A).

Measured Stratigraphic Section D-D'

Section D-D', in the South King Ranch area, begins at the Sand Hill fault and continues 52.5 meters up section, terminating at the top of the Llano de Albuquerque (Figure 9). QTouc dominates the base of this section, with medium-grained sand and minor gravel from 0 to 18 meters and again from 19 to 26.5 meters. From 18 to 19 meters and 26.5 to 29 meters there are 1 to 2.5 meter thick QToup beds. QTous is only found from 29 to 30.5 meters. QToum, dominated by silt, makes up the section from 30.5 to 44 meters. The top

of the section is again capped by rhythmically bedded coarse-grained sand and gravel of QToug from 44 to 52.5 meters.

Paleocurrent data were collected in QTous and QTouc at this site. One paleocurrent orientation was collected in QTous with a northwest/southeast flow orientation. Six paleocurrent orientations were collected from QTouc channels and they yielded a mean paleocurrent orientation of northwest/southeast (Figures 5 and 9; Appendix A).

Vertical Variation

The measured stratigraphic sections show that there is a great deal of variability in the thickness of the map units. QToug is approximately 1 to 17 meters in thickness. QTous is approximately 2 to 21 meters thick. QToum ranges in thickness from approximately 1.5 to 15 meters. QToup is approximately 1 to 37.5 meters thick. QTouc is less than 1 meter to 16 meters thick.

Some map units seem to remain in a consistent stratigraphic position and some units show variability in their stratigraphic position. QToug caps the stratigraphic sections throughout the study area. QToum and QTous occur in the middle portion of the stratigraphic sections, but have variability in their volumetric ratio to one another and in their stratigraphic position in relation to each other. QToup and QTouc are commonly interbedded (Figure 8, Section C, 0–25 m;

Figure 9, Section D, 0–29 m) and are exposed adjacent to the Sand Hill fault (Figure 5; Figure 6, Section A, 0–45 m; Figure 7, Section B, 0–8 m; Figure 8, Section C, 0–25 m; Figure 9, Section D, 0–29 m). The volumetric ratio of these two units and their stratigraphic position in relation to each other is variable.

Aerial Distribution

The relationships between the geologic units in the field area are fairly complex. Some of the map units are discontinuous (pinch out locally) in the general direction of the strike of the Sand Hill fault. In other places the units are buried by stratigraphically younger units.

The 1:8,000 scale lithofacies mapping was used to record the aerial distribution of the map units and the relationship of the map units to the Sand Hill fault. Because of scaling differences, the map units of Figure 5 commonly comprise assemblages of multiple lithologies presented in the measured stratigraphic sections.

QToug appears tabular because it caps all the stratigraphic sections in this study area, except where the younger stratigraphic units have been eroded. The unit is commonly only found on the hanging-wall block of the Sand Hill fault, but was deposited across the fault onto the footwall block at Red Hill.

The lower boundary of QToug is an unconformity, as described by Wright (1946) and Cather *et al.* (1997). Locally, a slight angular unconformity can be

seen in the field between the horizontal QToug and the gently dipping QTous below.

QTous is aurally the dominant map unit in the field area. The unit is pervasive in the central portion of the map area. However, QTous is locally discontinuous along strike where it is interrupted by lens-shaped bodies of QToum.

In the central and southern portions of the map area QToum forms small deposits within QTous. Because of its less tabular nature, QToum locally cuts across arroyos and ridge tops, as opposed to hugging specific stratigraphic elevations as many other units appear to. In this area QToum is discontinuous and lens-shaped in map view.

In the northern portion of the map area QToum is exposed adjacent to the Sand Hill fault at the base of the stratigraphic section. In the northern and central map area QToum extends for 0.9 to 1.75 kilometers parallel to the Sand Hill fault. This QToum deposit has QToup stratigraphically above it.

QTouc and QToup are exposed adjacent to the Sand Hill fault and are interbedded with one another. One exception is where a unit of QToum is sandwiched between the Sand Hill fault and QToup in the northern map area. In many cases, QTouc is not thick enough or laterally extensive enough to map separately from QToup on the geologic map or to break out on the measured

stratigraphic sections, and was therefore, commonly recorded as part of the volumetrically dominant QToup.

QTous and QTouc are very similar lithologically, and are distinguished by their position in the stratigraphic section, by association with QToup and by the presence or absence of micritic carbonate bodies and fragments. QTouc is found exclusively within QToup or exposed at the base of the stratigraphic section, directly adjacent to the Sand Hill fault. QTouc also has reworked carbonate fragments from QToup that are not found in QTous.

INTERPRETATIONS OF DEPOSITIONAL ENVIRONMENTS

QToug

There is not sufficient fine-grained material or fault-perpendicular paleocurrent data for QToug to have been deposited by debris flows originating from the Sand Hill fault. The sediments of QToug are also moderately to well-sorted and sediments from mass flow processes, such as debris flows would have a significant component of poorly sorted material (Nilsen, 1982; Boggs, 1995).

The abundance of trough cross-bedding and other sedimentary structures associated with dilute flow processes (Boggs, 1995) indicate that QTous was deposited by wind or water. The presence of channel forms further indicates deposition by water, such as fluvial processes. Some sedimentary structures

Such as mud balls are commonly found in fluvial sediments (Cant, 1982; Nilsen, 1982) in continental settings. Many of the sedimentary structures found in the unit, such as channel forms, are not associated with eolian deposition (Ahlbrandt and Fryberger, 1982).

The gravel channels record scour followed by waning flow and deposition of coarse bed loads. These types of channel deposits are typically found in fluvial (Miall, 1977; Cant, 1982; Collinson, 1996) or alluvial fan deposits (Nilsen, 1982; Collinson, 1996). The only local source for an alluvial fan would be the Sand Hill fault scarp but there is no evidence, such as a fan-shaped geometry or a change from coarse-grained proximal sediments to fine-grained distal sediments, to suggest an alluvial fan deposit originating from the scarp. There is no paleocurrent evidence suggesting fault-perpendicular flow directions as would be expected from an alluvial fan deposit (only flow sub-parallel to the fault scarp; Figures 5, and 7 through 9; Appendix A).

Miall (1977) presented four generic stratigraphic columns representing four end-members for sandy braided stream environments. These end-members are the Scott, Donjek, Platte and Bijou Creek types named after the fluvial systems they represent. When compared to the braided river end-members of Miall (1977), QToug falls in between the Scott and Platte types. It is non-cyclic, but rhythmic with grain sizes that fall between the two end-members. The rhythmic nature of QToug suggests high-energy event deposition of coarse-

grained sediments in a fluvial environment (Miall, 1977). The presence of multiple decimeter- to meter-scale gravel-channel forms with scoured bases, separated by predominantly trough cross-bedded sand suggests braided fluvial deposition of coarse-grained material based on descriptions by Miall (1977). Based on this information, QToug is interpreted as recording a braided fluvial environment dominated by high-energy event deposition of coarse-grained sediment.

QTous

As with QToug there is not sufficient fine-grained material or fault-perpendicular paleocurrent data for QTous to have been deposited by debris flows originating from the Sand Hill fault scarp. The sediments of QTous are also too well sorted to be debris flows. The gravel channel deposits, cross-stratification, and moderately sorted to well-sorted nature of the sediments, and the sedimentary structures, suggest deposition in a dilute flow environment instead.

The same arguments used to interpret QToug as a coarse-grained braided fluvial deposit, as opposed to alluvial fan deposits, can be used to interpret most of QTous as having a similar environment of deposition but with sandy material. When compared to the braided river end-members of Miall

(1977), QTous falls between the Donjek and Platte end-members. It has a weak cyclicity with a sand-dominated system punctuated by gravel channel fill.

Large-scale high-angle cross-stratification is commonly found in eolian deposits (Ahlbrandt and Fryberger, 1982; Boggs, 1995). The localized area with high-angle cross-stratification suggests that there could be a small component of eolian deposits in addition to the fluvial deposits within QTous. These sedimentary structures are inconclusive, but are suggestive. Cather *et al.* (1997) and Connell *et al.* (1999) documented eolian deposition adjacent to fluvial deposits in this portion of the Albuquerque Basin. Based on these sedimentary structures and arguments presented above, QTous is interpreted as recording a weakly cyclic braided fluvial environment with minor eolian deposition.

Some of the sedimentary structures seen in QTous suggest localized post-deposition deformation of the sediments. Convolute bedding within QTous likely represents subaqueous, post-depositional sediment slumping or folding. These sedimentary structures are usually due to differential overloading, oversteepening with rapid sediment accumulation on a slope or earthquake shocks (Boggs, 1995).

QToum

Numerous fining-upward sequences of sandy silt to silty clay, devoid of sedimentary structures, suggest deposition by water or turbidity currents (Boggs,

1995). However, isolated cross-stratification and ripples without additional elements of a Bouma sequence suggests deposition in dilute flow as opposed to turbidity currents. Laminated silt and clay are commonly found in overbank deposits (Miall, 1977).

Some of the characteristics found in QToum have been associated with pedogenic processes that occur in overbank deposition. Red and green soils have been interpreted as recording oxidation and reduction common in these environments (Birkeland *et al.*, 1991). Miall (1977) mentions pedogenic caliche nodules, like the ones in this unit, within silt and clay facies of braided rivers in some climates.

The fact that many of the QToum deposits are found vertically adjacent to QTous, which have been interpreted as braided fluvial deposits, strengthens the argument that QToum could be overbank floodplain and pond deposits. The larger deposit of QToum in the northern map section is adjacent to the Sand Hill fault. Because these sediments could be interpreted as pond deposits, it would seem possible that they could represent sag pond deposits where they are adjacent to the Sand Hill fault. Based on the data presented above, QToum is interpreted as recording deposition of fine-grained material in fluvial overbank deposits and possibly ponds. The likely origin of the ponds will be discussed in subsequent sections.

QToup

This lithofacies does not fit the typical profile of sediment deposited in a fluvial flow regime. The sediments are massive in nature with a conspicuous lack of any sedimentary features. QToup sediments are poorly to moderately sorted with a weak bimodal distribution. The primary grain size is found in the matrix and is fine- to medium-grained moderately to well-sorted sand. Secondary grain-size distribution comprises pebble-sized matrix-supported clasts.

Texturally, the matrix material fits the description of fine- to medium-grained eolian sands. Ahlbrandt and Fryberger (1982) describe inland dune sands as comprising fine- to medium-grained moderately to well-sorted sands. They also describe these sands as having laminations, crossbedding and a host of other sedimentary structures. Deflation surfaces are common within dune fields and have pebbles and coarse grained material that the wind is unable to transport. If the pebbles were representative of a deflation surface within an eolian dune field, however, then the pebbles would occur as stringers and not as individual matrix-supported clasts (Ahlbrandt and Fryberger, 1982; Boggs, 1995). The lack of sedimentary structures and the scattered distribution of the clasts within QToup precludes it as primary eolian deposition.

If the QToup sediments were deposited in a fluvial environment, however, the variable grain sizes should show some evidence of sediment layering or

sedimentary structures created with deposition by wind or water (Boggs, 1995). Locally massive pebbly sands were described by Browne and Plint (1994) as channel lags in a fluvial braidplain environment; however their deposits are no more than 4m thick, have sharp erosive bases and sharp boundaries at the top, and crude internal sedimentary structures. No sedimentary structures, layering of any kind, or erosive boundaries were observed in QToup. Therefore, it is unlikely that QToup represents primary sedimentation of material by fluvial deposition.

In addition to dilute flow, many sediment gravity flows commonly have sedimentary structures. Turbidity currents commonly display elements of a Bouma sequence. Liquefied flows have fluid escape structures, laminations, dish structures and other sedimentary structures (Boggs, 1995). Mud flows and muddy debris flows commonly have fine-grained matrices of silt and mud (Nilsen, 1982). QToup has no sedimentary structures and little to no silt or clay, which eliminates turbidity currents, liquefied flows, mud flows and muddy debris flows as likely depositional processes for the unit.

There are two types of sediment gravity flows that could create the moderately to poorly sorted, massive, sand-dominated sediment with pebble float seen in QToup. The first is a grain flow. Grain flows are commonly massive, poorly sorted, with no grading and have sand grain lineations with grains oriented parallel to transport (Boggs, 1995). In QToup the grains give no

vidence of flow direction. Commonly deposits of a single grain flow do not exceed approximately 5 cm in thickness (Lowe, 1976). Because QToup can be tens of meters thick locally, it is unlikely that this process is responsible for the local deposits of QToup observed.

Mud-free debris flows are debris flows that have a matrix composed predominantly of cohesionless sand and gravel (Boggs, 1995). These flows are poorly understood, but yield massive, poorly sorted sediments without significant silt or clay. These flows can continue to move over slopes as gentle as 1° or 2° , which implies they can deposit sediment over a fairly large area (Boggs, 1995). Even so, a debris flow commonly has some sedimentary structures within portions of the deposit (Boggs, 1995). QToup is devoid of sedimentary structures.

The poorly sorted material characterizing QToup could have been locally produced by classic colluvial deposition, where material is shed from a topographic high, such as a hillside or fault scarp, into a low area of accumulation below. These deposits are commonly poorly sorted and represent the types of material available from the source terrain (Nelson, 1992), in this instance, sand. One of the distinctive features of colluvium associated with normal faulting is that the colluvial sediment only occurs adjacent to the fault scarp on the hanging-wall block (Nelson, 1992). However, the thickness and lateral extent of the QToup unit prohibits its interpretation as a colluvial wedge unit. A typical colluvial wedge

s commonly not deposited very far from the fault scarp. An average single faulting event will produce a scarp less than 3 meters high and the colluvial process will produce a new scarp configuration with a slope from 25° to 40° (Nelson, 1992). Assuming a maximum scarp height of 3 meters and a 35° angle of sandy colluvium deposition, the maximum lateral extent of colluvial deposition would be a little more than 6 meter away from the fault scarp. In the study area QToup locally extends more than 700 meters from the fault scarp.

The carbonate bodies in QToup are distinctive because they are only found in the unit, but these are not interpreted as a primary feature of the deposit, but rather a secondary feature created after the sediment was in place. The consistent size and scattered, vertically oriented pattern is inconsistent with pedogenic carbonate formation. Carbonate soils, such as a K or Bk, commonly form in a horizon (Birkeland *et al.*, 1991). It is speculated that the carbonate bodies are trace fossils from burrowing insects because they are all approximately the same size and orientation, and do not form in horizons.

The only source for micritic carbonate clasts in the field area is carbonate soil horizons and the vertically oriented carbonate bodies. The irregular-shaped apparently randomly oriented micritic carbonate fragments are likely clasts from reworked carbonate material from the insect burrows described above, or from paleosol horizons.

Structureless sand with vertically oriented carbonate insect burrows suggests bioturbation. Bioturbation can have the effect of homogenizing any primary sedimentary structures (Collinson, 1996).

As stated previously, the fine- to medium-grained matrix material is very similar in texture to eolian sand. The original sedimentary structures within the eolian deposits could have been lost by reworking of the sands by burrowing creatures. The scattered, matrix-supported pebbles could be reworked by bioturbation from interdune deflation surfaces or interbedded stream deposits of QTouc.

Once the eolian sands were homogenized by bioturbation, any sandy fault-proximal colluvium would be very difficult to distinguish from the sandy eolian deposits. The boundary between the two depositional environments could easily be erased by bioturbation.

Based on the lack of sedimentary structures and abundant vertically oriented insect burrows in QTouc, I interpret most of this lithofacies as eolian sands that have been homogenized by bioturbation. In addition to bioturbated eolian sands, I suspect that the QTouc material adjacent to the fault could locally be colluvium shed from the scarp of the Sand Hill fault.

QTouc

The abundance of trough cross-bedding and other sedimentary structures associated with dilute flow processes (Boggs, 1995) suggests that QTouc was deposited by water or wind. The presence of multiple decimeter- to meter-scale gravel channel forms with scoured bases, separated by predominantly trough cross-bedded sand, suggests braided fluvial deposition.

The unit is almost identical to QTous, except for two things: (1) QTouc is only found exposed near the Sand Hill fault or within QToup and QTous is commonly found in the central portion of the stratigraphic section, and (2) QTouc has micritic carbonate fragments and QTous does not. The presence of apparently randomly oriented micritic carbonate fragments suggests that some of the material in these deposits could be reworked from QToup, as this is the only other lithofacies in the field area with an abundance of carbonate bodies and fragments. Another source for these carbonate fragments could be relict paleosols, which are also more abundant in QToup than in any other lithofacies in the field area. The size and physical properties of the carbonate fragments are consistent with formation as reworked carbonate bodies from QToup. For these carbonate fragments to be reworked soils, the soils would have to be Stage III or Stage IV carbonate soils (definitions of Giles *et al.*, 1966) to produce the observed fragments of micritic carbonate. Most of the soils observed in the study area, other than the Stage III under the Llano de Albuquerque, are only stage I

and II. Therefore, I interpret the carbonate fragments as reworked carbonate bodies.

The position of QTouc within QToup indicates that the two units were depositing simultaneously. The abundance of apparently randomly oriented micritic carbonate fragments suggests that some of the sediments in QTouc could be reworked QToup. The incorporation of pebbles from QTouc into QToup, as described above, strengthens this line of reasoning. I interpret QTouc as a braided fluvial environment, very similar to QTous. The differentiating factor is that QTouc was deposited within bioturbated eolian sands and colluvium of QToup. As QTouc was being deposited, it is likely that more QToup was being deposited and bioturbated simultaneously, which is how these two units became interbedded. QTouc is therefore, interpreted to have formed from streams flowing through the bioturbated eolian dune fields and colluvium of QToup.

GENETIC INTERPRETATIONS

Based on the interpretations of depositional environments presented above, inferences can be made about the genetic origins and basin-forming processes responsible for the sediments in the study area. The lithofacies in this field area fall into two categories: sediments that are exposed in the vicinity of the Sand Hill fault and those that are not. The sediments exposed near the Sand Hill fault consist of QToup and QTouc. Those that are not found in the vicinity of

The Sand Hill fault consist of QTous and QToug. It is possible that QToum has more than one depositional environment, and could have sediments that fall into both categories presented above.

Syntectonic Depositional Wedge Deposits

QToup and QTouc

Within this field area I interpret QToup and QTouc as possible STDW sediments. The STDW sediments, as described in the introduction, are those sediments that are preferentially deposited on the hanging-wall block of a fault as a result of the creation of a wedge-shaped space due to fault displacement.

QToup and QTouc are only exposed near the Sand Hill fault, and therefore, could represent STDW deposits similar to those seen elsewhere in the Albuquerque Basin. The Albuquerque Basin contains colluvial, eolian and fluvial STDW deposits. Machette (1978) recognized eolian deposition that was controlled by the fault scarp of the County Dump fault, with sediments deposited into the wedge-shaped space created by fault displacement. Connell *et al.* (1999) documented fault-parallel fluvial deposition in addition to fault-perpendicular colluvial deposition as part of a STDW north of this study area.

Even though QToup and QTouc seem to reasonably fit the description of STDW units seen elsewhere in the Albuquerque Basin, there is some ambiguity. Based on this study, it is unclear whether these units were only deposited near

the Sand Hill fault or if they are tabular units that dip below QTous and QToum. Because of this lack of information it is speculative to classify QToup and QTouc as STDW units, even though these types of sedimentary units are common in STDW environments within the Albuquerque Basin.

Regional Fluvial Sedimentation

Fluvial sediments of QToug, QTous, and part of QToum were part of the regional-scale deposition by rivers draining the western margin of the Albuquerque Basin (Connell *et al.*, 1999). The widespread fluvial deposits of the upper Santa Fe Group extend across the entire Albuquerque Basin (Figure 2) and are therefore, referred to as "regional fluvial deposits." These regional fluvial deposits have been interpreted by others as axial fluvial sediments within the Rio Grande rift (Machette 1978; Cather *et al.*, 1997; Connell *et al.*, 1999). I interpret the fluvial, overbank, and pond deposits of QTous, QToug and QToum as undifferentiated axial fluvial deposition.

The Arroyo Ojito Formation is a part of the regional fluvial sediments with south to southeast regional paleoflows in the Albuquerque Basin and Rio Grande rift. Connell *et al.* (1999) described these same sediments as axial fluvial sediments of the Sierra Ladrones, prior to the suggested nomenclature changes by Connell *et al.* (1999). My interpretation supports those made by Cather *et al.* (1997).

QToug

I interpret QToug as representing axial fluvial deposits in this area. The coarsening-upward sequence and the coarse-grained nature of these deposits in comparison to the underlying fluvial sediments of QTous suggest a change in one of the factors controlling particle/clast size.

Many workers have presented models suggesting mechanisms by which coarse-grained material prograde out into a basin. Some of these are listed below.

- A decrease in subsidence rates (Blair and Bilodeau, 1988; Paola *et al.*, 1992; Marr *et al.*, 2000)
- A change from high tectonic activity to relative tectonic quiescence (Blair and Bilodeau, 1988)
- A decrease in sediment flux (Marr *et al.*, 2000)
- A rapid increase in water flow (Marr *et al.*, 2000)

Marr *et al.* (2000) also found that an unconformity is typically produced during the progradation of gravel into the basin due to the decrease in subsidence rates or change in sediment flux, but not due to an increase in water flow. Based on these studies, the unconformity at the base of the unit and the coarsening upward of grain sizes from sand to gravel could be caused by a

duction of subsidence rates due to reduced tectonic activity or by an increase in coarse sediment input from the source terrain.

QTous

QTous represents channel deposits that are a part of the axial fluvial system in this area. Paleocurrent indicators confirm that QTous has paleoflow that matches that of the regional Santa Fe Group fluvial sediments. Locally the paleoflow orientation is sub-parallel to the strike of the Sand Hill fault.

QToum

QToum represents fine-grained material that is interpreted as overbank flood plains and ponds. Cather *et al.* (1997) interpret some of the fine-grained material in this area as recording deposition in ponds and overbank settings. Given the common association of QToum with QTous it is reasonable to interpret most of QToum as overbank floodplain and pond deposits that are part of the regional axial fluvial system.

In the northern map area a larger deposit of QToum is exposed adjacent to the Sand Hill fault. Due to the proximity to the Sand Hill fault, this deposit of QToum could fall within the STDW. This is the only occurrence of any unit except QToup or QTouc exposed adjacent to the Sand Hill fault in the field area. This indicates that, in this location, deposition of QToum may have been tectonically controlled.

Many workers have recognized the deposition of fine-grained material in small depressions or sag ponds adjacent to faults (Clark, 1983; Bowman and Gerson, 1986; Forman *et al.*, 1989; Salyards and Burciaga, 1994; Audemard *et al.*, 1999; Corcoran *et al.*, 1999). The fine-grained nature of the QToum sediments in this area is consistent with sag pond deposition. It is possible that the depocenter where the possible pond sediments were deposited was created in response to tectonic activity along the Sand Hill fault. This implies that the proximal portion QToum could be part of a STDW. However, even though it is possible that this area of QToum represents a sag pond, the data are inconclusive, and interpreting this area of QToum as a sag pond deposit is speculative at best.

Each of the map units discussed can be distinguished in the field by specific characteristics and the map units represent several environments of deposition. Table 3 summarizes the map units discussed and key features and the preferred interpretations of depositional environment for each map unit.

DISCUSSION

In the upper Arroyo Ojito Formation, axial fluvial sedimentation was synchronous with faulting and STDW deposition (Smyth and Connell, 1999; Figure 3). The Arroyo Ojito Formation was being deposited prior to fault displacement because it is in fault contact with the older Zia Formation. Because

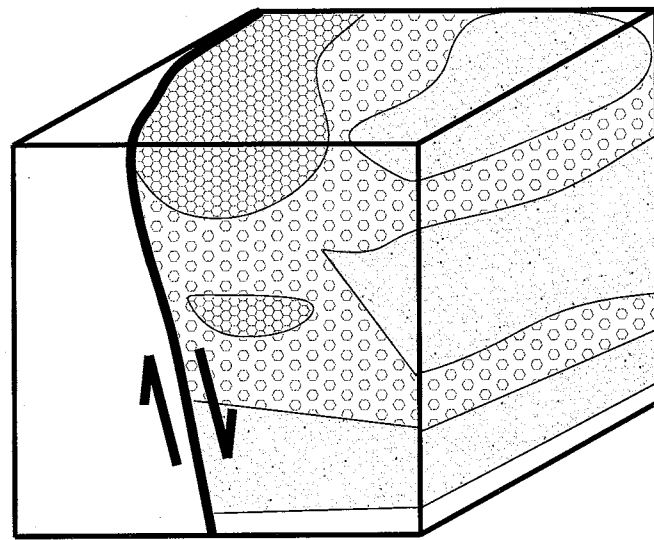
**Table 3:
Summary of Map Units and Lithofacies**

Map Unit	Distinguishing Features	Lithofacies	Environment of Deposition
Qc	Recent unconsolidated sediments that accumulate in swales, drainages, and other low-lying places (not studied).	Not studied.	Holocene colluvium and alluvium.
QTous	Massive laminated and cross-stratified sand with gravel channel deposits.	Fine-, medium-, and coarse-grained sand with minor silt, clay, and gravel.	Axial fluvial with minor eolian.
QToug	Coarsening-upward laminated and cross-stratified sand and gravel.	Coarse-grained sand and gravel.	Axial fluvial.
QToup	Massive bioturbated sand with scattered pebbles.	Bioturbated fine- to medium-grained sand with intermixed pebbles	STDW – bioturbated eolian sand with local colluvium derived from the Sand Hill fault.
QTouc	Cross-stratified sand with gravel channel deposits and reworked carbonate nodules.	Fine- to medium-grained sand with minor silt and gravel.	STDW – fluvial.
QToum	Interbedded silt and silty clay.	Silt and clay.	Axial fluvial overbank floodplains and ponds; STDW ponds.

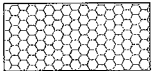
QTouc, the upper stratigraphic unit in the Arroyo Ojito Formation in the area, was deposited across the Sand Hill fault in at least one location (Plate I and Figure 5, just south of Section B) we know that the Arroyo Ojito Formation was still being deposited after fault displacement. If the Arroyo Ojito was being deposited before and after fault displacement then it is likely that any STDW sedimentation and regional fluvial sedimentation were synchronous.

At times when displacement produced a fault scarp along the Sand Hill fault, it would have created a local, wedge-shaped depression in which sediments could accumulate. This space was filled with STDW sediments in the form of colluvium and eolian sands that were subsequently mixed by bioturbation (QToup), fault-parallel fluvial deposits with reworked insect burrows from the eolian sands (QTouc), and possibly small pond deposits (QToum). Because (1) the STDW sedimentation occurred at the same time as the regional fluvial sedimentation, and (2) the Sand Hill fault experienced episodic motion, the STDW deposits and the regional fluvial deposits likely locally interfinger (Figure 15), even though no evidence of this was seen in the field due to poor exposure of this boundary.

QTouc may be a result of interfingering between the STDW and regional fluvial sedimentation. Paleocurrent indicators do not show a significant difference between the paleoflow orientations recorded in QTouc (STDW) and QTous (regional fluvial; Appendix A; Figures 5 through 9). QTous records north-



 QToup: STDW colluvial wedge lithofacies

 QTouc: STDW fluvial lithofacies

 QTous: Regional fluvial sand lithofacies

 Zia Formation


 Sand Hill fault: Arrows show direction of fault movement.

Figure 15: Schematic Interpretation of Lithofacies

Illustration of interfingering STDW and regional fluvial sediments. Such interfingering likely occurred because of episodic faulting. Regional fluvial sedimentation was coeval with locally derived STDW deposition along the fault.

northwest/south-southeast paleoflow orientations. QTouc records northwest-northeast/southeast to southwest paleoflow orientations. The extra variation in the QTouc paleocurrents is likely due to local variation in the trend of the Sand Hill fault. These paleocurrents roughly concur with Connell *et al.* (1999) for paleoflow of the Arroyo Ojito Formation (regional fluvial deposits). The Sand Hill fault is roughly sub-parallel to the regional paleoflow direction and therefore, any STDW fault-parallel fluvial deposits (QTouc) would also be sub-parallel to the regional fluvial paleoflow directions.

The wedge-shaped space created by movement on the Sand Hill fault was not large enough to control the regional fluvial deposition but likely became a preferred flow route for individual braided streams that were part of the regional axial fluvial system. These individual braided streams then reworked QToup material (and therefore, carbonate fragments) into stream deposits within that wedge-shaped space.

The lateral extent and thickness of STDW sediments along strike is variable. It is likely that the interaction of the STDW and the regional fluvial sediments caused differential erosion of the STDW sediments by the regional fluvial processes. If differential erosion of STDW sediments occurred it was probably before bioturbation of QToup because the carbonate bodies are not found intact or reworked in the QTous or QToug units.

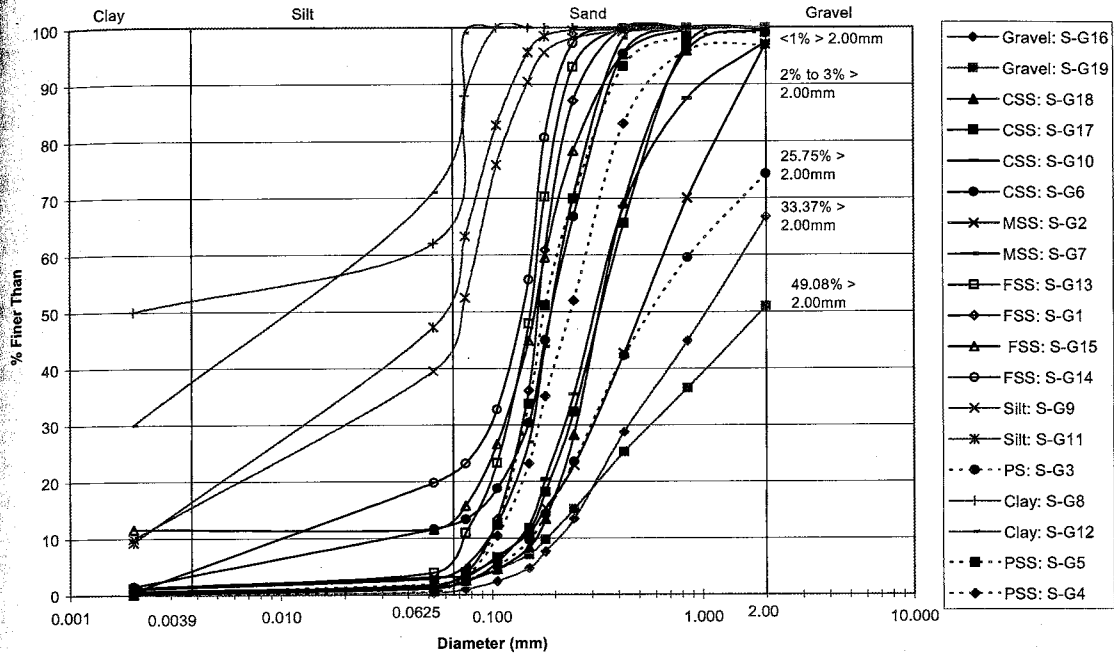
Based on the interpreted lithofacies, and speculative genetic and tectonic origin of the map units, unexposed geometries can be inferred for each map unit. Beds and units pinch out and grade into other facies both laterally and vertically, except for QToug, which is observed to be tabular and overlies all of the units in this area. At the map scale the deposits of QToum and QTous likely form discontinuous beds rather than tabular beds (Figure 5). In combination, the STDW units of QToup, QTouc and localized portions of QToum, likely form a wedge-shaped deposit with the thickest portion of the STDW forming adjacent to the fault and thinning away from the fault. Individually within the wedge-shaped space QTous and QToup units are likely discontinuous as they interfinger with each other.

HYDROLOGIC SIGNIFICANCE

GRAIN-SIZE ANALYSIS

The grain size data (Appendix B) were plotted with respect to (1) texture (Figure 16) and (2) the map units (Figure 17). There are some differences in the grain-size distribution of the individual lithofacies (Figure 16). The silt- and silty clay-dominated samples are approximately 50% clay and silt. The fine-grained sands are approximately 15% silt and clay. The medium-grained sands have less than 5% silt and clay and less than 5% gravel. The poorly sorted pebbly sand contains no silt or clay, but consists of approximately 75 to 98 % sand-sized material with 2 to 25% gravel-sized material. The coarse-grained sands contain 2 to 11% silt and clay, 89 to 95% sand, and less than 5% gravel. The gravels contain approximately 60% sand and 40% gravel (Figure 16; Appendix B).

When the data are arranged based on the map units, the same trend is seen. QToum stands out with high fines content, QToug stands out with high gravel and sand content and all other units (QTous, QToup, and QTouc) are composed primarily of sand (Figure 17). A summary of map units and their associated lithofacies, grain-size range and sorting is shown in Table 4.



CSS	MSS	FSS	PSS
Coarse-grained sand	Medium-grained sand	Fine-grained sand	Poorly-sorted, pebbly sand

Figure 16: Grain-size Analysis; Texture

Lithofacies are plotted with different symbols related to grain-size and sorting, as shown in the key. The X-axis is the log of the sieve opening size in millimeters, and the Y-axis is the percent of the sample finer than the various opening sizes.

The gravel and the silt and clay units display different grain-size distributions than the rest of the samples. The fine-grained sand displays slightly higher fines content than the other sands. The PSS unit has increased gravels over the rest of the sand-sized material. S-G8 and S-G12 are hydrometer samples; see Appendix B for additional details.

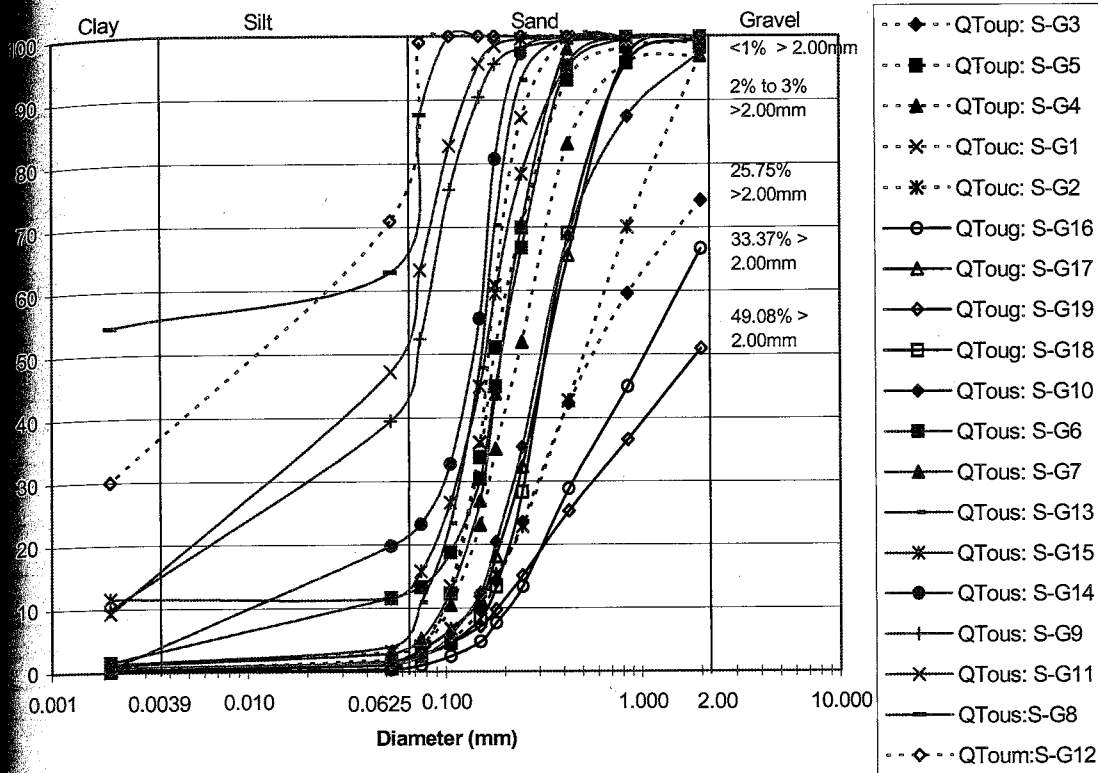


Figure 17: Grain-size Analysis; Lithofacies Map Units

Individual samples are identified by map unit. The X-axis is the log of the sieve opening size in millimeters, and the Y-axis is the percent of the sample finer than the various opening sizes. QToum and QToug have the most distinctive curves since they show a large amount of clay-sized particles and gravel-sized clasts respectively. QTous shows a wide range of grain sizes and sorting. S-G8 and S-G12 are hydrometer samples; see Appendix B for additional details.

**Table 4:
Grain Size and Sorting**

Map unit	Litho-facies	Sample number	Size of 80% of sample (in mm; subtract coarsest and finest 10%)	Grain size range	number of grain size categories	Sorting
@Toug	Gravel	S-G16	0.20-2.0+	Fine-grained sand to gravel	5	P-M*
	CSS	S-G17	0.14-0.72	Fine- to coarse-grained sand	3	M-W
	CSS	S-G18	0.18-0.70	Fine- to coarse-grained sand	3	M-W
	Gravel	S-G19	0.19-2.0+	Fine-grained sand to gravel	5	P-M*
@Tous	CSS	S-G6	0.03-0.40	Coarse silt to medium-grained sand	4	M
	MSS	S-G7	0.09-0.35	Very fine- to medium-grained sand	3	M-W
	Clay	S-G8	0.00025-0.075	Clay to coarse silt	5	P-M
	Silt	S-G9	0.002-0.16	Very fine silt to fine-grained sand	6	P
	CSS	S-G10	0.13-0.82	Fine- to coarse-grained sand	3	M-W
	Silt	S-G11	0.002-0.14	Very fine silt to fine-grained sand	6	P
	FSS	S-G13	0.075-0.12	Very fine-grained sand	1	VW
	FSS	S-G14	0.009-0.21	Fine silt to fine-grained sand	5	P-M
	FSS	S-G15	0.001-0.36	Clay to medium-grained sand	8	VP
QToum	Clay	S-G12	0.0014-0.014	Clay to medium silt	4	M
QToup	PSS	S-G3	0.15-2.0+	Fine-grained sand to gravel	5	P-M*
	PSS	S-G4	0.13-0.60	Fine- to coarse-grained sand	3	M-W
	PSS	S-G5	0.09-0.38	Very fine- to medium-grained sand	3	M-W
QTouc	FSS	S-G1	0.09-0.28	Very fine- to medium-grained sand	3	M-W
	MSS	S-G2	0.15-1.8	Fine- to very coarse-grained sand	4	M

Gravels were not subdivided into specific size categories, so this value represents the best possible sorting for the sample.

* See text for definitions of CSS, MSS, FSS, and PSS

Sorting	Number of Categories of Grain Sizes
Very well (VW)	0-1
Well (W)	1-3
Moderately (M)	3-5
Poorly (P)	5-7
Very Poorly (VP)	>7

The lithofacies categories are moderately to well-sorted fine-grained sand (FSS), moderately to well-sorted medium-grained sand (MSS), moderately to well-sorted coarse-grained sand (CSS) and poorly to moderately sorted fine- to medium-grained sand with pebbles (PSS). QToug contains poorly to moderately sorted gravel and moderately to well-sorted CSS. QTous consists of several sand-dominated lithologies with variable sorting, as well as minor amounts of silt and silty clay. The primary lithofacies associated with QTous is MSS, which is moderately to well-sorted predominantly medium-grained sand. Less prominent lithologies such as CSS, FSS, and silt and clay are moderately to well-sorted predominantly coarse-grained sand, poorly to moderately sorted predominantly fine-grained sand, and poorly sorted and poorly to moderately sorted silt and clay, respectively. QToum contains moderately sorted clay (silt from QToum was not analyzed). QToup contains moderately to well-sorted sand with local matrix-supported gravel which makes the overall unit locally poorly sorted. QTouc contains moderately to well-sorted FSS and MSS

Clear distinctions between each map unit cannot be made on the basis of grain size and sorting. The sand dominated map units QTouc, QToup and QTous cannot be distinguished on the basis of grain size (Figure 16; Appendix B). However, QToum, the silt and silty clay lithofacies, and QToug, the gravel and coarse sand lithofacies, both have distinctive grain-size distributions when compared to the sandy units.

When using grain size and sorting to estimate permeability, the more silt- and clay-sized material present in a sample, the lower the permeability should be, as the silt and clay fill in the pore spaces and consequently reduce permeability (Fetter, 1994). Based on the grain-size distribution and sorting, there should be at least three hydrogeologic units, gravel dominated (QToug), silt and clay dominated (QToum) and sand dominated (QTous, QTouc, and QToup). Of these three categories, the gravel dominated should have the highest permeability, the sand dominated should fall in the middle and the silt and silty clay dominated should have the lowest, according to Fetter (1994).

POROSITY

Porosity data were collected for four map units (Appendix C). Sand from QToug has the highest porosity with a mean of 32%; QTous is next with a mean of 26%, then QToup with a mean of 22%, and QTouc with a mean of 21% (Table 5; Figure 18). The porosity data indicate that the four measured map units fall into two groups on the basis of similar porosities. QToug and QTous make up the first group with median porosities of 32.65 and 27.34 respectively. QToup and QTouc make up the second group with median porosities of 19.59 and 17.089 respectively (Table 5). This is the only method of analysis that shows any real differences between any of the sand dominated units (Figure 18).

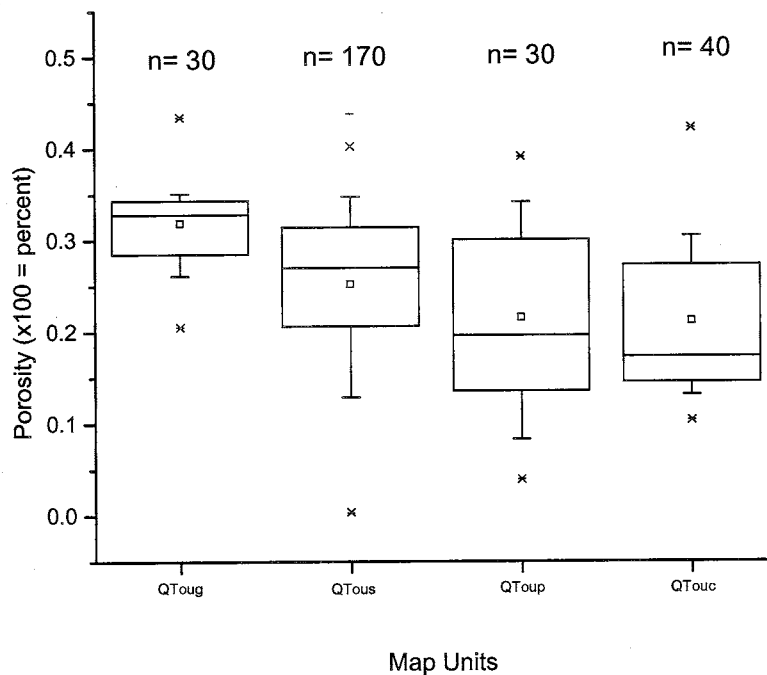
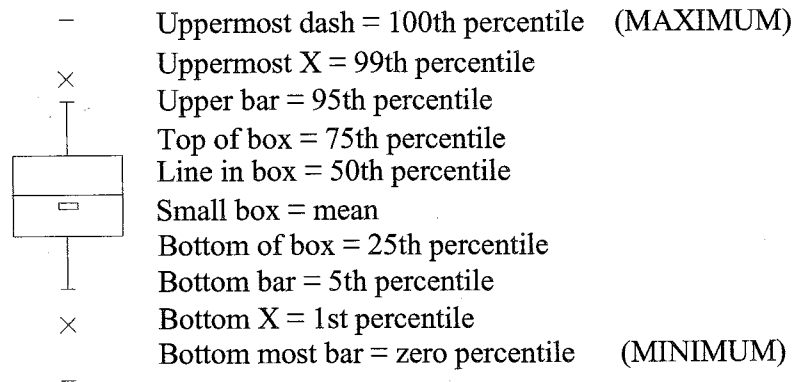
Legend

Figure 18: Statistical Analysis of Thin Section Porosity

Thin section porosity measurements grouped by map units (n = the number of measurements). The coarser-grained granular materials have higher porosities. The poorly-sorted, QToup has the lowest porosities.

<p align="center">Table 5:</p> <p align="center">Porosity of Map Units</p> <p align="center">(number of samples analyzed from each unit is indicated below)</p>				
	QToug (n = 40)	QTous (n = 170)	QToup (n = 30)	QTouc (n = 40)
Mean % ±Standard Deviation	31.86±4.95	25.81±8.45	21.54±10.28	21.15±8.06
Median %	32.65	27.34	19.59	17.09

IN-SITU PERMEABILITY MEASUREMENTS

The raw permeability data (Appendix E) have been grouped in two ways. The first grouping is based strictly on lithology as defined by grain size and sorting (Figure 19; Table 6). The lithofacies categories are moderately to well-sorted fine-grained sand (FSS), moderately to well-sorted fine- to medium-grained sand (FMSS), moderately to well-sorted medium-grained sand (MSS), moderately to well-sorted medium- to coarse-grained sand (MCSS), moderately to well-sorted coarse-grained sand (CSS) and poorly to moderately sorted fine-

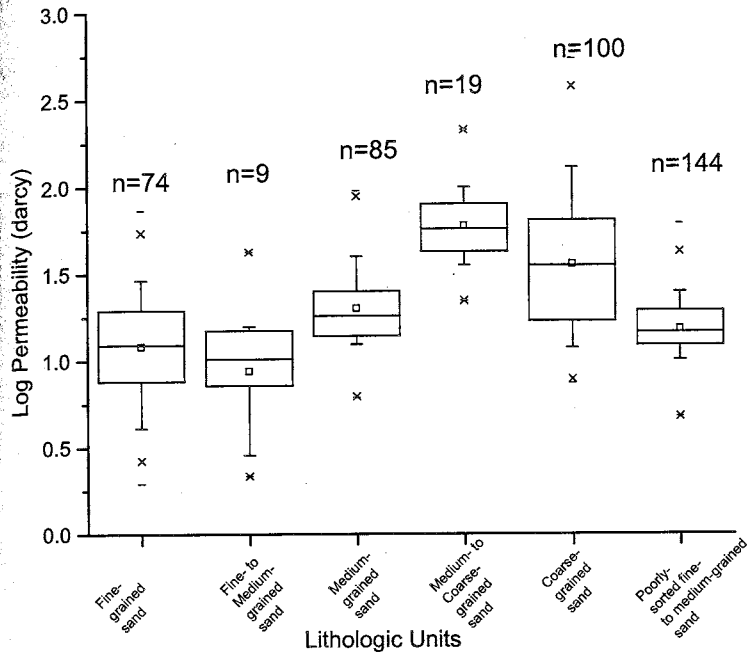


Figure 19: Air Minipermeability Box Plots; Lithologic Units

These data are grouped by grain size and sorting of sediments. All groups are moderately to well-sorted sand except for the poorly sorted sand. Note the distinctive differences in mean permeabilities for each textural category. See Figure 18 for the Legend to the box plots.

to medium-grained sand with pebbles (PSS). The mean and standard deviations for each of the categories are presented in Table 6.

	FSS	FMSS	MSS	MCSS	CSS	PSS
Mean ± Standard Deviation	1.08±0.32	0.94±0.41	1.25±0.17	1.78±0.23	1.68±0.39	1.14±0.17
Median	1.09	0.94	1.25	1.76	1.66	1.15

The second plot represents these same data grouped into the mappable lithofacies: QTous, QToup and QTouc (Table 7; Figure 20).

	QTous	QToup	QTouc
Mean ± Standard Deviation	1.32±0.40	1.18±0.16	1.42±0.38
Median	1.26	1.17	1.41

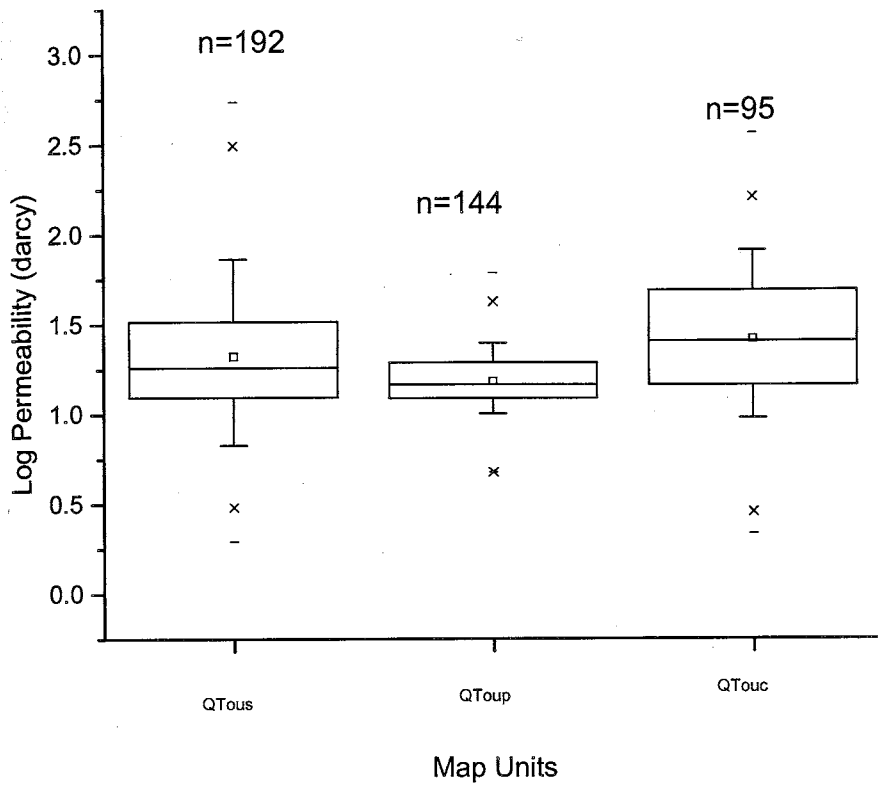


Figure 20: Air Minipermeability Box Plots; Map Units

These data show the range of permeabilities of the sandy map units (n equals the number of measurements in each unit). See Figure 18 for the Legend to the box plots.

The data for the lithologies as defined by texture (Figure 19) show that the fine sands have a lower permeability than the coarse sands, with medium sands falling in the middle. This fits the general notion that fine-grained sediments have lower permeability because the intergranular pore spaces are smaller (Fetter, 1994). The mean permeability of the poorly sorted sand facies is slightly greater than that of the fine sand, but lower than that of the better sorted medium- and coarse-grained sands. This general trend suggests that units of finer grain size have lower permeabilities than units of coarser grain size and when materials have a similar grain size, the material that is poorly sorted has a lower permeability.

Using these general observations regarding grain size and sorting, it can be inferred that the silt and silty clay unit should have lower permeabilities than the sand-sized material. The inability of the air-minipermeameter used in the study to measure the silt and silty clay unit, because the sediment permeabilities fall below the permeability range of the instrument (0.5–200 Darcies), confirms that the permeabilities for the silt and silty clay materials are lower than the sandy units. Even though the gravel unit could not be measured using the air minipermeameter, by following the trends in texture and sorting, it is likely that the gravel and coarse sand unit has the highest permeabilities in this area.

When the permeability data are grouped based on the mappable lithofacies units (QTous, QToup, and QTouc; Figure 20), which commonly consist of more than one grain-size lithofacies, the resulting map unit data sets have overlapping permeability ranges. QTous, QToup, and QTouc are virtually indistinguishable from one another by permeability, because they are all fine- to medium-grained sand. This indicates that the mappable units may only comprise three hydrogeologic units based on permeability: silt and clays (QToum), sand dominated (including QTous, QToup, and QTouc), and the gravel and coarse sand-dominated unit (QToug). Because these hydrogeologic units do not correspond to the map units, they have been given different designations for the hydrogeologic map (Figure 21): silt and silty clay is QTom, the undifferentiated sands are QTos and the gravel and coarse sand is QTog.

HYDROGEOLOGIC IMPLICATIONS

Of the three hydrogeologic units described above, the gravel unit (QTog) has the coarsest grain-size, highest porosity and likely the highest permeability and therefore, should be the best conduit for fluid flow. The sand units (QTos) should be the second best conduits for fluid flow based on grain size, porosity and permeability, regardless of depositional environment. The silt and silty clay unit (QTom) is the next lowest permeability unit and may act as a local barrier to fluid flow due to the fine grain-size, low porosity and low permeability. However,

Explanation

Adjacent Units: Not incorporated into this study

QC: Undifferentiated Quaternary colluvium and alluvium.

Tz: Zia Formation

Hydrogeologic Units

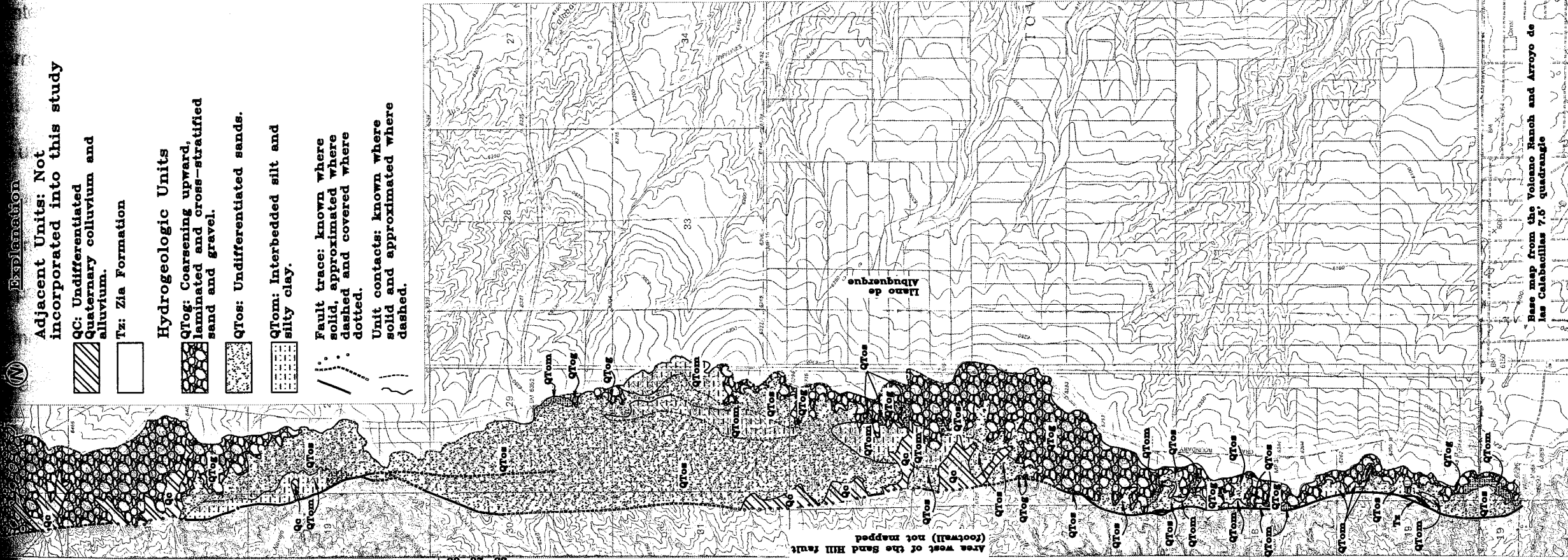
QTog: Coarsening upward, laminated and cross-stratified sand and gravel.

QTos: Undifferentiated sands.

QTom: Interbedded silt and silty clay.

Fault trace: known where solid, approximated where dashed and covered where dotted.

Unit contacts: known where solid and approximated where dashed.



the laterally discontinuous nature of the unit should prevent it from being an effective barrier to regional flow.

The inferred facies architecture of these units should also play a key role in the ability of the units to act as barriers or conduits to fluid flow due to lateral and vertical interconnectedness. The three dimensional geometries of the map units are inferred based on the interpreted environment of deposition of each unit. In the study area QToug is interpreted to be tabular, which would be very conducive to unrestricted fluid flow. However, in the study area, erosion has removed the unit everywhere except for the structurally highest exposures. The laterally discontinuous nature of QToum and QTous would make it more difficult to anticipate possible fluid pathways in these units. The low-permeability QToum sediments are elongate and lenticular sub-parallel to the fault zone. QToum may act as a local median in the groundwater highway, but the groundwater would not be impeded, merely locally diverted away from the QToum into the higher permeability sand and gravel rich units. QToup and QTouc collectively are interpreted as wedge-shaped, high-permeability sediments of a STDW adjacent to the fault zone, even though individually they are discontinuous in nature. Because the fault zone is a low permeability feature capable of impeding flow (Rawling *et al.*, 2001), the STDW sediments in this location would provide an alternative route for fluid flow.

Paleocurrent data for the STDW units and the regional fluvial units (Appendix A; Figure 5; Plate I) primarily show north–northwest to south–southeast paleoflow. Because the permeability anisotropy of the fluvial units is assumed to be parallel to the paleoflow direction, it is reasonable to assume that the preferential flow directions through this field area would be to the south–southeast.

The Sand Hill fault strikes roughly north–south, as would the interpreted high–permeability, wedge–shaped STDW sediments adjacent to the fault. Based on work by Rawling *et al.* (2001), the fault would act as a low–permeability barrier. The Sand Hill fault would likely retard cross–fault groundwater flow. The high permeability STDW sands (QToup and QTouc) would act as a preferential pathway for fluids parallel to the low–permeability fault zone. Although faulting reduced cross–fault fluid flow by creating a low–permeability barrier, it increased fault–parallel fluid flow by creating a high permeability wedge of STDW sediments. This would not always be the case, as the parent material for the STDW plays a large role in determining the permeability of the fault–parallel sediments. Had the STDW material been clay or silt rich, the STDW would have been much less permeable.

CONCLUSIONS

Sediments on the hanging-wall block of the Sand Hill fault were likely deposited in two main depositional environments with five mappable lithofacies units: coarsening upward, laminated and cross-stratified sands and gravels (QToug); massive, laminated and cross-stratified sands with gravel channel deposits (QTous); interbedded silt and silty clay (QToum); massive sands (QToup); and cross-stratified sands with gravel channel deposits (QTouc). QToug, QTous, and part of QToum represent channel deposits, overbank floodplain and pond deposits, and minor eolian deposits recording deposition in a regionally extensive fluvial system that developed in the axial portion of the Rio Grande rift. QToup, QTouc, and part of QToum are comprised of bioturbated colluvium, bioturbated eolian, a possible sag pond deposit, and fluvial deposits. Based on similarities of QToup, QTouc, and QToum to other STDW sediments in the Albuquerque Basin and their exposure adjacent to the Sand Hill fault these sediments may represent deposition in a STDW. If so, QToup, QTouc, and portions of QToum would be restricted to the proximity of the Sand Hill fault; this cannot be verified because the contact between the possible STDW and the regional fluvial sediments is not exposed in the study area.

The map units (lithofacies), QToug, QTous, QToum, QToup, and QTouc can be grouped into three hydrogeologic units in the study area. The hydrogeologic units are:

- QTog which is comprised of QToug,
- QTom, which is comprised of QToum, and
- QTos, which is comprised of QTous, QToup, and QTouc.

QToum and QToug each make up their own hydrogeologic unit. QToum, the finest-grained unit in the study area, has a mean permeability of less than 0.5 Darcy. Because QToug is coarse-grained and moderately to well-sorted, it is interpreted to have the highest permeability in the field area, even though this unit was not measurable with the instrument used in this study. Most important the sands in the hanging wall of the Sand Hill fault have similar permeabilities, which are all high, regardless of depositional environment: QTous has a mean permeability of approximately 1.32 Darcy; QToup has a mean permeability of 1.18 Darcy; and QTouc, has a mean permeability of 1.42 Darcy. For these sediments, the permeability corresponded to grain size and to a lesser extent sorting which is a function of the depositional environment. However, the depositional environment did not determine the hydrogeologic boundaries of the sediments. In short, this study has demonstrated that mapping based on depositional environments is not always the most accurate representation of

permeability characteristics; rather, lithofacies with similar grain-size distributions should have similar permeabilities.

Improved understanding of the relationship between sedimentology and permeability in poorly lithified sediments associated with normal faults will enhance fluid flow modeling of such systems. In many cases, it is not financially realistic to measure the permeabilities of every unit in an area the size of the Albuquerque Basin. My work will help researchers and consultants such as those in hydrology, water resources, environmental remediation, and the petroleum industry make informed decisions about how to use physical descriptions of the sediments on geologic maps to determine appropriate hydrogeologic units for flow models.

REFERENCES

- Ahlbrandt, T.S., and Fryberger, S.G., 1982, Introduction to Eolian Deposits, *in* Scholle, P.A., and Spearing, D., eds., Sandstone Depositional Environments: Tulsa, Oklahoma, American Association of Petroleum Geologists, p. 11-47.
- Amit, R., Harrison, J.B., and Enzel, Y., 1995, Use of soils and colluvial deposits in analyzing tectonic events; the southern Arava rift, Israel: *Geomorphology*, v. 12, p. 91-107.
- Anderson, T.W., Welder, G.E., Lesser, G., and Trujillo, A., 1988, Region 7, central alluvial basins, *in* Back, W., Rosenshein, J.S., and Seaber, P.R., eds., The Geology of North America, Hydrogeology: Boulder, Colorado, Geological Society of America, v. O-2, p. 81-86.
- Audemard, F., Costa, C., Okumura, K., Cowan, H., Diederix, H., Ferrer, C., Pantosti, D., and Machette, M., 1999, Trench investigation along the Mirida section of the Bocono fault (central Venezuelan Andes), Venezuela: *Tectonophysics*, v. 308, p. 1-21.
- Baldrige, W.S., Olsen, K.H., and Callender, J.F., 1984, Rio Grande rift: Problems and perspectives, *in* Baldrige, W.S., Dickerson, P.W., Rieker, R.E., and Zidek, J., eds., New Mexico Geological Society Guidebook, 35th Field Conference, Rio Grande rift: Northern New Mexico: New Mexico Geological Society, p. 1-12.
- Beckner, J.R., 1996, Cementation processes and sand petrography of the Zia Formation, Albuquerque Basin, New Mexico, [M.S. Thesis]: Socorro, NM, New Mexico Institute of Mining and Technology, 146 p.
- Beckner, J.R., and Mozley, P.S., 1998, Origin and spatial distribution of early phreatic and vadose calcite cements in the Zia Formation, Albuquerque Basin, New Mexico, USA, *in* Monrad, S., ed., Carbonate Cements in Sandstones: International Association of Sedimentologists Special Publication, v. 26, p. 27-51.

- Birkeland, P.W., Machette, M.N., and Haller, K.M., 1991, Soils as a tool for applied Quaternary geology: Utah Geological and Mineral Survey Miscellaneous Publication 91-3, 63 p.
- Blair, T.C., and Bilodeau, W.L., 1988, Development of tectonic cyclotherms in rift, pull-apart, and foreland basins: Sedimentary response to episodic tectonism: *Geology*, v. 16, p. 517-520.
- Boggs, S., 1995, *Principles of Sedimentology and Stratigraphy, Second Edition*: Englewood Cliffs, New Jersey, Prentice Hall, 774p.
- Bowman, D., and Gerson, R., 1986, Morphology of the latest Quaternary surface-faulting in the Gulf of Elat region, eastern Sinai: *Tectonophysics*, v. 128, p. 97-119.
- Browne, G.H., and Plint, A.G., 1994, Alternating braidplain and lacustrine deposition in a strike-slip setting: The Pennsylvanian Boss Pointe Formation of the Cumberland Basin, Maritime Canada: *Journal of Sedimentary Research*, v. B64, p. 40-59.
- Bryan, K., and McCann, F.T., 1937, The Ceja del Rio Puerco: A border feature of the Basin and Range Province in New Mexico: *Journal of Geology*, v. 45, p. 801-828.
- Caine, J.S., Evans, J.P., and Forster, C.B., 1996, Fault zone architecture and permeability structure: *Geology*, v. 24, p. 1025-1028.
- Cant, D.J., 1982, Fluvial Facies Models, in Scholle, P.A., and Spearing, D., eds., *Sandstone Depositional Environments*: Tulsa, Oklahoma, American Association of Petroleum Geologists, p. 115-138.
- Cather, S.M., 1997, Toward a hydrogeologic classification of map units in the Santa Fe Group, Rio Grande rift, New Mexico: *New Mexico Geology*, v. 19, p. 15-21.
- Cather, S.M., Connell, S.D., Heynekamp, M.R., and Goodwin, L.B., 1997, Geology and map of the Sky Village SE 7.5-minute quadrangle, Sandoval County, New Mexico: New Mexico Bureau of Mines and Mineral Resources Open-File report, DMG 9, 8 p.

- Chow, J., Angelier, J., Hua, J.J., Lee, J.C., and Sun, R., 2001, Paleoseismic event and active faulting; from ground penetrating radar and high-resolution seismic reflection profiles across the Chihshang fault, eastern Taiwan, *in* Lallemand, S.L., Liu, C., Angelier, J., and Tsai, Y.B., eds., *Active Subduction and Collision in Southeast Asia: Tectonophysics*, v. 33, p. 241–259.
- Clarke, A.O., 1983, Radiocarbon dating of a peat deposit in the Cucamonga fault zone, California: *Professional Geographer*, v. 35, p. 178–183.
- Collinson, J.D., 1996, Alluvial Sediments, *in* Reading, H.G., ed., *Sedimentary Environments: Processes Facies and Stratigraphy*: Oxford, England, Blackwell Science Ltd., p. 37–82.
- Compton, R.R., 1985, *Geology in the Field: United States*, John Wiley and Sons, Inc., 398 p.
- Connell, S.D., Koning, D.J., and Cather, S.M., 1999, Revisions to the stratigraphic nomenclature of the Santa Fe Group, northwestern Albuquerque Basin, New Mexico, *in* Pazzaglia, F.J., and Lucus, S.G., eds., *New Mexico Geological Society Guidebook, 50th Field Conference, Albuquerque Geology*: New Mexico Geological Society, p. 337–354.
- Corcoran, P.L., Mueller, W.U., and Padgham, W.A., 1999, Influence of Tectonism and climate on lithofacies distribution and sandstone and conglomerate composition in the Archean Beaulieu Rapids Formation, Northwest Territories, Canada: *Precambrian Research*, v. 94, p. 175–204.
- Davis, J.M., Lohman, R.C., Phillips, F.M., Wilson, J.L., and Love, D.W., 1993, Architecture of the Sierra Ladrones Formation, Central New Mexico: Depositional controls on the permeability correlation structure: *Geological Society of America Bulletin*, v. 105, p. 998–1007.
- Davis, J.M., Wilson, J.L., and Phillips, F.M., 1994, A portable air-minipermeameter for rapid in situ field measurements: *Ground Water*, v. 32, p. 258–266.
- Fetter, C.W., 1994, *Applied Hydrogeology*: New Jersey, Prentice Hall Incorporated, 691 p.

- Forman, S.L., Machette, M.N., Jackson, M.E., and Matt, P., 1989, An evolution of thermoluminescence dating of paleoearthquakes on the American Fork segment, Wasatch fault zone, Utah: *Journal of Geophysical Research*, v. 94, p. 1622–1630.
- Forman, S.L., Nelson, A.R., and McCalpin, J.P., 1991, Thermoluminescence dating of fault–scarp–derived colluvium; deciphering the timing of paleoearthquakes on the Weber segment of the Wasatch fault zone, north central Utah: *Journal of Geophysical Research*, v. 96, p. 595–605.
- Galusha, T., 1966, The Zia Sand Formation, new early to medial Miocene beds in New Mexico: *American Museum Novitates*, v. 2271, 12 p.
- Gile, L.H., Peterson, F.F., and Grossman, R.B., 1966, Morphological and genetic sequences of carbonate accumulation in desert soils: *Soil Science*, v. 101, p. 347–360.
- Haneberg, W.C., 1995, Steady–state groundwater flow across idealized faults: *Water Resources Research*, v. 31, p. 1815–1820.
- Hawley, J.W., ed., 1978, Guidebook to the Rio Grande rift in New Mexico and Colorado: New Mexico Bureau of Mines and Mineral Resources Circular 163, 241 p.
- Hawley, J.W., and Haase, C.S., 1992, Hydrogeologic framework of the northern Albuquerque Basin: New Mexico Bureau of Mines and Mineral Resources Open–File Report 387, 148 p.
- Hawley, J.W., Haase, C.S., and Lozinsky, R.P., 1995, An underground view of the Albuquerque Basin, *in* Ortega–Klett, C.T., ed., *The Water Future of the Albuquerque and the Middle Rio Grande Basin*: New Mexico Water Resources Research Institute, p. 27–55.
- Herrin, J.M., 2001, Characteristics of deformation bands in poorly lithified sand: Rio Grande rift, New Mexico [MS Thesis]: Socorro, New Mexico, New Mexico Institute of Mining and Technology, 44p.
- Heynekamp, M.R., Goodwin, L.B., and Mozley, P.S., and Haneberg, W.C., 1999, Controls on fault–zone architecture in poorly lithified sediments, Rio Grande Rift, New Mexico: Implications for fault–zone permeability and fluid flow, *in* Haneberg, W.C., Mozley, P.S., Moore, J.C., and Goodwin, L.B., eds., *Faults and Subsurface Fluid Flow in the Shallow Crust*: American Geophysical Union Monograph 113, p. 27–49.

- Hong, S., 1999, Anisotropic hydraulic conductivity of faulted poorly consolidated eolian sands: Bosque, New Mexico [M.S. Thesis]: Socorro, New Mexico, New Mexico Institute of Mining and Technology, 50 p.
- Kelly, V.C., 1977, Geology of the Albuquerque Basin, New Mexico: New Mexico Bureau of Mines and Mineral Resources Memoir 33, 59 p.
- Knipe, R.J., 1993, The influence of fault zone processes and diagenesis on fluid flow, in Hornbury, A.D., and Robinson, A.G., eds., Diagenesis and Basin Development: American Association of Petroleum Geologists, Studies in Geology no. 36, p. 135–148.
- Lowe, D.R., 1976, Subaqueous liquefied and fluidized sediment flows and their deposits: *Sedimentology*, v. 23, p. 285–308.
- Lozinsky, R.P., 1994, Cenozoic stratigraphy, sandstone petrology and depositional history of the Albuquerque Basin, central New Mexico; in Keller, G.R., and Cather, S.M., eds., Basins of the Rio Grande Rift: Structure Stratigraphy and Tectonic Setting: Geological Society of America, Special Paper 291, p. 73–82.
- Lozinsky, R.P., and Tedford, R.H., 1991, Geology and paleontology of the Santa Fe Group, southwestern Albuquerque Basin, Valencia County, New Mexico: New Mexico Bureau of Mines and Mineral Resources, Bulletin 132, 35 p.
- Machette, M.N., 1978, Dating Quaternary faults in the southwestern United States by using buried calcic paleosols: *Journal of Research, U.S. Geological Survey*, v. 6, p. 369–381.
- Machette, M.N., 1978b, Geologic map of the San Acacia quadrangle, Socorro County, New Mexico: US Geological Survey, Geologic quadrangle Map GQ-1415, scale 1:24,000.
- Marr, J.G., Swenson, J.B., Paola, C., and Voller, V.R., 2000, A two-diffusion model of fluvial stratigraphy in closed depositional basins: *Basin Research*, v. 12, p. 381–398.
- Masch, F.E., and Denny, K.J., 1966, Grain size distribution and its effect on the permeability of unconsolidated sands: *Water Resources Research*, v. 2, p. 665–677.

- McCalpin, J.P., 2000, The Wasatch fault megatrench of 1999, evidence for temporal clustering of post-Bonneville paleoearthquakes [abstract]: Geological Society of America, Abstracts with Programs, v. 32, p. A-16.
- McCalpin, J.P., and Nelson C.V., 2000, Long Recurrence intervals from the Wasatch fault zone, Utah: Reston, Virginia, United States Geological Survey, 60 p.
- Miall, A.D., 1977, A review of braided river depositional environment: Earth Science Reviews, v. 13, p. 1-62.
- Mifflin, M.D., 1988, Region 5, Great Basin, *in* Back, W, Rosenheim, J.S., and Seaber, P.R., eds., The Geology of North America, Hydrogeology: Boulder Colorado, Geological Society of America, v. 0-2, p 69-78.
- Morey, D.M., 1998, Seismic CAT scan of an ancient earthquake along the Oquirrh fault, Utah [Master's Thesis]: University of Utah, Salt Lake City, Utah, 72 p.
- Mozley, P.S., and Davis, J.M., 1996, Relationship between oriented calcite concretions and permeability correlation structure in an alluvial aquifer, Sierra Ladrones Formation, New Mexico: Journal of Sedimentary Research, v. 66, p. 11-16.
- Mozley, P.S., and Goodwin, L.B., 1995, Patterns of cementation along a Cenozoic normal fault: A record of paleoflow orientations: Geology, v. 23, p. 6771-6780.
- Nelson, A.R., 1992, Lithofacies analysis of colluvial sediments - an aid in interpreting the recent history of Quaternary normal faults in the Basin and Range Province, Western United States: Journal of Sedimentary Petrology, v. 62, p. 607-621.
- Nelson, A.R., Personius, S.F., Rimando, R.E., Punongbayan, R.S., Tungol, N., Mirabueno, H., and Rasdas, A., 2000, Multiple large earthquakes in the past 1500 years on a fault in metropolitan Manila, the Philippines: Bulletin of the Seismological Society of America, v. 90, p. 73-85.
- Nilsen, T.H., 1982, Eolian Deposits, *in* Scholle, P.A., and Spearing, D., eds., Sandstone Depositional Environments: Tulsa, Oklahoma, American Association of Petroleum Geologists, p. 49-86.

- Paola, C., Heller, P.L., and Angevine, C.L., 1992, The large-scale dynamics of grain-size variation in alluvial basins, 1: Theory: *Basin Research*, v. 4, p. 73-90.
- Rawling, G.C., Goodwin, L.B., and Wilson, J.L., 2001, Internal Architecture, permeability structure, and hydrologic significance of contrasting fault-zone types: *Geology*, v. 29, 43-46.
- Reading, H.G., and Levell, B.K., 1996, Controls on the sedimentary rock record, *in* Reading, H.G., ed., *Sedimentary Environments: Processes Facies and Stratigraphy*: Oxford, England, Blackwell Science Ltd., p. 37-82.
- Rubin, C.M., Thompson, S., Abdrakhmatov, K., and Weldon, R., 1999, Thrust fault paleoseismology in an intercontinental tectonic setting, Kyrgyz Tien Shan, Central Asia [abstract]: *Geological Society of America, Abstract with Programs*, v. 31, p. 376.
- Salyards, S.L., and Burciaga, A., 1994, Styles of distributed deformation across a sag pond, San Andreas fault, San Mateo County, California [Abstract]: *Geological Society of America, Abstracts with Programs*, v. 26, p. 87.
- Sigda, J.M., Goodwin, L.B., and Mozley, P.S., and Wilson, J.L., 1999, Permeability alteration in small-displacement faults in poorly consolidated sediments: Rio Grande rift, New Mexico, *in* Haneberg, W.C., Mozley, P.S., Moore, J.C., and Goodwin, L.B., eds., *Faults and Subsurface Fluid Flow in the Shallow Crust: American Geophysical Union Monograph 113*, p. 51-68.
- Sigda, J.M., 1995, Examining the impacts of faults on aquifer flow systems: Implications for regional groundwater flow modeling [abstract], *in* *The Water Future of Albuquerque and Middle Rio Grande Basin (Proceedings of the 39th Annual New Mexico Water Conference, Albuquerque, New Mexico, November 3-4, 1994)*: New Mexico Water Resources Research Institute Report n. 290, p. 237-244.
- Smith, J.A., and Kuhle, A.J., 1998, Hydrostratigraphic implications of new geologic mapping in the Santo Domingo Basin, New Mexico: *New Mexico Geology*, v. 20, p. 21-27.

Smyth, D.G., and Connell, S., 1999, Hydrogeology of the upper Santa Fe Group, adjacent to the Sand Hill fault, Albuquerque Basin, New Mexico [Abstract]: *New Mexico Geology*, v. 21, p. 40.

Tedford, R.H., 1982, Neogene stratigraphy of the northwestern Albuquerque Basin: *New Mexico Geological Society Guidebook 33*, p. 271–278.

Walters, M., 1997, Stereopro: Stereographic projections: MWsoftware, version 1.00.

Wright, H.E., 1946, Tertiary and Quaternary geology of the lower Rio Puerco area, New Mexico: *Geological Society of America Bulletin*, v. 57, p. 383–456.

APPENDIX A: PALEOCURRENT DATA

All paleocurrent data come from the measurement of gravel channel orientations along the measured sections (Figures 6 through 9).

105
Appendix A:
Paleocurrent Data

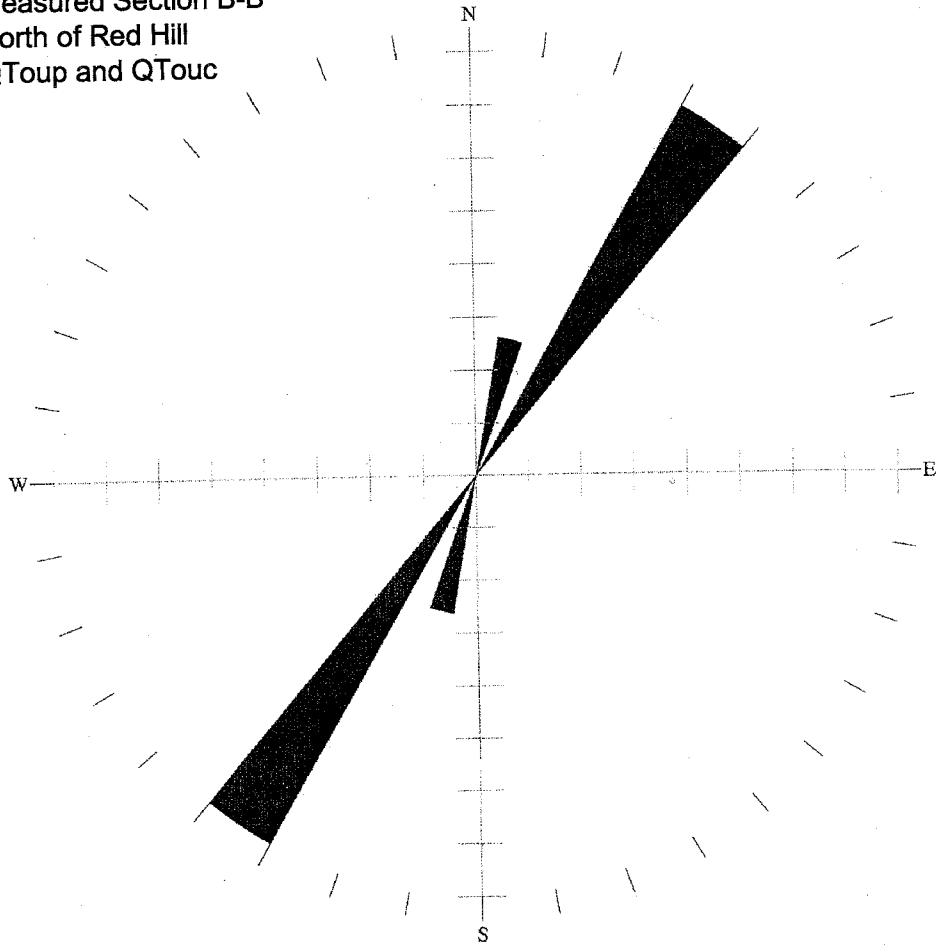
Measured Section B - B': North of Red Hill
QToup and QTouc

Data Point	Azimuth in Degrees	Type of Indicator
B1	210	Channel Orientation
B2	30	Channel Orientation
B3	190	Channel Orientation
B4	215	Channel Orientation

Mean \pm Standard deviation 206 \pm 11

106
Appendix A:
Paleocurrent Data

Measured Section B-B'
North of Red Hill
QToup and QTouc



Key

Rose Diagram Bi-Directional
Total Number of Points = 4
Bucket Size = 10 degrees

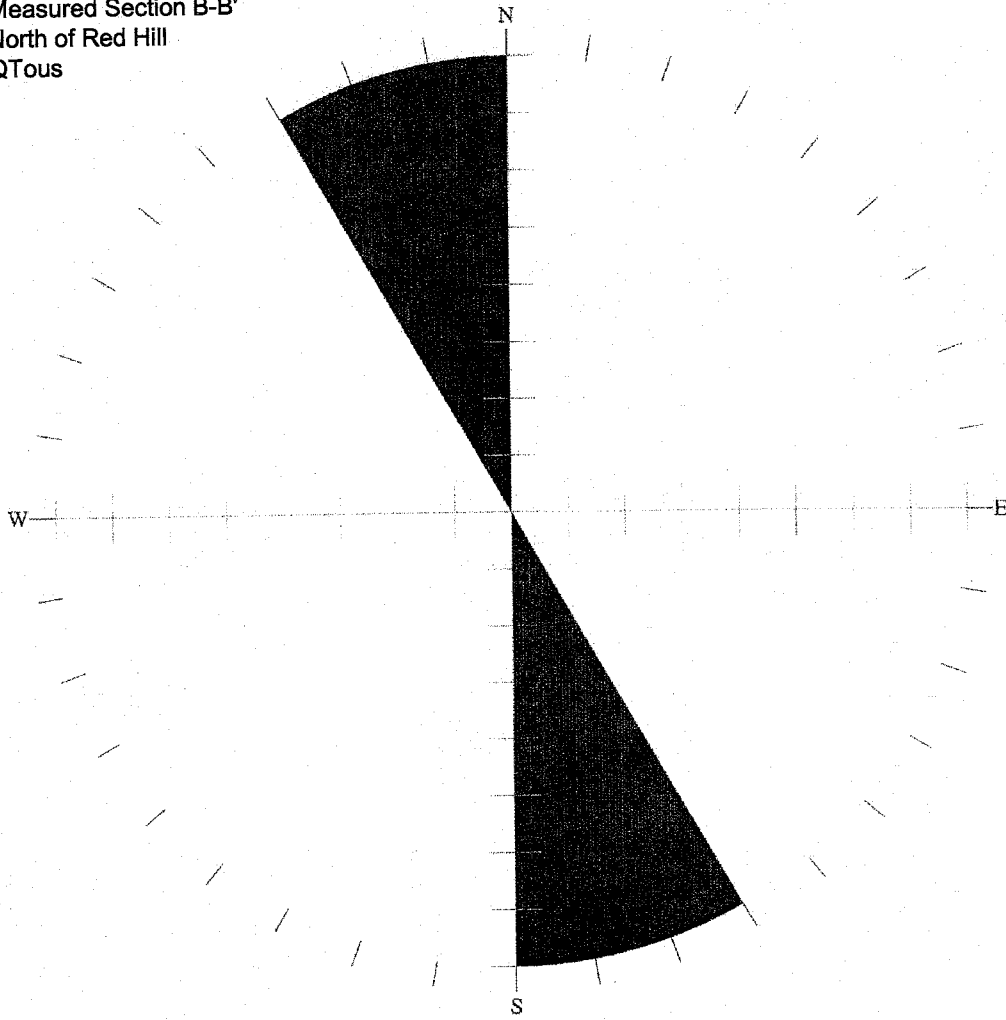
107
Appendix A:
Paleocurrent Data

Measured Section B - B': North of Red Hill
QTous

Data Point	Azimuth in Degrees	Type of Indicator
B5	345	Channel Orientation
B6	335	Channel Orientation
B7	355	Channel Orientation
Mean ± Standard deviation	345 ± 10	

108
Appendix A:
Paleocurrent Data

Measured Section B-B'
North of Red Hill
QTous



Key

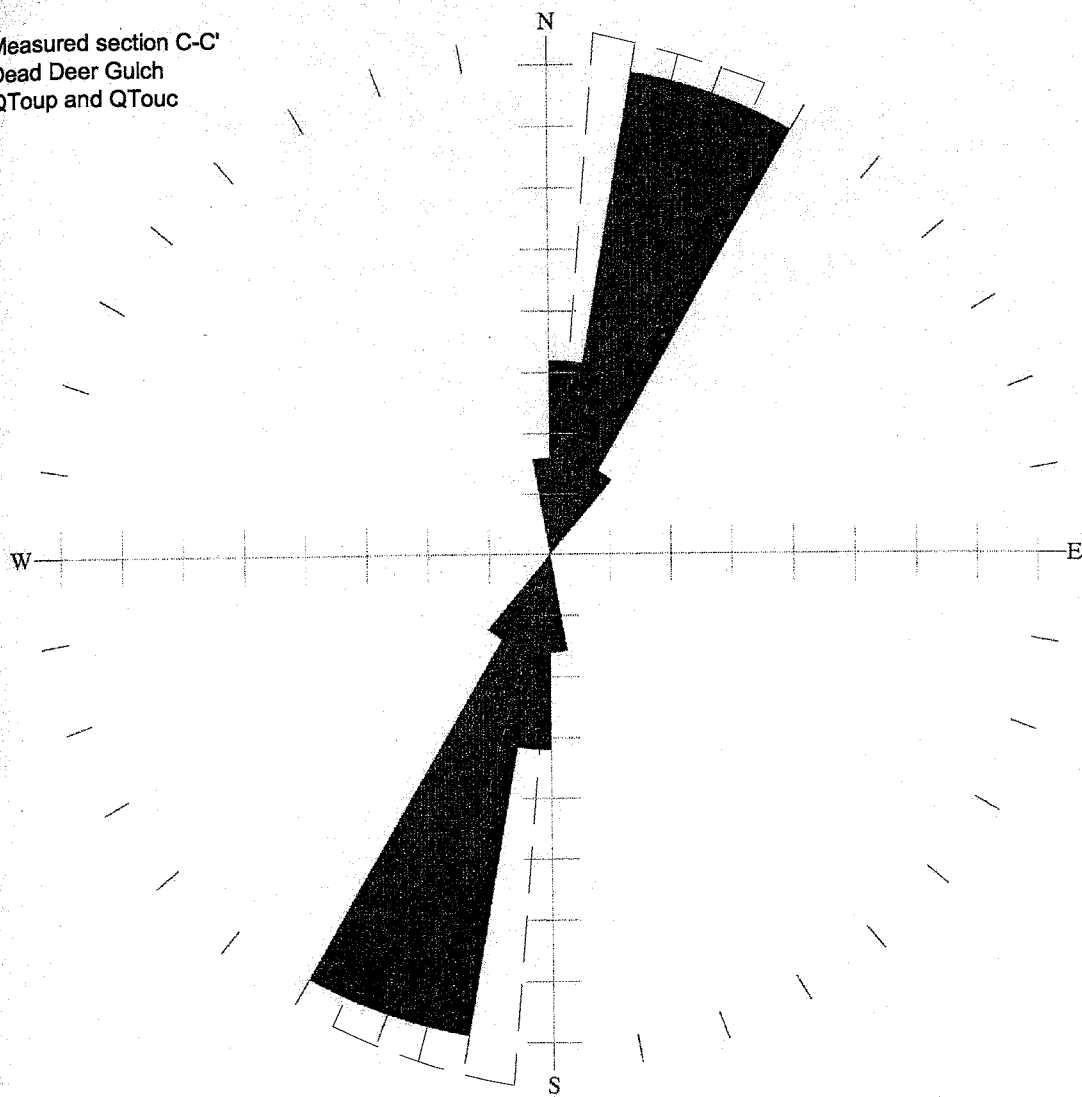
Rose Diagram Bi-Directional
Total Number of Points = 3
Bucket Size = 10 degrees

109
Appendix A:
Paleocurrent Data

Measured Section C - C': Dead Deer Gulch
QToup and QTouc

Data Point	Azimuth in Degrees	Type of Indicator
C1	25	Channel Orientation
C2	20	Channel Orientation
C3	25	Channel Orientation
C4	25	Channel Orientation
C5	30	Channel Orientation
C6	10	Channel Orientation
C7	10	Channel Orientation
C8	355	Channel Orientation
C9	15	Channel Orientation
C10	0	Channel Orientation
C11	5	Channel Orientation
C12	10	Channel Orientation
C13	15	Channel Orientation
C14	20	Channel Orientation
Mean \pm Standard deviation		15 \pm 10

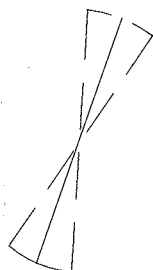
Measured section C-C'
Dead Deer Gulch
QToup and QTouc



Mean \pm standard deviation = $15^{\circ} \pm 10^{\circ}$

Key

Rose Diagram Bi-Directional
Total Number of Points = 14
Bucket Size = 10 degrees



Mean = solid line
Standard deviation = dashed lines

111
Appendix A:
Paleocurrent Data

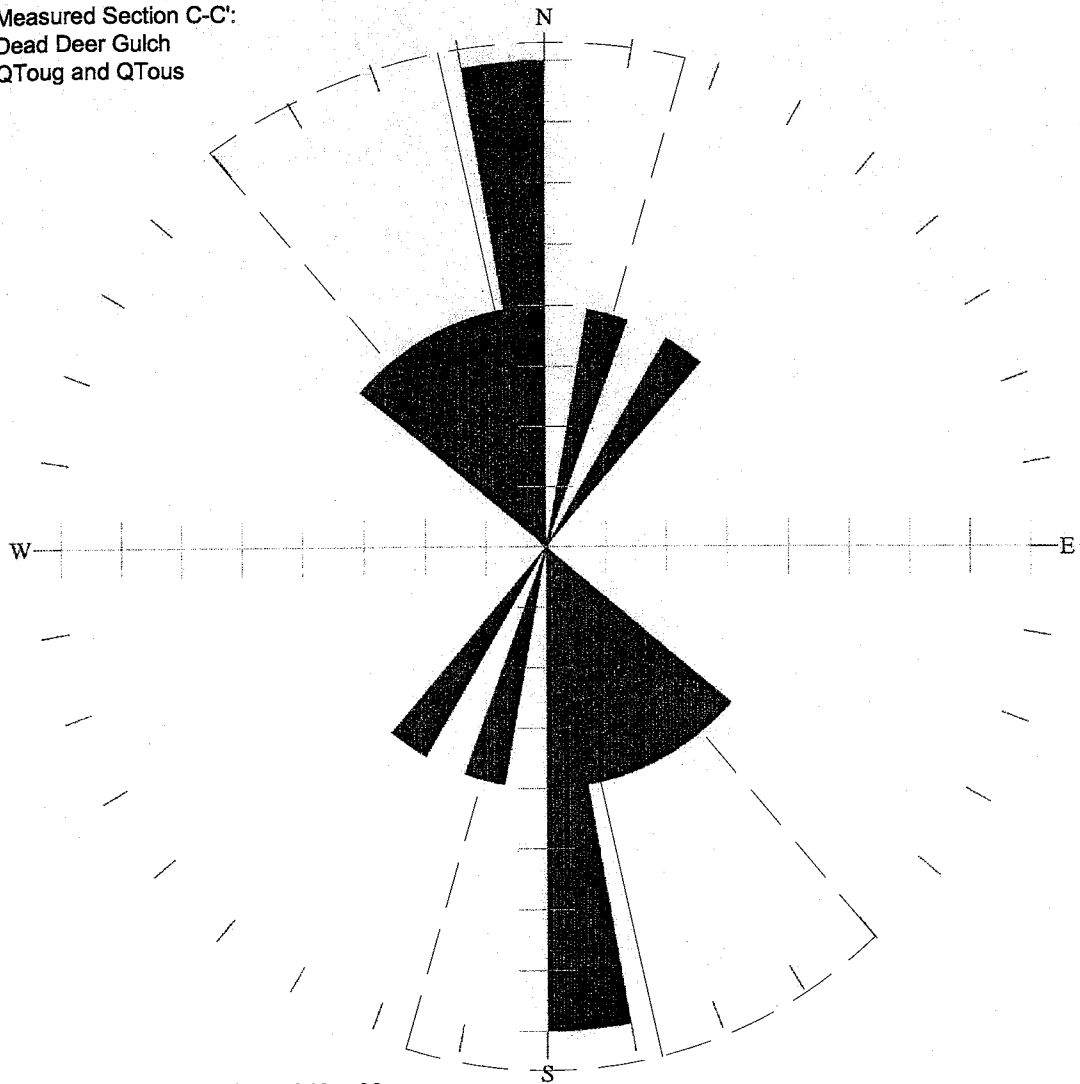
Measured Section C - C': Dead Deer Gulch
QToug and QTous

Data Point	Azimuth in Degrees	Type of Indicator
C15	323	Channel Orientation
C16	330	Channel Orientation
C17	345	Channel Orientation
C18	310	Channel Orientation
C19	350	Channel Orientation
C20	15	Channel Orientation
C21	355	Channel Orientation
C22	36	Channel Orientation

Mean \pm Standard deviation 348 \pm 28

112
Appendix A:
Paleocurrent Data

Measured Section C-C':
Dead Deer Gulch
QToug and QTous



Mean \pm standard deviation = 348 \pm 28

Key

Rose Diagram Bi-Directional
Total Number of Points = 8
Bucket Size = 10 degrees



Mean = solid line
Standard deviation = dashed lines

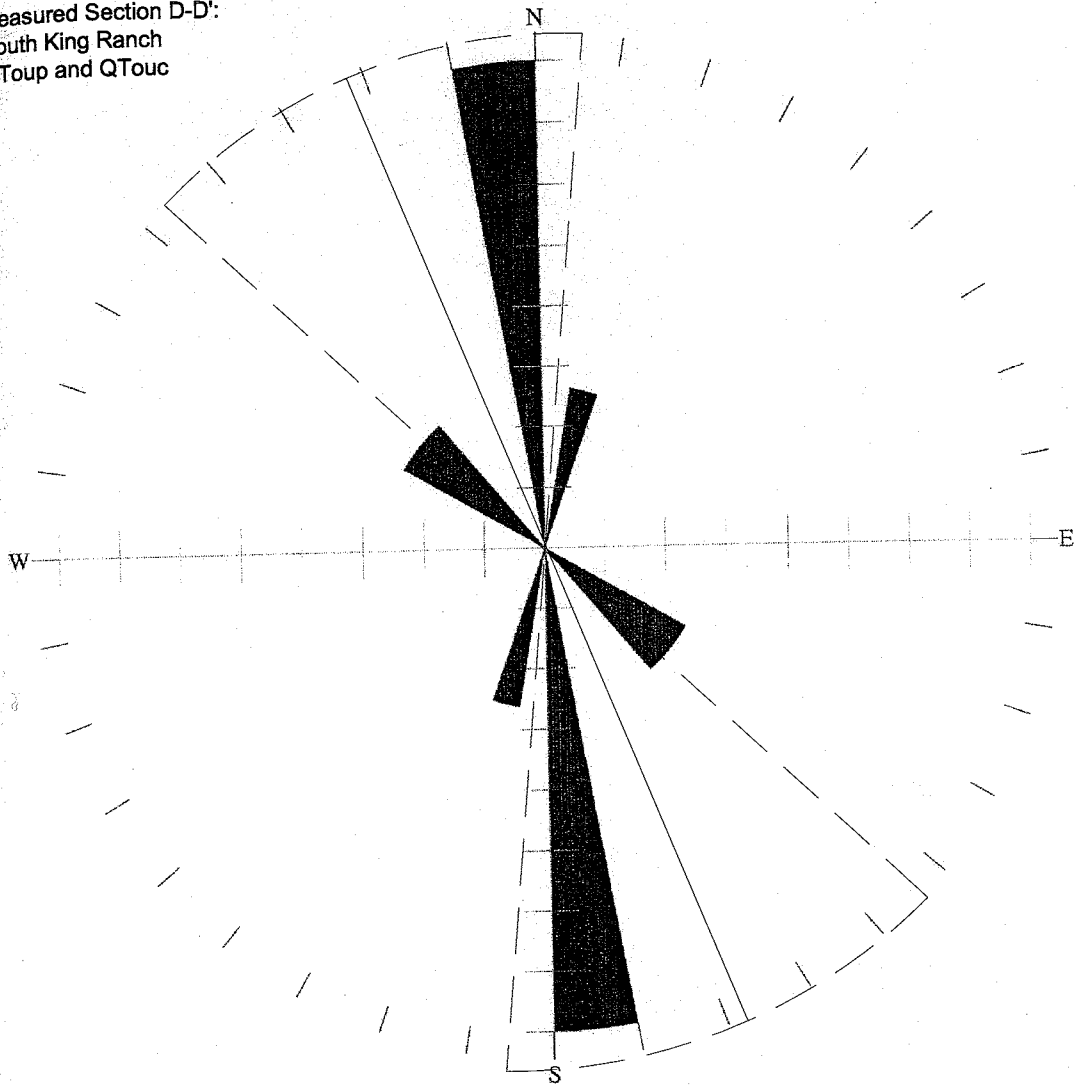
113
Appendix A:
Paleocurrent Data

Measured Section D - D': South King Ranch
QToup and QTouc

Data Point	Azimuth in Degrees	Type of Indicator
D1	310	Channel Orientation
D2	302	Channel Orientation
D3	350	Channel Orientation
D4	350	Channel Orientation
D5	350	Channel Orientation
D6	10	Channel Orientation
Mean \pm Standard deviation		339 \pm 27

114
Appendix A:
Paleocurrent Data

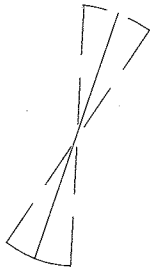
Measured Section D-D':
South King Ranch
QTouc and QTouc



Mean \pm standard deviation = 339 \pm 27

Key

Rose Diagram Bi-Directional
Total Number of Points = 6
Bucket Size = 10 degrees Error Size = 0 degrees



Mean = solid line
Standard deviation = dashed lines

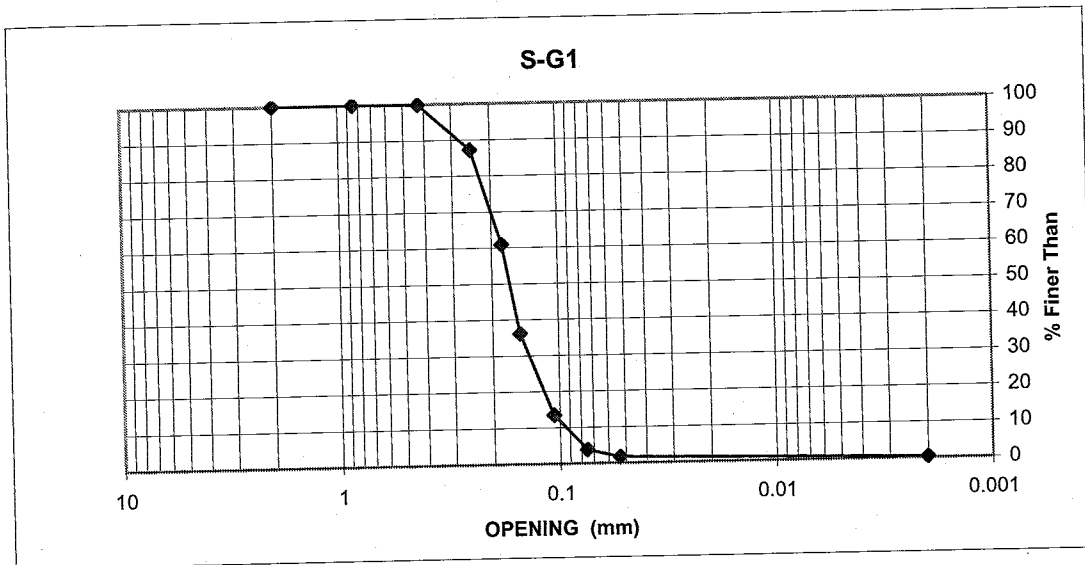
APPENDIX B: GRAIN-SIZE ANALYSES

Grain-size distribution of sand- and gravel-sized material was determined by separating the sediments using standard sieves. Two samples from the QToum map unit were analyzed using a hydrometer. Sample locations are presented on the measured stratigraphic sections (Figures 6 through 9).

116
Appendix B:
Grain Size Analyses

Percent finer than

Sample	Grain Size	Opening size (mm)	% Finer than
S-G1	> Sand (Gravel)	2	100.00
	Sand <2, >0.075	0.85	100.00
		0.425	99.84
		0.246	87.17
		0.18	60.85
		0.15	36.07
		0.106	13.39
	Silt <0.075, >0.002	0.075	3.77
		0.053	1.73
	Clay <0.002	0.002	0.29



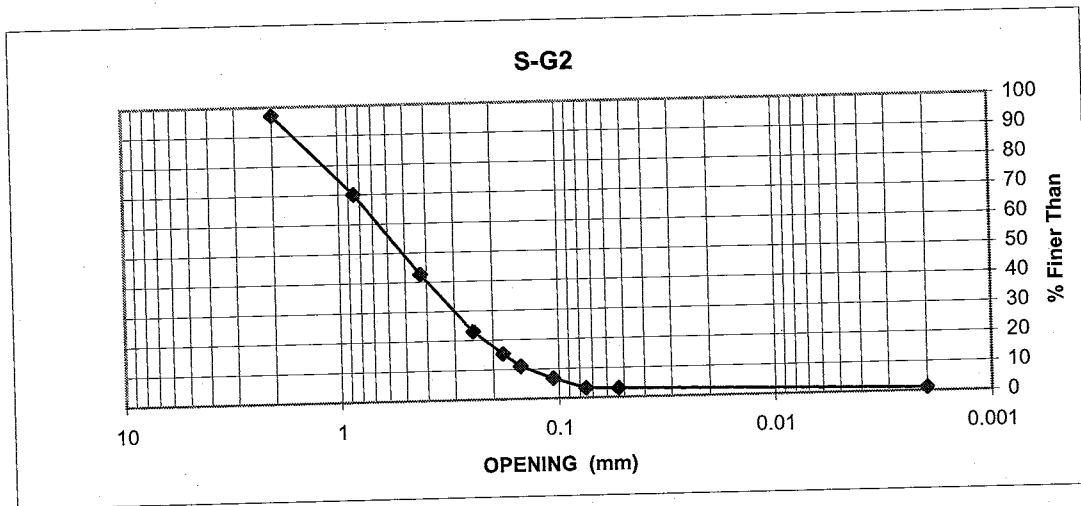
Results

Sample	Grain size	Mass	% of Total
S-G1	>Sand (Gravel)	0.00	0.00
	Sand (#10-200)	123.45	96.23
	Silt <0.075, >0.002	4.47	3.48
	Clay <0.002	0.37	0.29

Appendix B:
Grain Size Analyses

Percent finer than

Sample	Grain Size	Opening size (mm)	% Finer than
S-G2	> Sand (Gravel)	2	97.03
	Sand <2, >0.075	0.85	70.05
		0.425	42.69
		0.246	22.93
		0.18	15.30
		0.15	10.96
	Silt <0.075, >0.002	0.106	6.73
		0.075	3.24
		0.053	3.06
	Clay <0.002	0.002	1.08



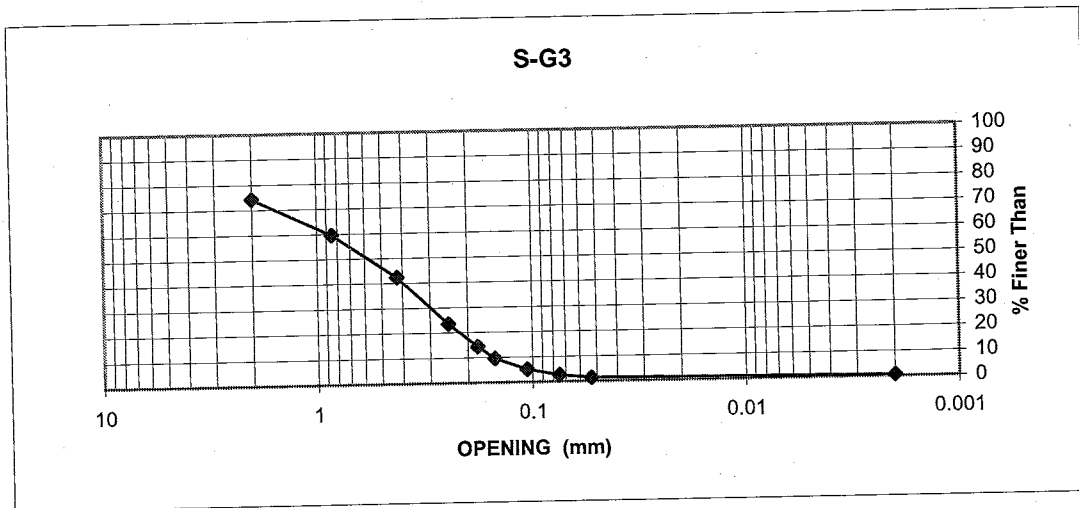
Results

Sample	Grain Size	Mass	% of total
S-G2	>Sand (Gravel)	5.77	2.97
	Sand (#10-200)	182.23	93.79
	Silt <0.075, >0.002	4.19	2.16
	Clay <0.002	2.10	1.08

Appendix B:
Grain Size Analyses

Percent finer than

Sample	Grain Size	Opening size (mm)	% Finer than
S-G3	> Sand (Gravel)	2	74.25
	Sand <2, >0.075	0.85	59.60
		0.425	42.31
		0.246	23.51
		0.18	14.22
		0.15	9.61
	Silt <0.075, >0.002	0.106	5.00
		0.075	2.67
		0.053	1.34
	Clay <0.002	0.002	0.47



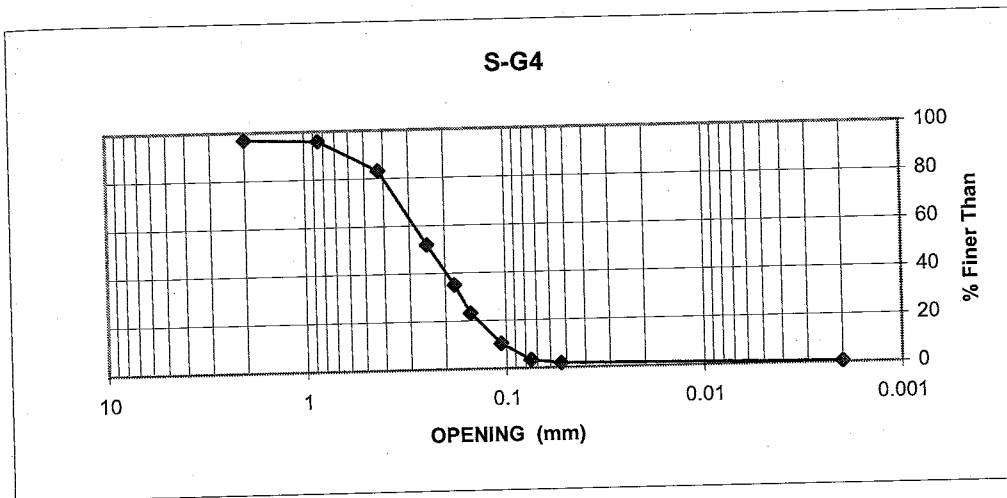
Results

Sample	Grain Size	Mass	% of total
S-G3	>Sand (Gravel)	147.72	25.75
	Sand (#10-200)	410.58	71.58
	Silt <0.075, >0.002	12.62	2.20
	Clay <0.002	2.67	0.47

119
Appendix B:
Grain Size Analyses

Percent finer than

Sample	Grain Size	Opening size (mm)	% Finer than
S-G4	> Sand (Gravel)	2	96.93
	Sand <2, >0.075	0.85	95.90
		0.425	83.12
		0.246	51.95
		0.18	35.08
		0.15	23.18
		0.106	10.45
	Silt <0.075, >0.002	0.075	3.32
		0.053	1.88
	Clay <0.002	0.002	0.35



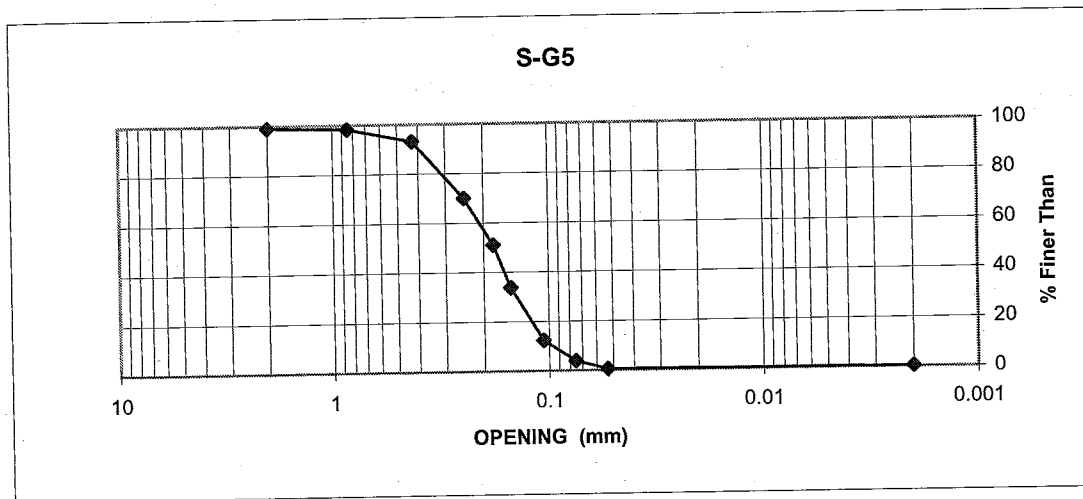
Results

Sample	Grain Size	Mass	% of total
S-G4	>Sand (Gravel)	6.04	3.07
	Sand (#10-200)	184.45	93.61
	Silt <0.075, >0.002	5.86	2.98
	Clay <0.002	0.69	0.35

120
Appendix B:
Grain Size Analyses

Percent finer than

Sample	Grain Size	Opening size (mm)	% Finer than
S-G5	> Sand (Gravel)	2	99.07
	Sand <2, >0.075	0.85	98.35
		0.425	93.18
		0.246	69.94
		0.18	51.08
		0.15	33.74
	Silt <0.075, >0.002	0.106	12.28
		0.075	3.92
		0.053	0.55
	Clay <0.002	0.002	0.20



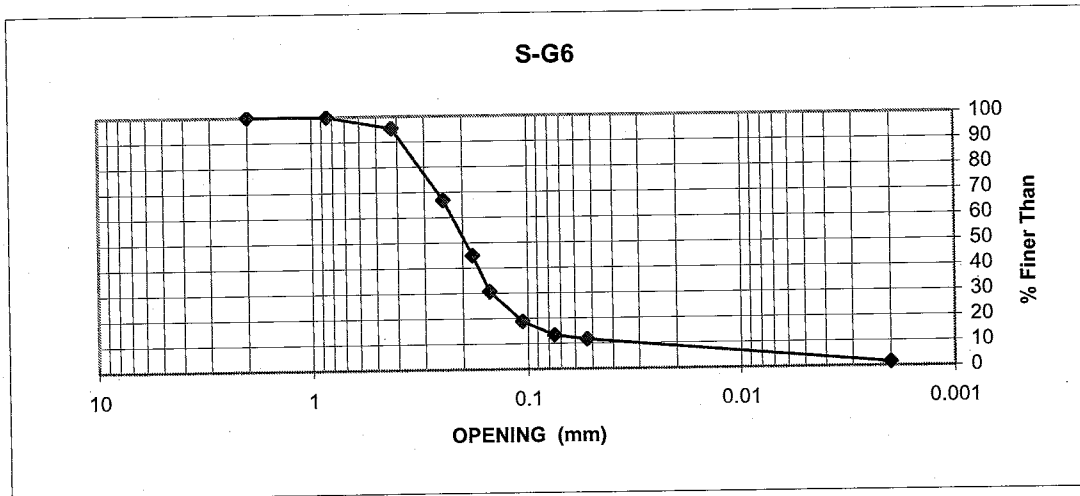
Results

Sample	Grain Size	Mass	% of total
S-G5	>Sand (Gravel)	2.69	0.93
	Sand (#10-200)	274.90	95.14
	Silt <0.075, >0.002	10.75	3.72
	Clay <0.002	0.59	0.20

121
Appendix B:
Grain Size Analyses

Percent finer than

Sample	Grain Size	Opening size (mm)	% Finer than
S-G6	> Sand (Gravel)	2	100.00
	Sand <2, >0.075	0.85	99.87
		0.425	95.37
		0.246	66.78
		0.18	44.94
		0.15	30.69
	Silt <0.075, >0.002	0.106	18.76
		0.075	13.29
	Clay <0.002	0.053	11.62
		0.002	1.50



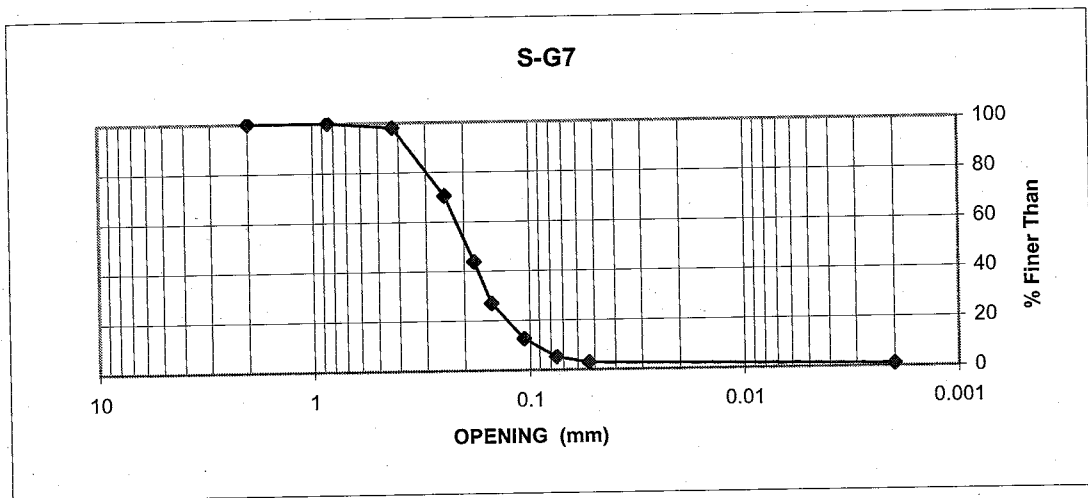
Results

Sample	Grain Size	Mass	% of total
S-G6	>Sand (Gravel)	0.00	0.00
	Sand (#10-200)	186.48	86.71
	Silt <0.075, >0.002	25.36	11.79
	Clay <0.002	3.23	1.50

122
Appendix B:
Grain Size Analyses

Percent finer than

Sample	Grain Size	Opening size (mm)	% Finer than
S-G7	> Sand	2	100.00
	Sand <2, >0.075	0.85	100.00
		0.425	98.06
		0.246	70.45
		0.18	43.84
		0.15	26.95
	Silt <0.075, >0.002	0.106	12.66
		0.075	5.14
		0.053	2.85
	Clay <0.002	0.002	1.07



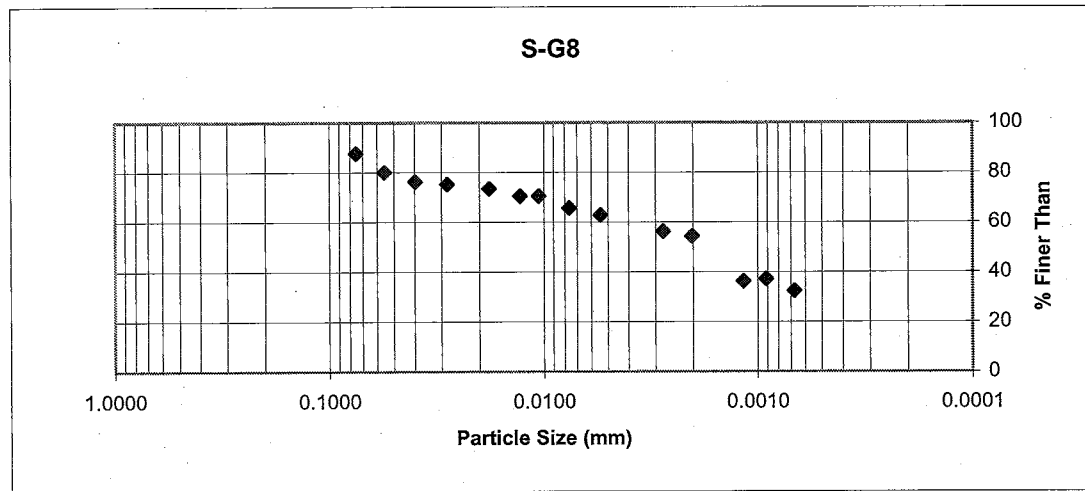
Results

Sample	Grain Size	Mass	% of total
S-G7	>Sand (Gravel)	0.00	0.00
	Sand (#10-200)	130.51	94.86
	Silt <0.075, >0.002	5.59	4.07
	Clay <0.002	1.48	1.07

Appendix B:
Grain Size Analyses

Percent finer than - Hydrometer

Sample	Grain Size	Particle Diameter <i>d</i> (mm)	% Finer than (%)
S-G8	Silt <0.075, >0.002	0.0750	87.65
		0.0553	80.03
		0.0398	76.22
		0.0282	75.27
		0.0180	73.36
		0.0129	70.50
		0.0105	70.50
		0.0076	65.74
		0.0054	62.88
		0.0028	56.21
		Clay <0.002	0.0020
0.0012	36.20		
0.0009	37.16		
0.0007	32.39		



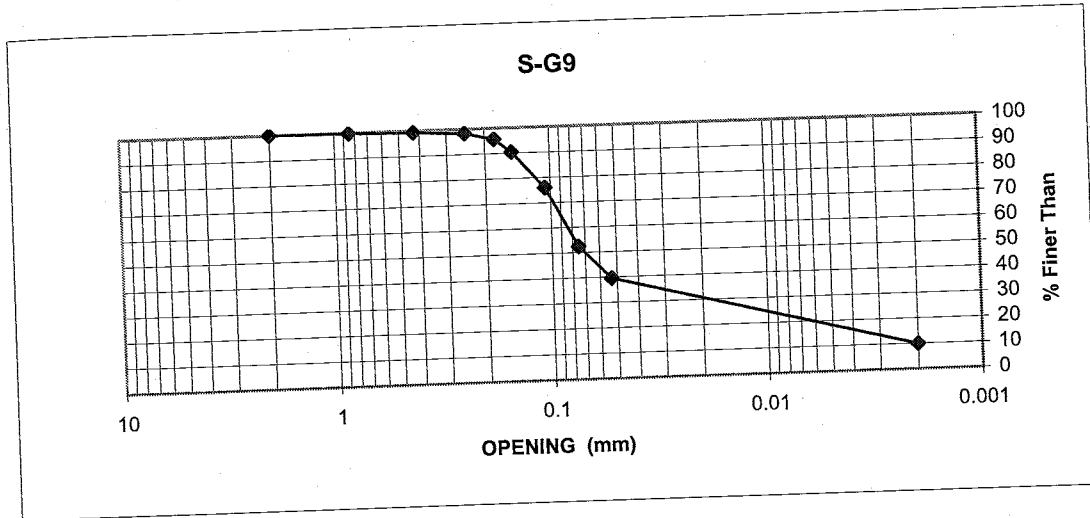
Results

Sample	Grain Size	% of total
S-G8	>Sand (Gravel)	0.00 Extrapolated
	Sand (#10-200)	12.00 from graphs
	Silt <0.075, >0.002	38.00
	Clay <0.002	50.00

124
Appendix B:
Grain Size Analyses

Percent finer than

Sample	Grain Size	Opening size (mm)	% Finer than
S-G9	> Sand (Gravel)	2	100.00
	Sand <2, >0.075	0.85	99.71
		0.425	99.29
		0.246	98.18
		0.18	95.59
		0.15	90.44
	Silt <0.075, >0.002	0.106	75.89
		0.075	52.43
		0.053	39.50
	Clay <0.002	0.002	9.92



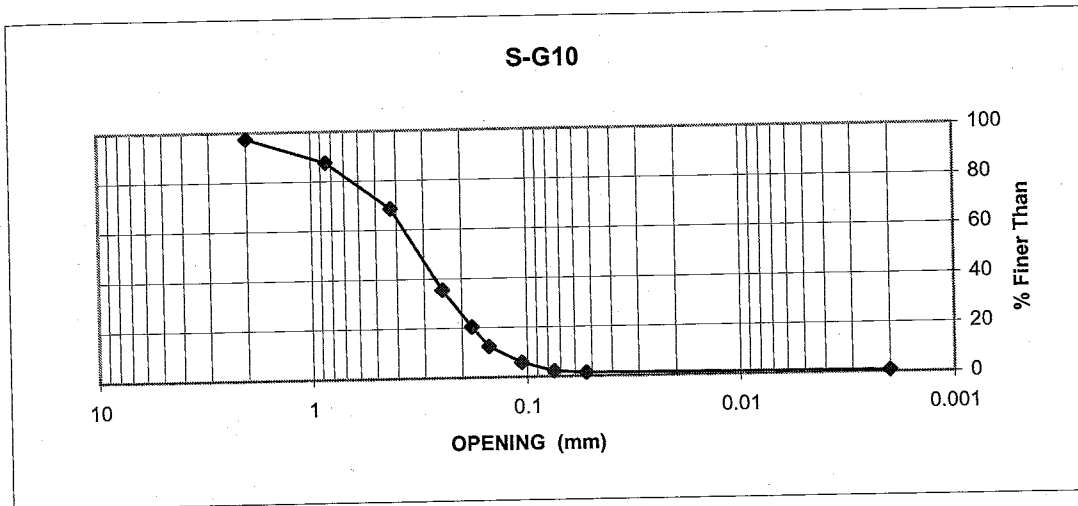
Results

Sample	Grain Size	Mass	% of total
S-G9	>Sand (Gravel)	0.00	0.00
	Sand (#10-200)	51.77	47.57
	Silt <0.075, >0.002	46.25	42.51
	Clay <0.002	10.80	9.92

125
Appendix B:
Grain Size Analyses

Percent finer than

Sample	Grain Size	Opening size (mm)	% Finer than
S-G10	> Sand (Gravel)	2	97.44
	Sand <2, >0.075	0.85	87.50
		0.425	68.57
		0.246	35.43
		0.18	20.43
		0.15	12.39
	Silt <0.075, >0.002	0.106	5.77
		0.075	2.23
		0.053	1.36
	Clay <0.002	0.002	0.70



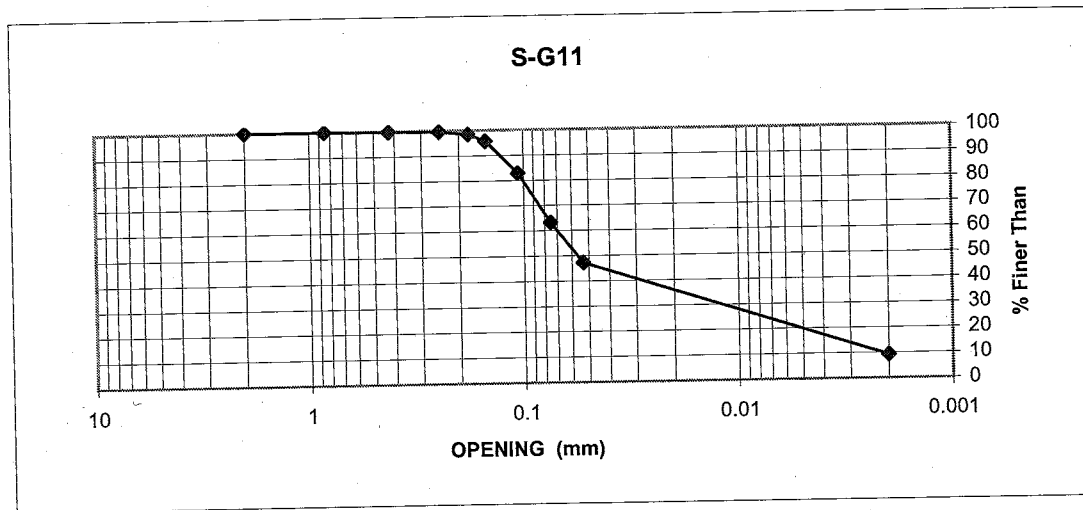
Results

Sample	Grain Size	Mass	% of total
S-G10	>Sand (Gravel)	3.67	2.56
	Sand (#10-200)	136.27	95.21
	Silt <0.075, >0.002	2.19	1.53
	Clay <0.002	1.00	0.70

126
Appendix B:
Grain Size Analyses

Percent finer than

Sample	Grain Size	Opening size (mm)	% Finer than
S-G11	> Sand (Gravel)	2	100.00
	Sand <2, >0.075	0.85	99.94
		0.425	99.75
		0.246	99.53
		0.18	98.48
		0.15	95.64
	Silt <0.075, >0.002	0.106	82.80
		0.075	63.24
		0.053	47.26
	Clay <0.002	0.002	9.28



Results

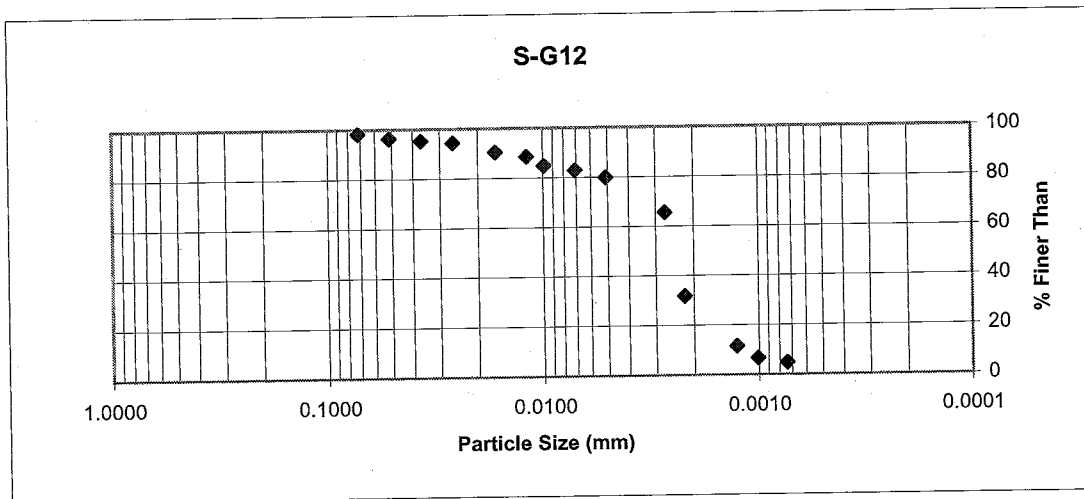
Sample	Grain Size	Mass	% of total
S-G11	>Sand (Gravel)	0.00	0.00
	Sand (#10-200)	38.61	36.76
	Silt <0.075, >0.002	56.67	53.96
	Clay <0.002	9.75	9.28

127
Appendix B:
Grain Size Analyses

Percent finer than - Hydrometer

Sample	Grain Size	Particle diameter <i>d</i> (mm)	% Finer than (%)	
S-G12	Silt <0.075, >0.002	0.0717	98.17	
		0.0514	96.25	
		0.0366	95.28	
		0.0260	94.32	
		0.0166	90.47	
		0.0119	88.55	
		0.0099	84.70	
		0.0071	82.77	
		0.0051	79.88	
		0.0027	65.45	
		Clay <0.002	0.0022	31.76
			0.0013	11.55
			0.0010	6.74
			0.0007	4.81

Note: Flocculation likely caused the a portion of the clay fraction to fall out of suspension prematurely. It is believed that a more accurate representation of the clay fraction would be represented by extending the initial slope.



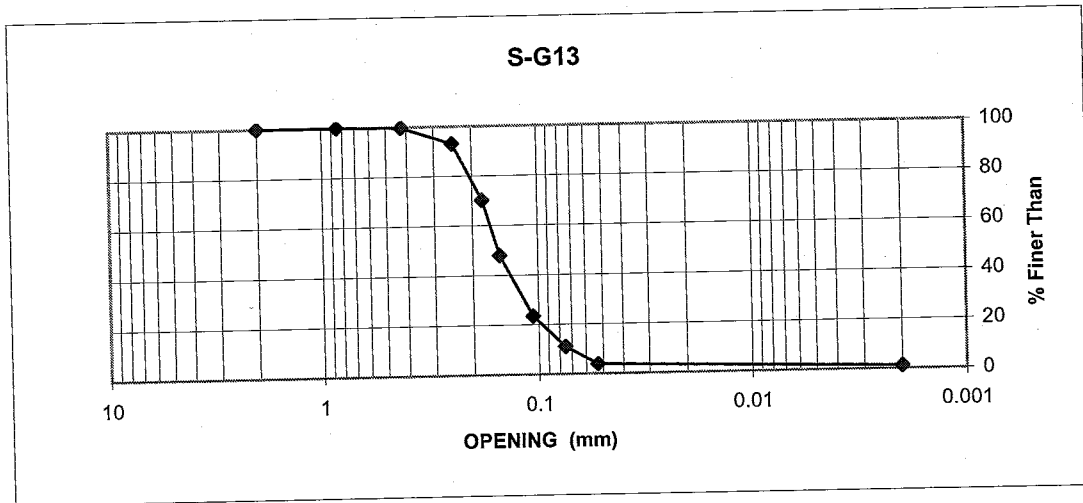
Results

Sample	Grain size	% OF TOTAL
S-G12	>Sand (Gravel)	0.00 Extrapolated
	Sand (#10-200)	1.00 from graphs
	Silt <0.075, >0.002	29.00
	Clay <0.002	70.00

Appendix B:
Grain Size Analyses

Percent finer than

Sample	Grain Size	Opening size (mm)	% Finer than
S-G13	> Sand (Gravel)	2	100.00
	Sand <2, >0.075	0.85	99.96
		0.425	99.76
		0.246	93.09
		0.18	70.28
		0.15	47.89
	Silt <0.075, >0.002	0.106	23.35
		0.075	10.94
		0.053	3.90
	Clay <0.002	0.002	1.22



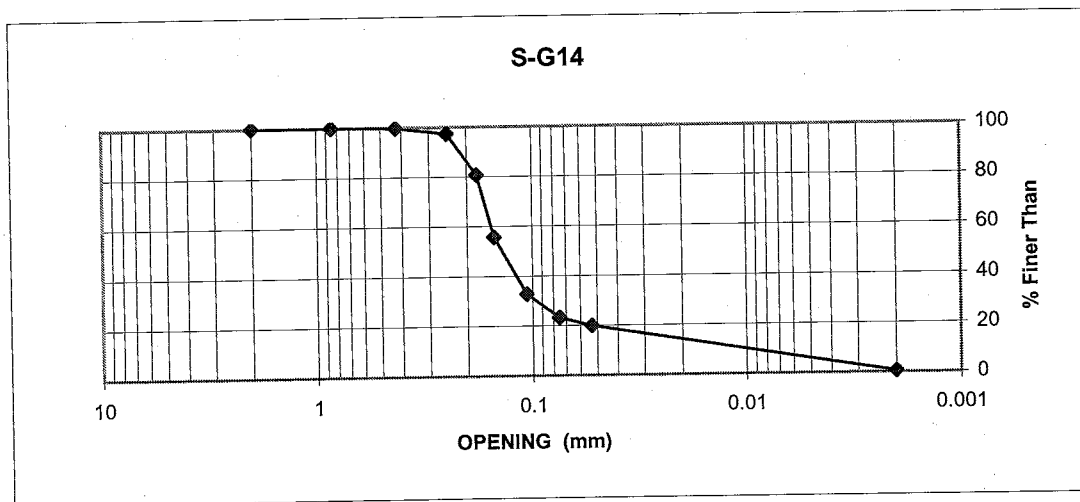
Results

Sample	Grain Size	Mass	% of total
S-G13	>Sand (Gravel)	0.00	0.00
	Sand (#10-200)	203.57	89.06
	Silt <0.075, >0.002	22.23	9.73
	Clay <0.002	2.78	1.22

129
Appendix B:
Grain Size Analyses

Percent finer than

Sample	Grain Size	Opening size (mm)	% Finer than
S-G14	> Sand (Gravel)	2	100.00
	Sand <2, >0.075	0.85	99.95
		0.425	99.76
		0.246	97.25
		0.18	80.67
		0.15	55.61
	Silt <0.075, >0.002	0.106	32.74
		0.075	23.20
		0.053	19.80
	Clay <0.002	0.002	0.58



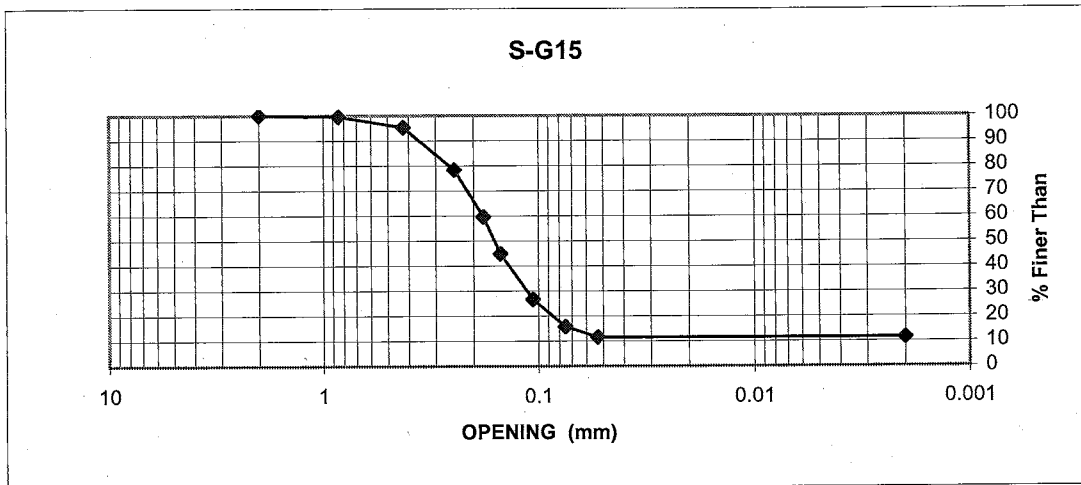
Results

Sample	Grain Size	Mass	% of total
S-G14	>Sand (Gravel)	0.00	0.00
	Sand (#10-200)	201.66	76.80
	Silt <0.075, >0.002	59.41	22.62
	Clay <0.002	1.51	0.58

130
Appendix B:
Grain Size Analyses

Percent finer than

Sample	Grain Size	Opening size (mm)	% Finer than
S-G15	> Sand (Gravel)	2	99.96
	Sand <2, >0.075	0.85	99.56
		0.425	95.23
		0.246	78.36
		0.18	59.56
		0.15	44.87
	Silt <0.075, >0.002	0.106	26.63
		0.075	15.77
		0.053	11.56
	Clay <0.002	0.002	11.56



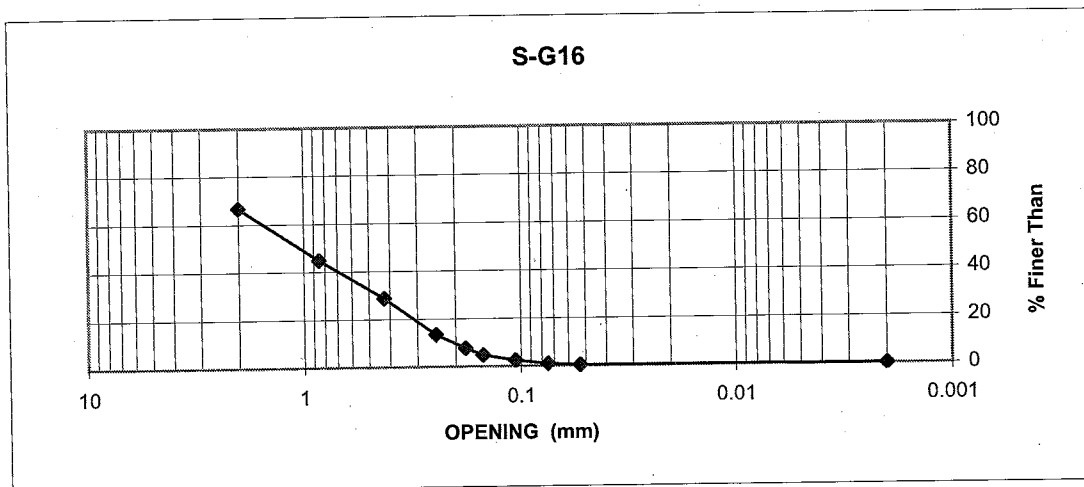
Results

Sample	Grain Size	Mass	% of total
S-G15	>Sand (Gravel)	0.05	0.04
	Sand (#10-200)	101.14	84.18
	Silt <0.075, >0.002	5.06	4.21
	Clay <0.002	13.89	11.56

131
Appendix B:
Grain Size Analyses

Percent finer than

Sample	Grain Size	Opening size (mm)	% Finer than
S-G16	> Sand (Gravel)	2	66.63
	Sand <2, >0.075	0.85	44.91
		0.425	28.78
		0.246	13.41
		0.18	7.65
		0.15	4.69
		0.106	2.39
	Silt <0.075, >0.002	0.075	0.97
		0.053	0.32
	Clay <0.002	0.002	0.07



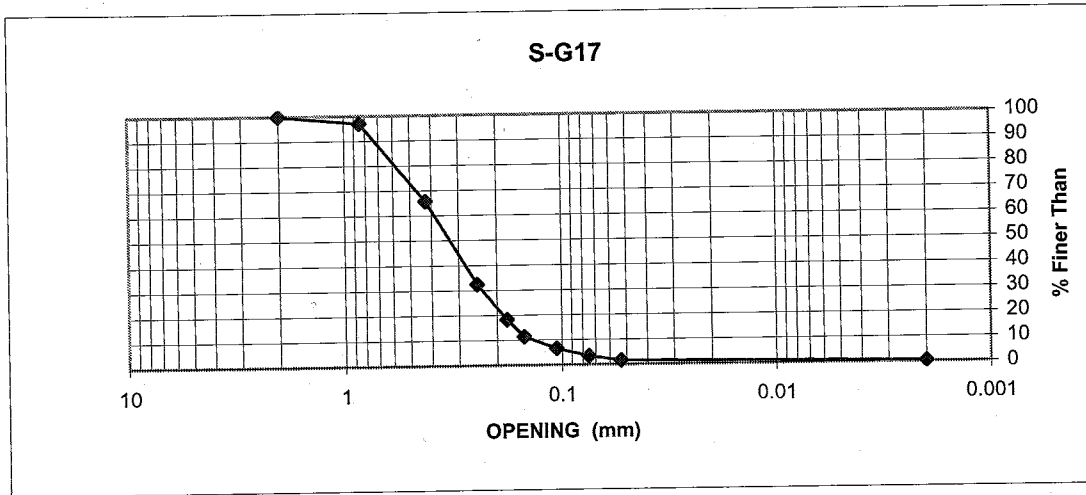
Results

Sample	Grain Size	Mass	% of total
S-G16	>Sand (Gravel)	167.68	33.37
	Sand (#10-200)	330.02	65.67
	Silt <0.075, >0.002	4.48	0.89
	Clay <0.002	0.38	0.07

Appendix B:
Grain Size Analyses

Percent finer than

Sample	Grain Size	Opening size (mm)	% Finer than
S-G17	> Sand (Gravel)	2	99.87
	Sand <2, >0.075	0.85	96.88
		0.425	65.65
		0.246	32.34
		0.18	18.19
		0.15	11.39
	Silt <0.075, >0.002	0.106	6.52
		0.075	3.46
		0.053	1.59
	Clay <0.002	0.002	0.42



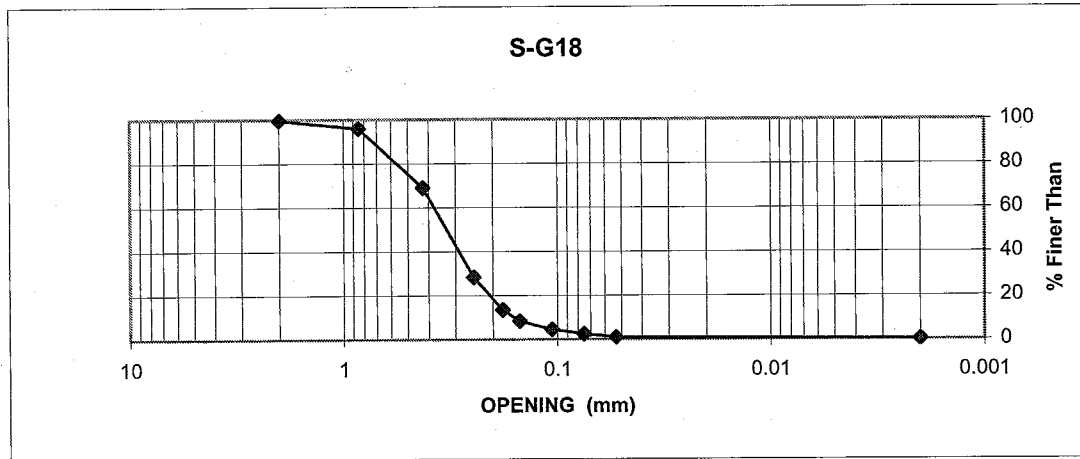
Results

Sample	Grain Size	Mass	% of total
S-G17	>Sand (Gravel)	0.42	0.13
	Sand (#10-200)	315.99	94.41
	Silt <0.075, >0.002	9.95	3.04
	Clay <0.002	1.39	0.42

133
Appendix B:
Grain Size Analyses

Percent finer than

Sample	Grain Size	Opening size (mm)	% Finer than
S-G18	> Sand (Gravel)	2	99.61
	Sand <2, >0.075	0.85	95.86
		0.425	69.06
		0.246	28.29
		0.18	13.39
		0.15	8.36
	Silt <0.075, >0.002	0.106	4.50
		0.075	2.49
		0.053	1.07
	Clay <0.002	0.002	0.11



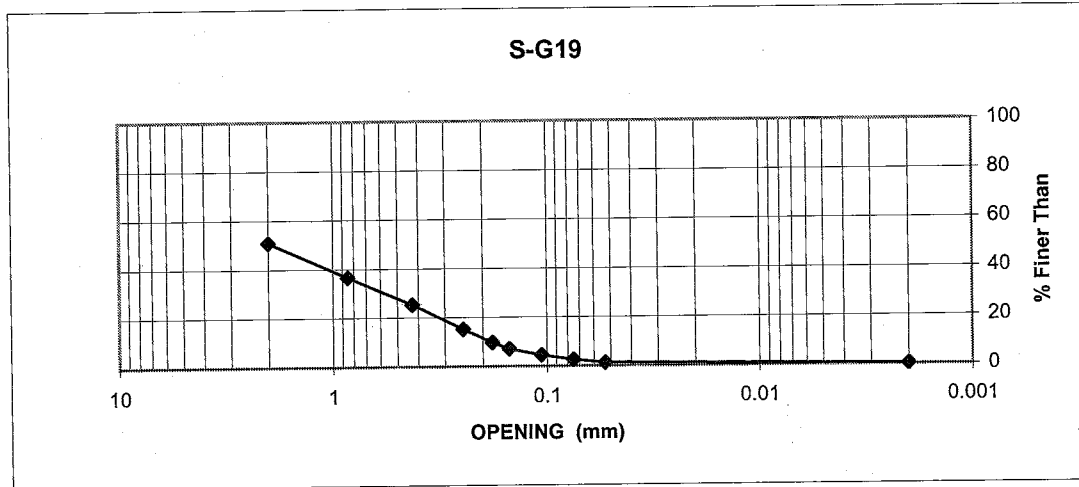
Results

Sample	Grain Size	Mass	% of Total
S-G18	>Sand (Gravel)	0.83	0.39
	Sand (#10-200)	208.83	97.13
	Silt <0.075, >0.002	5.11	2.38
	Clay <0.002	0.24	0.11

134
Appendix B:
Grain Size Analyses

Percent finer than

Sample	Grain Size	Opening size (mm)	% Finer than
S-G19	> Sand (Gravel)	2	50.92
	Sand <2, >0.075	0.85	36.58
		0.425	25.31
		0.246	15.14
		0.18	9.75
		0.15	7.13
	Silt <0.075, >0.002	0.106	4.48
		0.075	2.64
	Clay <0.002	0.053	1.34
		0.002	0.21



Results

Sample	Grain size	Mass	% of total
S-G19	>Sand (Gravel)	204.90	49.08
	Sand (#10-200)	201.54	48.28
	Silt <0.075, >0.002	10.10	2.42
	Clay <0.002	0.90	0.21

APPENDIX C: POROSITY DATA

These tables contain porosity data from thin section image analysis. Sample locations are presented on the measured stratigraphic sections (Figures 6 through 9). For each sample, one thin section was made. The porosity column includes the percent porosity of each of the ten locations measured from each slide. The base of each column displays the mean porosity \pm the standard deviation.

136
Appendix C:
Thin Section Porosity Data

sample	porosity	sample	porosity	sample	porosity
ST-a1	0.1424	ST-b3	0.1257	ST-c1	0.1029
	0.1580		0.1679		0.0829
	0.1451		0.1902		0.1955
	0.1540		0.1370		0.1560
	0.1550		0.0731		0.1716
	0.1631		0.2532		0.0754
	0.1515		0.2795		0.0393
	0.1453		0.2813		0.1356
	0.1637		0.2324		0.0885
	0.1634		0.1649		0.1962
Mean +- Std. Dev.	0.1542± 0.0065	0.1905± 0.0569	0.1244± 0.0466		
ST-d3	0.1392	ST-d4	0.2804	ST-d5	0.2363
	0.1039		0.2766		0.2137
	0.1090		0.2728		0.2535
	0.1685		0.2776		0.2772
	0.1038		0.2219		0.1732
	0.1314		0.2884		0.3472
	0.1635		0.2654		0.3045
	0.1393		0.2687		0.2705
	0.1255		0.3252		0.3665
	0.1341		0.2567		0.4226
Mean± Std. Dev.	0.1318± 0.0171	0.2734± 0.0163	0.2865± 0.589		
ST-e1	0.3414	ST-f2	0.2228	ST-f5	0.2091
	0.2893		0.2952		0.2214
	0.3003		0.3484		0.3001
	0.3910		0.3459		0.2801
	0.3293		0.2526		0.1948
	0.3185		0.2852		0.2745
	0.3673		0.2732		0.2857
	0.3773		0.2853		0.2290
	0.3218		0.2907		0.2867
	0.2755		0.2806		0.2759
Mean± Std. Dev.	0.3312± 0.0305	0.2880± 0.0256	0.2557± 0.0337		

Appendix C:
Thin Section Porosity Data

ST-g4	0.2186	ST-g6	0.2928	ST-h2	0.0785
	0.0542		0.0759		0.0027
	0.2067		0.3629		0.0529
	0.2169		0.2934		0.0821
	0.1890		0.3378		0.1418
	0.1809		0.4021		0.1302
	0.2222		0.2877		0.0037
	0.1900		0.1225		0.0380
	0.2601		0.1781		0.1698
	0.2233		0.2803		0.0533
Mean± Std.	0.1962±	0.2634±		0.0753±	
Dev.	0.0341	0.0827		0.0452	
ST-h3	0.1791	ST-h4	0.3174	ST-i1	0.2857
	0.2833		0.2734		0.1353
	0.1965		0.2244		0.1170
	0.1184		0.2587		0.1754
	0.0027		0.3132		0.2673
	0.1814		0.2542		0.2222
	0.0618		0.2598		0.2423
	0.0833		0.2635		0.1284
	0.0842		0.3091		0.3535
	0.0706		0.2673		0.1800
Mean± Std.	0.1261±	0.2741±		0.2107±	
Dev.	0.0672	0.0235		0.0635	
ST-i2	0.2427	ST-i3	0.3050	ST-j3	0.2742
	0.1958		0.3085		0.2736
	0.2292		0.2674		0.2696
	0.2618		0.3372		0.2978
	0.3474		0.2544		0.2452
	0.3768		0.3090		0.3516
	0.2059		0.4379		0.2588
	0.2916		0.2868		0.2886
	0.2298		0.2774		0.2804
	0.3328		0.2509		0.2612
Mean± Std.	0.2714±	0.3035±		0.2801±	
Dev.	0.0526	0.0361		0.0196	

138
Appendix C:
Thin Section Porosity Data

ST-k1	0.3234	ST-k4	0.3379	ST-l2	0.2944
	0.3188		0.3202		0.2001
	0.3323		0.2988		0.2384
	0.3872		0.3106		0.2210
	0.3749		0.2680		0.2284
	0.3659		0.2944		0.1473
	0.3311		0.2757		0.1868
	0.3312		0.3017		0.1677
	0.3317		0.2658		0.1601
	0.3321		0.3145		0.1566
Mean± Std.	0.3429±		0.2988±		0.2001±
Dev.	0.0199		0.0182		0.0364
ST-l3	0.1739	ST-l5	0.3197	ST-m1	0.2987
	0.1923		0.3783		0.3031
	0.2550		0.3848		0.2586
	0.2897		0.3388		0.3454
	0.2506		0.3557		0.3358
	0.2140		0.3140		0.3257
	0.1666		0.3864		0.4209
	0.2151		0.3493		0.3192
	0.2151		0.3599		0.3260
	0.2182		0.3259		0.3186
Mean± Std.	0.2191±		0.3513±		0.3252±
Dev.	0.0276		0.0217		0.0256
ST-n2	0.2052	ST-n3a	0.2808	ST-n3	0.2828
	0.2682		0.3288		0.3308
	0.3251		0.3308		0.3316
	0.3428		0.3503		0.3516
	0.2612		0.3173		0.3189
	0.3195		0.2902		0.2915
	0.4343		0.2731		0.2742
	0.2920		0.2847		0.2865
	0.2508		0.3123		0.3134
	0.2366		0.3431		0.3443
Mean± Std.	0.2936±		0.3111±		0.3126±
Dev.	0.0495		0.0232		0.0230

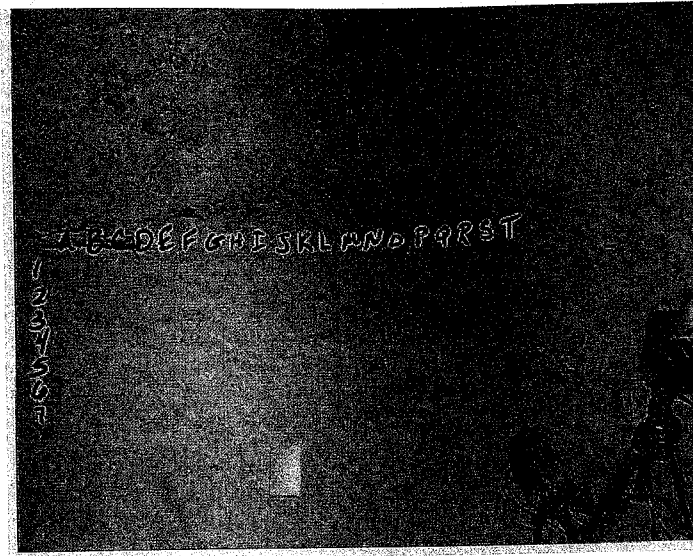
Appendix C:
Thin Section Porosity Data

ST-n4	0.3168
	0.3506
	0.3418
	0.3984
	0.4119
	0.3510
	0.3446
	0.3292
	0.3279
	0.3397
Mean± Std.	0.3512±
Dev.	0.0216

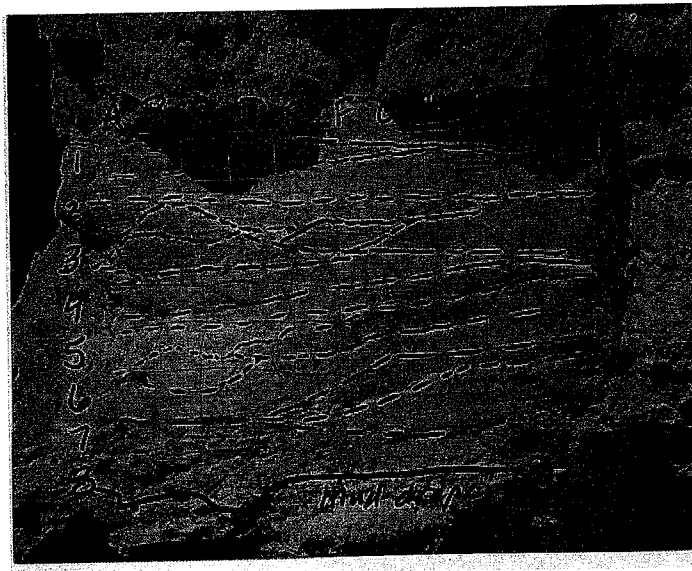
APPENDIX D: AIR MINIPERMEAMETER OUTCROP PHOTOS

This appendix includes outcrop photos of air minipermeameter data collection sites illustrating the grid layout of each site. The sample locations are noted on the measured stratigraphic sections (Figures 6 through 9). All outcrops used for data collection were either north- or south-facing. The grids were numbered along the horizontal axis and lettered along the vertical axis in order to record data in a systematic fashion. Where applicable, sedimentary structures were traced on the photos. Fractures, cracks and roots were avoided during data collection as these features appear to be discontinuous and site specific and do not represent the unit as a whole.

Appendix D
Air Minipermeameter Outcrop Photographs

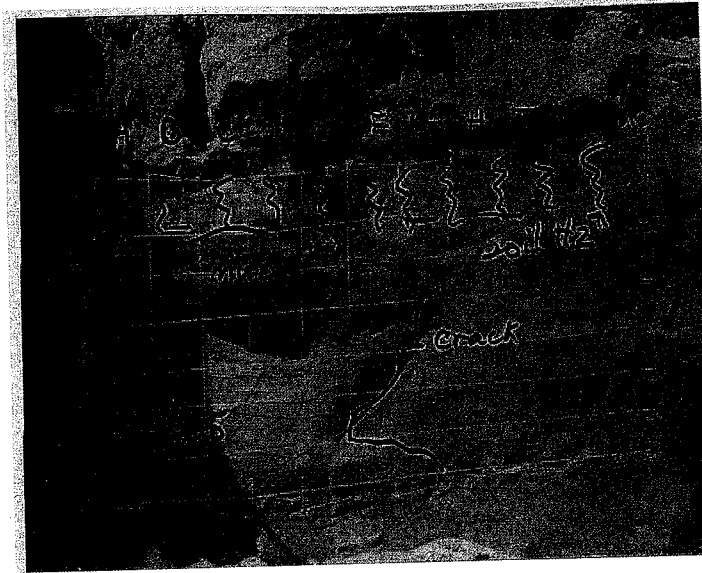


S-P1: QToup
Poorly to moderately sorted massive sand.



S-P2: QTous
Massive laminated and cross-stratified sand with gravel channel deposits.

Appendix D
Air Minipermeameter Outcrop Photographs

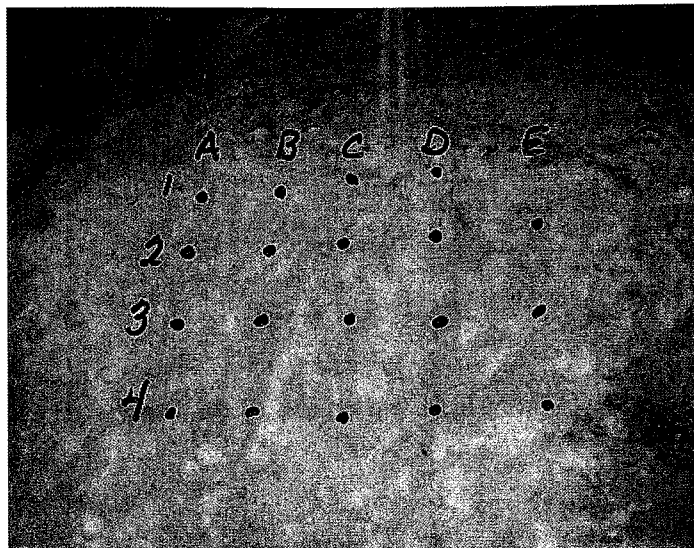


S-P3: QTous
Massive laminated and cross-stratified sand with gravel channel deposits, with a very weak carbonate soil denoted by the vertical squiggly lines at the top of the measurement grid.

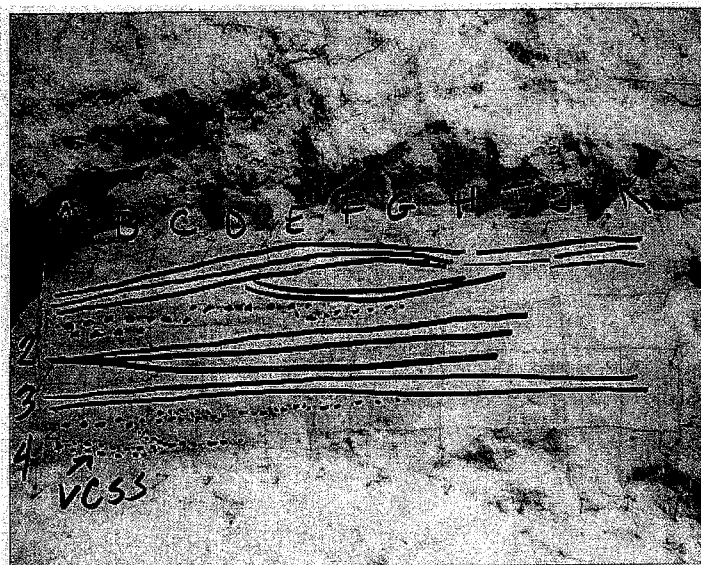


S-P4: QToup
Poorly to moderately sorted massive sand.

Appendix D
Air Minipermeameter Outcrop Photographs

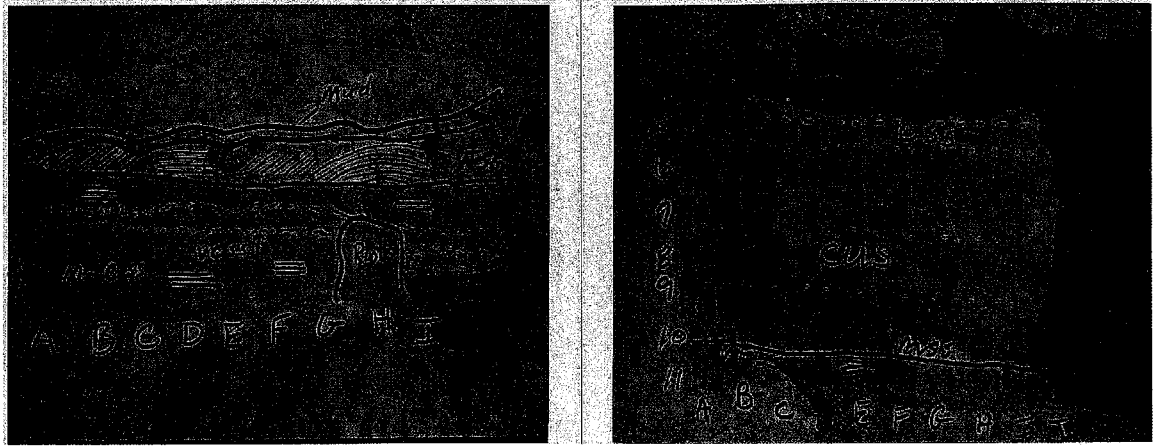


S-P5: QToup
Poorly to moderately sorted massive sand with carbonate soil development.



S-P6: QTous
Massive laminated and cross-stratified sand with gravel channel deposits.

Appendix D
Air Minipermeameter Outcrop Photographs



S-P7 Part A: QTouc

S-P7 Part B: QTouc

Cross-stratified sand with gravel channel deposits. These two photographs represent two portions of the same outcrop, located side by side as shown above (with approximately 0.5 meters between the two photographs). The measurements could not be performed on one large, continuous grid as there were obstructions between area A and area B.

APPENDIX E: PERMEABILITY DATA

Permeability measurements were taken with an air minipermeameter. At each outcrop sampled (e.g. S-P1), three time readings from the air minipermeameter were recorded for each grid location (1A, 4G, etc.) in seconds. The mean and standard deviation for the time readings at each grid location are provided in the second and third columns from the right. Below is a list of abbreviations used to conserve space in the descriptions column of the tables on the following pages.

List of Abbreviations

X-bed	Cross-bedded
Lam	Laminated
Ps sand	poorly sorted sand
Md	mud drape
Fss	fine-grained sand
Fmss	fine- to medium-grained sand
Mss	medium-grained sand
Mcss	medium- to coarse-grained sand

Css coarse-grained sand

Hydraulic conductivity (K , in Darcies) is defined as (from Fetter, 1994):

$$K = K_i \left(\frac{\gamma}{\mu} \right)$$

K_i is intrinsic permeability, which is defined as:

$$K_i = Cd^2$$

C is a constant called a shape factor and d is the mean pore diameter.

λ is the specific weight of the fluid.

μ is the dynamic viscosity of the fluid.

Appendix E:
Permeability Data

S-P1: QToup (Dead Deer Gulch): Poorly to moderately sorted massive, fine- to medium-grained sand with scattered pebbles and vertically-oriented carbonate bodies.

#meas	sample	time (s)		description	mean	std dev	K (darcy)
3	1A	6.49	6.52	5.49 Ps sand	6.17	0.59	10.62
3	1B	5.58	4.68	4.54 Ps sand	4.93	0.56	13.39
3	1C	4.11	2.88	2.87 Ps sand	3.29	0.71	20.61
3	1D	5.50	5.24	5.27 Ps sand	5.34	0.14	12.34
3	1E	6.54	6.47	6.40 Ps sand	6.47	0.07	10.11
3	1F	2.06	6.47	6.65 Ps sand	5.06	2.60	13.04
3	1G	6.31	6.33	6.63 Ps sand	6.42	0.18	10.18
3	1H	6.45	6.52	6.53 Ps sand	6.50	0.04	10.06
3	1I	4.46	4.43	4.39 Ps sand	4.43	0.04	15.00
3	1J	4.18	4.11	3.78 Ps sand	4.02	0.21	16.60
3	1K	5.24	2.79	3.88 Ps sand	3.97	1.23	16.83
3	1L	7.39	4.58	4.69 Ps sand	5.55	1.59	11.84
3	1M	3.49	2.87	3.16 Ps sand	3.17	0.31	21.41
3	1N	10.10	10.04	9.47 Ps sand	9.87	0.35	6.56
3	1O	4.83	2.97	4.30 Ps sand	4.03	0.96	16.55
3	1P	5.61	5.76	5.37 Ps sand	5.58	0.20	11.78
3	1Q	5.52	5.48	4.94 Ps sand	5.31	0.32	12.39
3	1R	2.11	2.84	2.15 Ps sand	2.37	0.41	29.68
3	1S	4.58	3.97	4.46 Ps sand	4.34	0.32	15.33
3	1T	14.20	13.36	13.03 Ps sand	13.53	0.60	4.76
3	2A	5.15	5.20	5.24 Ps sand	5.20	0.05	12.68
3	2B	4.50	3.89	4.82 Ps sand	4.40	0.47	15.09
3	2C	5.60	5.30	5.36 Ps sand	5.42	0.16	12.14
3	2D	2.79	3.12	2.45 Ps sand	2.79	0.34	24.70
3	2E	3.41	3.40	3.53 Ps sand	3.45	0.07	19.58
3	2F	2.03	1.51	1.72 Ps sand	1.75	0.26	42.41
3	2G	6.14	6.42	6.38 Ps sand	6.31	0.15	10.37
3	2H	6.20	6.20	6.28 Ps sand	6.23	0.05	10.52
3	2I	3.42	3.05	2.36 Ps sand	2.94	0.54	23.25
3	2J	2.15	5.40	4.12 Ps sand	3.89	1.64	17.20
3	2K	4.36	5.05	5.90 Ps sand	5.10	0.77	12.93
3	2L	6.15	5.75	5.78 Ps sand	5.89	0.22	11.13
3	2M	5.07	2.82	2.90 Ps sand	3.60	1.28	18.71
3	2N	3.18	2.24	2.78 Ps sand	2.73	0.47	25.23
3	2O	6.17	5.94	4.80 Ps sand	5.64	0.73	11.66
3	2P	4.66	4.48	4.60 Ps sand	4.58	0.09	14.48
3	2Q	4.47	4.65	3.06 Ps sand	4.06	0.87	16.44
3	2R	4.76	5.56	2.60 Ps sand	4.31	1.53	15.44
3	2S	5.19	5.36	5.34 Ps sand	5.30	0.09	12.43
3	2T	2.61	2.70	2.84 Ps sand	2.72	0.12	25.41
3	3A	4.34	3.26	2.05 Ps sand	3.22	1.15	21.10
3	3B	2.78	3.23	3.06 Ps sand	3.02	0.23	22.58

Appendix E:
Permeability Data

#meas	sample	time (s)		description	mean	std dev	K (darcy)
3	3C	2.71	3.02	2.96 Ps sand	2.90	0.16	23.66
3	3D	6.20	5.85	6.69 Ps sand	6.25	0.42	10.48
3	3E	4.67	4.39	4.45 Ps sand	4.50	0.15	14.73
3	3F	6.52	6.88	5.67 Ps sand	6.36	0.62	10.29
3	3G	4.27	5.92	6.57 Ps sand	5.59	1.19	11.76
3	3H	4.00	5.30	3.32 Ps sand	4.21	1.01	15.83
3	3I	6.36	7.50	6.21 Ps sand	6.69	0.71	9.77
3	3J	3.15	4.44	4.66 Ps sand	4.08	0.82	16.34
3	3K	6.48	6.58	4.66 Ps sand	5.91	1.08	11.10
3	3L	6.20	6.04	6.17 Ps sand	6.14	0.09	10.67
3	3M	9.67	9.72	6.56 Ps sand	8.65	1.81	7.50
3	3N	4.91	6.92	4.91 Ps sand	5.58	1.16	11.78
3	3O	6.67	6.75	5.86 Ps sand	6.43	0.49	10.18
3	3P	3.32	2.91	6.24 Ps sand	4.16	1.82	16.03
3	3Q	3.28	2.54	2.47 Ps sand	2.76	0.45	34.93
3	3R	4.50	4.38	4.90 Ps sand	4.59	0.27	14.43
3	3S	4.01	2.97	4.72 Ps sand	3.90	0.88	17.16
3	3T	8.03	6.38	6.77 Ps sand	7.06	0.86	9.24
3	4A	4.97	4.82	3.53 Ps sand	4.44	0.79	14.96
3	4B	6.42	6.42	6.46 Ps sand	6.43	0.02	10.17
3	4C	3.00	2.94	3.84 Ps sand	3.26	0.50	20.80
3	4D	1.67	4.27	4.57 Ps sand	3.50	1.59	19.24
3	4E	6.83	6.52	6.70 Ps sand	6.68	0.16	9.78
3	4F	6.03	5.88	6.03 Ps sand	5.98	0.09	10.96
3	3G	4.27	4.12	3.78 Ps sand	4.06	0.25	16.45
3	4H	5.42	5.01	4.88 Ps sand	5.10	0.28	12.93
3	4I	6.94	6.30	7.48 Ps sand	6.91	0.59	9.45
3	4J	4.45	4.57	4.56 Ps sand	4.53	0.07	14.66
3	4K	4.19	3.24	3.93 Ps sand	3.79	0.49	17.70
3	4L	4.15	4.70	4.94 Ps sand	4.60	0.41	14.42
3	4M	6.45	3.09	3.78 Ps sand	4.44	1.77	14.96
3	4N	14.22	12.79	10.00 Ps sand	12.34	2.15	5.23
3	4O	3.82	4.16	4.12 Ps sand	4.03	0.19	16.55
3	3P	3.84	4.61	4.89 Ps sand	4.45	0.54	14.93
3	4Q	2.81	2.59	2.50 Ps sand	2.63	0.16	26.31
3	4R	3.38	3.08	3.29 Ps sand	3.25	0.15	20.87
3	4S	3.48	3.48	3.45 Ps sand	3.47	0.02	19.44
3	4T	5.22	5.45	4.79 Ps sand	5.15	0.34	12.80

Appendix E:
Permeability Data

S-P2: QTous (Dead Deer Gulch): Fine- to medium-grained sand with laminations and crossbeds.

#meas	sample	time (s)		Description	mean	std dev	K (darcy)
3	1A	6.21	6.66	5.88 Fmss	6.25	0.39	10.47
3	1B	5.94	5.25	5.64 Fmss	5.61	0.35	11.71
3	1C	7.95	6.79	7.00 Fmss	7.25	0.62	9.00
3	1D	5.36	5.48	5.64 Fmss	5.49	0.14	11.97
3	1E	5.36	3.60	4.20 X-bed	4.39	0.89	15.15
3	1F	4.15	6.48	5.48 Fmss	5.37	1.17	12.26
3	1G	6.76	6.76	6.55 Lam	6.69	0.12	9.77
3	1H	9.79	9.51	9.52 Lam	9.61	0.16	6.74
3	1I	6.30	6.00	7.87 Lam	6.72	1.00	9.72
3	1J	1.94	1.88	3.39 Fracture	2.40	0.86	29.16
3	1K	1.41	1.94	1.37 Fracture	1.57	0.32	48.68
3	2A	9.90	22.06	13.43 Lam	15.13	6.26	4.25
3	2B	16.86	16.97	12.04 Lam	15.29	2.82	4.21
3	2C	6.56	8.18	6.89 X-bed	7.21	0.86	9.04
3	2D	14.83	8.54	4.98 Lam	9.45	4.99	6.86
3	2E	2.85	2.72	2.08 Lam	2.55	0.41	27.27
3	2F	2.59	2.18	3.67 Lam	2.81	0.77	24.44
3	2G	5.63	11.54	8.27 Lam	8.48	2.96	7.66
3	2H	12.91	11.30	11.50 Lam	11.90	0.88	5.42
3	2I	9.03	5.71	7.58 Lam	7.44	1.66	8.76
3	2J	13.99	12.68	11.64 Lam	12.77	1.18	5.05
3	2K	13.59	14.03	15.04 Fmss	14.22	0.74	4.53
3	3A	13.99	19.33	22.95 Fmss	18.76	4.51	3.43
3	3B	16.39	16.58	15.32 X-bed	16.10	0.68	4.00
3	3C	8.68	8.55	13.28 Md	10.17	2.69	6.36
3	3D	20.83	15.70	16.40 Lam	17.64	2.78	3.64
3	3E	4.84	8.44	12.68 Lam	8.65	3.92	7.50
3	3F	22.18	12.03	26.04 Lam	20.08	7.24	3.20
3	3G	32.12	33.06	29.54 Lam	31.57	1.82	2.03
3	3H	10.55	11.22	8.52 Lam	10.10	1.41	6.41
3	3I	15.76	15.76	17.07 Fmss	16.20	0.76	3.97
3	3J	7.62	10.10	11.09 Fmss	9.60	1.79	6.75
3	3K	7.79	4.45	8.64 Fmss	6.96	2.21	9.38
3	4A	4.38	4.06	5.52 Fmss	4.65	0.77	14.24
3	4B	6.06	6.04	6.04 Lam	6.05	0.01	10.84
3	4C	7.16	5.40	5.90 Lam	6.15	0.91	10.64
3	4D	7.57	7.43	5.46 Lam	6.82	1.18	9.57
3	4E	8.32	8.65	8.63 Lam	8.53	0.19	7.61
3	4F	9.14	10.20	10.13 Lam	9.82	0.59	6.59
3	4G	2.87	3.50	4.54 Md	3.64	0.84	18.48
3	4H	4.42	3.76	3.66 X-bed	3.95	0.41	16.94
3	4I	5.36	6.61	6.27 Md	6.08	0.65	10.78
3	4J	6.76	5.15	5.76 Lam	5.89	0.81	11.14
3	5A	4.36	5.36	5.30 X-bed	5.01	0.56	13.19

Appendix E:
Permeability Data

#meas	sample time (s)		Description	mean	std dev	K (darcy)
3 5B	4.66	5.33	5.36 X-bed	5.12	0.40	12.89
3 5C	7.70	8.25	6.39 Ripple	7.45	0.96	8.75
3 5D	4.61	5.33	5.75 Lam	5.23	0.58	12.60
3 5E	3.37	4.00	3.49 Lam	3.62	0.33	18.58
3 5F	3.82	3.72	3.76 Lam	3.77	0.05	17.80
3 5G	3.41	3.67	3.12 Lam	3.40	0.28	19.87
3 5H	3.84	4.21	4.07 Lam	4.04	0.19	16.52
3 5I	7.05	7.18	7.56 Lam	7.26	0.27	8.97
3 5J	3.59	3.94	3.59 Lam	3.71	0.20	18.11
3 5K	4.55	3.78	4.12 Lam	4.15	0.39	16.06
3 6A	3.58	3.76	3.38 Lam	3.57	0.19	18.84
3 6B	3.41	3.60	3.24 Lam	3.42	0.18	19.77
3 6C	3.85	2.09	4.97 Lam	3.64	1.45	18.48
3 6D	3.35	3.88	2.75 Lam	3.33	0.57	21.35
3 6E	1.51	3.79	3.52 Lam	2.94	1.25	23.28
3 6F	2.67	1.18	1.18 X-bed	1.68	0.86	44.86
3 6G	4.19	2.97	1.41 X-bed	2.86	1.39	24.03
3 6H	3.69	3.27	2.19 Fmss	3.05	0.77	22.36
3 6I	5.27	4.97	5.49 X-bed	5.24	0.26	12.57
3 6J	4.72	4.57	4.00 Fmss	4.43	0.38	14.99
3 6K	3.67	1.98	2.43 Fmss	2.69	0.88	25.65
3 7B	1.19	3.86	3.52 Md	2.86	1.45	24.03
3 7C	1.68	3.97	1.68 Md	2.44	1.32	28.62
3 7D	1.21	1.51	1.51 Md	1.41	0.17	56.38
3 7E	4.00	3.00	2.06 Md	3.02	0.97	22.60
3 7F	1.21	1.10	2.72 Md	1.68	0.91	44.86
3 7G	2.38	4.18	2.12 Fmss	2.89	1.12	23.69
3 7H	2.88	2.00	1.65 Md	2.18	0.63	32.69
3 7I	1.82	1.51	1.52 Fmss	1.62	0.18	47.00
3 7J	1.54	3.24	2.76 Lam	2.51	0.88	27.72
3 7K	3.42	2.39	2.59 Fmss	2.80	0.55	24.57
3 8A	2.21	2.98	1.74 Fmss	2.31	0.63	30.52
3 8B	1.20	1.83	2.67 Md	1.90	0.74	38.42
3 8C	1.90	1.76	1.82 Md	1.83	0.07	40.31
3 8D	2.19	2.19	2.78 X-bed	2.39	0.34	29.40
3 8E	4.60	4.40	3.12 Fmss	4.04	0.80	16.52
3 8F	6.64	2.30	2.55 Fracture near	3.83	2.44	17.49
3 8G	4.51	1.40	7.09 Lam	4.33	2.85	15.34
3 8H	4.85	4.54	4.15 Lam	4.51	0.35	14.70
3 8I	1.94	3.97	5.72 Lam	3.88	1.89	17.27
3 8J	1.20	1.52	1.63 Fmss	1.45	0.22	54.26

Appendix E:
Permeability Data

S-P3: QTous (Dead Deer Gulch): Medium-grained sand, homogeneous.

#meas	sample	time (s)	Description	mean	std dev	K (darcy)
3	1A	2.67 2.82 2.64	Mss	2.71	0.10	25.78
3	1B	5.37 5.15 4.76	Mss	5.09	0.31	12.95
3	1C	4.84 3.82 3.79	Mss	4.15	0.60	16.06
3	1D	10.37 10.50 10.72	Mss	10.53	0.18	6.14
3	1E	4.19 6.18 6.21	Mss	5.53	1.16	11.90
3	1F	3.82 3.79 3.88	Mss	3.83	0.05	17.49
3	1G	6.64 6.27 4.34	Mss	5.75	1.24	11.42
3	1H	10.71 9.16 10.10	Mss	9.99	0.78	6.48
3	1I	2.57 3.81 4.27	Mss	3.55	0.88	18.97
3	1J	2.79 3.31 4.06	Mss	3.39	0.64	19.96
3	1K	3.44 3.49 2.59	Mss	3.17	0.51	21.41
3	2A	2.60 2.42 1.58	Mss	2.20	0.54	32.29
3	2B	3.40 3.00 2.72	Mss	3.04	0.34	22.44
3	2C	2.01 2.27 2.09	Mss	2.12	0.13	33.65
3	2D	5.84 4.03 2.40	Mss	4.09	1.72	16.31
3	2E	3.60 3.72 3.91	Mss	3.74	0.16	17.92
3	2F	2.21 2.43 1.39	Mss	2.01	0.55	35.91
3	2G	3.09 2.89 3.33	Mss	3.10	0.22	21.94
3	2H	3.41 3.93 2.69	Mss	3.34	0.62	20.24
3	2I	2.30 5.77 5.04	Mss	4.37	1.83	15.21
3	2J	5.02 2.97 4.07	Mss	4.02	1.03	16.61
3	2K	2.00 3.34 3.39	Mss	2.91	0.79	23.54
3	3A	4.11 4.09 2.80	Mss	3.67	0.75	18.32
3	3B	1.30 4.80 4.84	Mss	3.65	2.03	18.43
3	3C	3.67 2.54 3.43	Mss	3.21	0.60	21.12
3	3D	5.31 5.39 5.92	Mss	5.54	0.33	11.87
3	3E	4.45 5.46 5.25	Mss	5.05	0.53	13.06
3	3F	5.09 5.40 5.16	Mss	5.22	0.16	12.63
3	3G	1.38 2.42 1.56	Mss	1.79	0.56	41.43
3	3H	3.92 3.82 3.52	Mss	3.75	0.21	17.87
3	3I	5.04 5.38 5.47	Mss	5.30	0.23	12.43
3	3J	4.84 4.54 4.75	Mss	4.71	0.15	14.06
3	3K	3.48 3.65 4.82	Mss	3.98	0.73	16.77
3	4A	5.37 4.29 1.30	Mss	3.65	2.11	18.39
3	4B	5.63 5.94 5.30	Mss	5.62	0.32	11.69
3	4C	5.17 4.46 4.95	Mss	4.86	0.36	13.60
3	4D	4.60 5.97 4.94	Mss	5.17	0.71	12.75
3	4E	6.06 4.66 4.42	Mss	5.05	0.89	13.08
3	4F	5.05 4.11 1.88	Mss	3.68	1.63	18.25
3	4G	6.94 4.59 4.34	Mss	5.29	1.43	12.45
3	4H	4.67 1.20 5.33	Mss	3.73	2.22	17.97
3	4I	4.82 5.48 5.39	Mss	5.23	0.36	12.60

Appendix E:
Permeability Data

#meas	sample	time (s)		description	mean	std dev	K (darcy)
3	4J	3.04	2.62	4.12 Mss	3.26	0.77	20.80
3	4K	5.52	4.02	1.36 Mss	3.63	2.11	18.50
3	5A	1.58	2.65	3.02 Mss	2.42	0.75	28.98
3	5B	3.61	4.49	3.04 Mss	3.71	0.73	18.08
3	5C	3.72	4.02	3.63 Mss	3.79	0.20	17.69
3	5D	4.67	4.42	4.48 Mss	4.52	0.13	14.67
3	5E	5.51	4.70	4.64 Mss	4.95	0.49	13.34
3	5F	1.90	4.88	3.50 Mss	3.43	1.49	19.70
3	5G	2.48	1.21	3.02 Mss	2.24	0.93	31.67
3	5H	1.34	4.70	3.30 Mss	3.11	1.69	21.86
3	5I	3.38	4.33	4.12 Mss	3.94	0.50	16.96
3	5J	5.54	3.27	4.26 Mss	4.36	1.14	15.26
3	5K	5.08	3.50	2.55 Mss	3.71	1.28	18.09
3	6A	2.85	2.68	2.79 Mss	2.77	0.09	24.83
3	6B	3.84	3.06	2.27 Mss	3.06	0.79	22.31
3	6C	3.42	3.24	3.09 Mss	3.25	0.17	20.87
3	6D	2.44	2.36	2.45 Mss	2.42	0.05	28.98
3	6E	2.45	2.92	1.90 Mss	2.42	0.51	28.89
3	6F	3.55	3.47	3.40 Mss	3.47	0.08	19.42
3	6G	3.80	3.77	3.76 Mss	3.78	0.02	17.75
3	6H	3.76	3.76	3.72 Mss	3.75	0.02	17.90
3	6I	3.67	3.84	3.74 Mss	3.75	0.09	17.89
3	6J	3.79	3.78	3.49 Mss	3.69	0.17	18.22
3	6K	4.89	4.03	4.36 Mss	4.43	0.43	15.00
3	7A	2.67	2.72	2.55 Mss	2.65	0.09	26.16
3	7B	1.60	2.30	2.08 Mss	1.99	0.36	36.27
3	7C	2.21	2.03	2.12 Mss	2.12	0.09	33.72
3	7D	1.88	1.48	1.34 Mss	1.57	0.28	48.95
3	7E	3.22	3.03	3.18 Mss	3.14	0.10	21.64
3	7F	2.76	2.24	2.01 Mss	2.34	0.38	30.12
3	7G	2.82	2.94	3.03 Mss	2.93	0.11	23.37
3	7H	1.79	2.34	2.00 Mss	2.04	0.28	35.21
3	7I	3.12	2.96	3.36 Mss	3.15	0.20	21.61
3	7J	3.06	3.24	3.53 Mss	3.28	0.24	20.68
3	7K	3.15	3.24	3.21 Mss	3.20	0.05	21.22

Appendix E:
Permeability Data

S-P4: QToup (Waterfall Site): Medium-grained sand with scattered pebbles and vertically-oriented carbonate bodies.

#meas	sample	time (s)		Description	mean	std dev	K (darcy)
3	1A	4.42	4.40	4.28 Ps sand	4.37	0.08	15.22
3	1B	4.40	4.40	4.43 Ps sand	4.41	0.02	15.06
3	1C	4.26	4.48	4.45 Ps sand	4.40	0.12	15.11
3	1D	5.25	5.30	5.45 Ps sand	5.33	0.10	12.35
3	1E	1.70	1.40	0.88 Ps sand	1.33	0.41	61.42
3	2A	5.30	5.43	5.25 Ps sand	5.33	0.09	12.36
3	2B	5.04	4.91	4.89 Ps sand	4.95	0.08	13.35
3	2C	4.49	4.54	4.87 Ps sand	4.63	0.21	14.30
3	2D	5.33	5.39	5.45 Ps sand	5.39	0.06	12.21
3	2E	4.62	4.43	4.27 Ps sand	4.44	0.18	14.96
3	3A	3.16	2.76	2.33 Ps sand	2.75	0.42	25.06
3	3B	4.90	4.21	3.96 Ps sand	4.36	0.49	15.26
3	3C	6.14	5.88	5.85 Ps sand	5.96	0.16	11.01
3	3D	4.72	4.58	4.75 Ps sand	4.68	0.09	14.14
3	3E	6.51	6.54	6.36 Ps sand	6.47	0.10	10.11
3	3F	5.42	5.41	5.25 Ps sand	5.36	0.10	12.28
3	3G	2.70	1.96	1.90 Ps sand	2.19	0.45	32.52
3	3H	5.27	5.17	5.02 Ps sand	5.15	0.13	12.80
3	3I	5.59	5.57	4.88 Ps sand	5.35	0.40	12.31
3	4A	2.99	2.70	2.14 Ps sand	2.61	0.43	26.57
3	4B	4.36	3.00	2.03 Ps sand	3.13	1.17	21.74
3	4C	5.36	5.31	5.40 Ps sand	5.36	0.05	12.29
3	4D	4.24	4.18	4.09 Ps sand	4.17	0.08	15.98
3	4E	5.58	5.51	5.64 Ps sand	5.58	0.07	11.79
3	4F	7.44	6.93	6.72 Ps sand	7.03	0.37	9.28
3	4G	6.00	5.61	5.66 Ps sand	5.76	0.21	11.40
3	4H	1.97	1.99	2.20 Near fracture	2.05	0.13	35.01
3	4I	4.45	4.18	4.04 Ps sand	4.22	0.21	15.77
3	5A	6.48	6.18	5.58 Ps sand	6.08	0.46	10.78
3	5B	4.76	4.48	4.34 Ps sand	4.53	0.21	14.66
3	5C	4.90	4.73	4.59 Ps sand	4.74	0.16	13.96
3	5D	4.12	3.67	3.73 Ps sand	3.84	0.24	17.44
3	5E	5.06	4.84	3.67 Ps sand	4.52	0.75	14.67
3	5F	4.27	4.82	4.47 Ps sand	4.52	0.28	14.68
3	5G	3.53	3.75	3.59 Ps sand	3.62	0.11	18.56
3	5H	4.94	3.97	3.51 Ps sand	4.14	0.73	16.10
3	5I	3.37	3.46	2.85 Ps sand	3.23	0.33	21.03
3	6A	4.60	5.56	3.96 Ps sand	4.71	0.81	14.07
3	6B	3.70	3.03	3.85 Ps sand	3.53	0.44	19.10
3	6C	3.55	3.06	3.00 Ps sand	3.20	0.30	21.20
3	6D	3.72	3.36	3.70 Ps sand	3.59	0.20	18.72

Appendix E:
Permeability Data

#meas	sample	time (s)		description	mean	std dev	K (darcy)
3	6E	4.03	4.15	4.21 Ps sand	4.13	0.09	16.14
3	6F	3.19	3.23	2.56 Ps sand	2.99	0.38	22.82
3	6G	4.30	4.24	4.17 Ps sand	4.24	0.07	15.71
3	6H	3.69	2.91	1.47 Ps sand	2.69	1.13	25.69
3	6I	1.85	3.88	4.49 Ps sand	3.41	1.38	19.83
3	7A	3.82	3.67	3.18 Ps sand	3.56	0.33	18.93
3	7B	4.27	4.01	3.27 Ps sand	3.85	0.52	17.39
3	7C	5.21	3.50	4.30 Ps sand	4.34	0.86	15.33
3	7D	5.27	5.51	4.40 Ps sand	5.06	0.58	13.04
3	7E	3.43	3.23	2.87 Ps sand	3.18	0.28	21.39
3	7F	2.82	2.40	2.66 Ps sand	2.63	0.21	26.38
3	7G	4.12	4.46	4.50 Ps sand	4.36	0.21	15.25
3	7H	6.36	3.65	5.50 Ps sand	5.17	1.38	12.75
3	7I	5.96	5.94	5.30 Ps sand	5.73	0.38	11.45
3	8A	4.92	4.63	4.33 Ps sand	4.63	0.30	14.32
3	8B	2.60	2.60	2.68 Ps sand	2.63	0.05	26.38
3	8C	2.91	2.37	3.22 Ps sand	2.83	0.43	24.25
3	8D	4.40	3.55	3.36 Ps sand	3.77	0.55	17.79
3	8E	2.91	2.94	2.44 Ps sand	2.76	0.28	24.93
3	8F	2.00	3.08	3.82 Ps sand	2.97	0.92	23.05
3	8G	5.06	4.81	4.91 Ps sand	4.93	0.13	13.41
3	8H	2.48	2.45	2.57 Ps sand	2.50	0.06	27.89
3	8I	4.45	3.09	3.62 Ps sand	3.72	0.69	18.04

Appendix E:
Permeability Data

S-P5: QToup (Waterfall Site): Medium-grained sand with scattered pebbles, vertically-oriented carbonate bodies and carbonate soil. Highly variable readings.

#meas	sample	time (s)		Description	mean	std dev	K (darcy)
3	1A	2.49	9.46	8.45 Ps sand	6.80	3.77	9.60
2	1C	3.36	3.35	Rough surface	3.36	0.01	20.16
3	2A	5.04	6.00	4.20 Ps sand	5.08	0.90	12.99
3	2B	8.60	9.74	6.42 Ps sand	8.25	1.69	7.87
1	2C	10.00	10.00	10.00 Rough surface	10.00	0.00	6.47
3	2D	12.27	18.67	23.50 Ps sand Rough	18.15	5.63	3.54
3	2E	11.69	12.10	14.04 surface/	12.61	1.26	5.12
2	3A	60+	43.26	60.00 Ps sand	51.63	11.84	1.24
3	3B	7.96	7.20	6.24 Rough surface	7.13	0.86	9.14
3	3C	2.39	1.61	3.37 Sandy	2.46	0.88	28.45
3	3D	2.06	6.04	9.06 Fracture	5.72	3.51	11.48
1	3E	5.15	5.15	5.15 Ps sand	5.15	0.00	12.80
3	4A	3.42	1.34	1.76 Rough surface	2.17	1.10	32.75
3	4B	10.59	13.94	8.97 Ps sand	11.17	2.53	5.79
3	4C	7.00	5.57	8.12 Ps sand	6.90	1.28	9.46
3	4D	11.79	8.28	16.95 Ps sand	12.34	4.36	5.23
3	4E	6.88	8.33	2.94 Ps sand	6.05	2.79	10.83

Appendix E:
Permeability Data

S-P6: QTous (South King Ranch): Medium-grained and coarse-grained sand.

#meas	sample	time (s)		Description	mean	std dev	K (darcy)
3	1A	1.20	1.18	1.25 Mcss/lam	1.21	0.04	70.37
3	1B	1.21	1.03	0.87 Mcss/lam	1.04	0.17	90.65
3	1C	2.09	2.00	2.03 Mcss/lam	2.04	0.05	35.28
3	1D	1.57	1.63	1.58 Mcss/lam	1.59	0.03	47.89
3	1E	0.91	0.85	0.84 css	0.87	0.04	129.29
3	1F	1.60	1.61	1.60 css	1.60	0.01	47.50
3	1G	2.15	2.85	2.21 css	2.40	0.39	29.16
3	1H	1.00	0.97	1.00 Mcss/lam	0.99	0.02	98.54
3	1I	1.50	1.42	1.40 Mcss/lam	1.44	0.05	54.78
3	1J	1.43	1.40	1.36 Mcss/lam	1.40	0.04	57.13
3	1K	1.27	1.24	1.24 Mcss/lam	1.25	0.02	67.00
3	2A	1.57	1.26	1.73 Mcss/lam	1.52	0.24	50.94
3	2B	3.15	3.04	3.03 Mcss/lam	3.07	0.07	22.17
3	2C	1.82	1.82	1.62 Mcss/lam	1.75	0.12	42.41
3	2D	2.12	2.18	2.21 Mcss/lam	2.17	0.05	32.81
3	2E	1.00	1.02	0.94 Mcss/lam	0.99	0.04	99.16
3	2F	1.76	1.76	1.78 Mcss/lam	1.77	0.01	42.01
3	2G	1.95	1.90	1.85 Mcss/lam	1.90	0.05	38.42
3	2H	1.40	1.21	1.29 Mcss/lam	1.30	0.10	63.25
3	2I	1.87	1.81	1.86 mss	1.85	0.03	39.78
3	2J	1.34	1.19	1.19 mss	1.24	0.09	67.81
3	2K	1.72	1.73	1.65 mss	1.70	0.04	44.08
3	3A	0.78	0.67	0.72 Mcss	0.72	0.06	211.73
3	3B	1.00	0.91	1.00 css	0.97	0.05	102.41
3	3C	0.97	0.64	0.61 css	0.74	0.20	196.52
3	3D	0.62	0.59	0.59 css	0.60	0.02	544.56
3	3E	0.94	0.81	0.75 Mcss	0.83	0.10	141.69
3	3F	1.52	1.42	1.25 Mcss	1.40	0.14	57.13
3	3G	1.14	1.12	1.12 Mss	1.13	0.01	78.74
3	3H	1.15	0.85	1.16 Mss	1.05	0.18	88.15
3	3I	1.88	1.94	1.90 Mss	1.91	0.03	38.26
3	3J	1.90	1.97	1.52 Mss	1.80	0.24	41.14
3	3K	0.85	1.12	1.06 Mss	1.01	0.14	94.98
3	4C	0.88	0.84	0.82 Css	0.85	0.03	136.42
3	4D	2.05	1.99	1.87 Css	1.97	0.09	36.78
3	4E	0.72	0.76	0.76 Css	0.75	0.02	191.08
3	4F	0.73	0.63	0.61 Css	0.66	0.06	311.77
3	4G	1.22	1.12	1.20 Css	1.18	0.05	73.16
3	4I	0.94	0.88	1.00 Css	0.94	0.06	108.87
3	4J	0.62	0.82	0.81 Css	0.75	0.11	188.48
3	4K	0.82	0.54	0.54 Css	0.63	0.16	376.86

Appendix E:
Permeability Data

S-P7: QTouc (South King Ranch): Fine- to coarse-grained sand with reworked pebbles and randomly-oriented carbonate fragments.

#meas	sample	time (s)		Description	mean	std dev	K (darcy)
3	1A	1.30	1.36	1.24 Lam css	1.30	0.06	63.25
3	1B	0.54	0.61	0.76 Lam css	0.64	0.11	365.83
3	1C	1.58	1.60	1.49 Lam css	1.56	0.06	49.36
3	1D	0.97	1.09	1.00 Lam css	1.02	0.06	93.30
3	1E	1.10	1.06	1.05 Lam css	1.07	0.03	85.81
3	1F	1.37	1.42	1.25 Lam css	1.35	0.09	60.13
3	1G	1.12	1.08	0.99 Lam css	1.06	0.07	86.73
3	1H	0.84	0.81	0.82 Lam css	0.82	0.02	145.93
3	1I	1.76	7.64	1.59 Lam css	3.66	3.44	18.34
3	1J	0.47	0.90	1.00 Lam css	0.79	0.28	162.38
3	2A	1.94	1.95	1.94 Lam css	1.94	0.01	37.39
3	2B	1.08	1.09	0.97 Lam css	1.05	0.07	89.13
3	2C	1.12	1.30	1.08 Lam css	1.17	0.12	74.47
3	2D	1.87	1.79	1.80 Lam css	1.82	0.04	40.49
3	2E	1.14	1.18	1.09 Lam css	1.14	0.05	77.63
3	2F	1.27	0.97	1.12 Lam css	1.12	0.15	79.51
3	2G	1.14	1.10	1.05 Lam css	1.10	0.05	82.32
3	2H	1.54	1.53	1.44 Lam css	1.50	0.06	51.69
3	2I	1.61	1.75	1.72 Lam css	1.69	0.07	44.30
3	2J	1.39	1.35	1.33 Lam css	1.36	0.03	59.50
3	3A	1.43	1.44	1.45 Lam css	1.44	0.01	54.78
3	3B	2.18	1.30	1.93 Lam css	1.80	0.45	40.95
3	3C	2.09	2.03	2.01 Lam css	2.04	0.04	35.21
3	3D	1.57	1.48	1.00 Lam css	1.35	0.31	59.91
3	3E	1.50	1.62	1.56 Lam css	1.56	0.06	49.22
3	3F	1.34	1.32	1.37 Lam css	1.34	0.03	60.34
3	3G	1.93	2.03	2.00 Lam css	1.99	0.05	36.41
3	3I	0.83	1.30	0.91 Lam css	1.01	0.25	94.41
3	3J	1.31	1.25	1.30 Lam css	1.29	0.03	64.20
3	4A	2.01	2.50	2.48 Lam css	2.33	0.28	30.22
3	4B	1.67	1.51	1.32 Lam css	1.50	0.18	51.84
3	4C	2.18	1.40	1.77 Lam css	1.78	0.39	41.52
3	4D	2.22	2.27	1.64 Lam css	2.04	0.35	35.21
3	4E	0.91	1.51	1.18 Lam css	1.20	0.30	71.28
3	4F	1.66	1.72	1.67 Lam css	1.68	0.03	44.63
3	4G	2.17	2.28	2.27 Lam css	2.24	0.06	31.62
3	4I	1.95	1.90	1.84 Lam css	1.90	0.06	38.50
3	4J	1.87	1.91	1.89 Lam css	1.89	0.02	38.67
3	5A	2.94	2.40	2.28 Lam css	2.54	0.35	27.39
3	5B	1.13	4.30	2.48 Lam css	2.64	1.59	26.27

Appendix E:
Permeability Data

#meas	sample	time (s)		Description	mean	std dev	K (darcy)
3	5C	2.73	4.21	4.21 Lam css	3.72	0.85	18.06
3	5D	2.30	2.71	3.28 Lam css	2.76	0.49	24.93
3	5E	4.45	4.60	4.75 Lam css	4.60	0.15	14.41
3	5F	4.49	2.97	2.20 Lam css	3.22	1.17	21.08
3	5G	7.48	7.01	6.77 Lam css	7.09	0.36	9.20
3	5H	2.68	2.36	2.38 Lam css	2.47	0.18	28.23
3	5I	3.66	3.60	4.11 Lam css	3.79	0.28	17.69
3	5J	4.39	4.15	3.71 Lam css	4.08	0.34	16.34
3	6A	3.63	3.81	3.12 Lam css	3.52	0.36	19.14
3	6B	3.37	2.42	4.01 Lam css	3.27	0.80	20.75
3	6C	4.73	3.93	3.97 Lam css	4.21	0.45	15.82
3	6D	5.30	5.85	5.48 Lam css	5.54	0.28	11.86
3	6E	3.58	3.83	3.97 Lam css	3.79	0.20	17.67
3	6F	4.61	4.43	3.64 Lam css	4.23	0.52	15.75
3	6G	4.36	4.14	4.09 Lam css	4.20	0.14	15.87
3	6H	3.85	3.78	3.79 Lam css	3.81	0.04	17.60
3	6I	4.58	4.70	4.37 Lam css	4.55	0.17	14.58
3	6J	3.05	2.25	2.75 Lam css	2.68	0.40	25.76
3	7A	5.03	5.96	2.43 Lam css	4.47	1.83	14.84
3	7B	2.48	4.01	3.66 Lam css	3.38	0.80	19.98
3	7C	1.57	4.46	2.78 Lam css	2.94	1.45	23.31
3	7D	6.24	6.24	5.27 Lam css	5.92	0.56	11.09
3	7E	3.50	2.69	4.85 Lam css	3.68	1.09	18.25
3	7F	3.58	5.72	5.36 Lam css	4.89	1.15	13.53
3	7G	6.63	3.78	4.95 Lam css	5.12	1.43	12.88
3	7H	5.00	4.09	5.46 Lam css	4.85	0.70	13.63
3	7I	3.79	1.18	3.31 Lam css	2.76	1.39	24.96
3	8A	1.67	1.44	2.09 Lam css	1.73	0.33	43.02
3	8B	1.40	2.32	2.66 Lam css	2.13	0.65	33.59
3	8C	0.91	0.47	0.97 Lam css	0.78	0.27	166.17
3	8D	6.39	6.83	5.86 Lam css	6.36	0.49	10.29
3	8E	7.51	6.02	6.92 Lam css	6.82	0.75	9.58
3	8F	1.97	1.21	4.57 Lam css	2.58	1.76	26.88
3	8G	9.20	3.95	7.42 Lam css	6.86	2.67	9.52
3	8H	3.00	4.72	4.32 Lam css	4.01	0.90	16.64
3	8I	1.27	2.88	2.03 Lam css	2.06	0.81	34.88
3	9A	3.77	4.60	3.69 Lam css	4.02	0.50	16.61
3	9B	5.00	5.35	5.13 Lam css	5.16	0.18	12.78
3	9C	4.30	5.57	6.01 Lam css	5.29	0.89	12.44
3	9D	7.72	4.90	2.27 Lam css	4.96	2.73	13.31
3	9E	2.29	5.60	3.85 Lam css	3.91	1.66	17.09
3	9F	8.27	8.80	9.15 Lam css	8.74	0.44	7.43
3	9G	4.65	4.35	4.85 Lam css	4.62	0.25	14.36
3	9H	7.25	6.97	6.70 Lam css	6.97	0.28	9.36
3	9I	7.70	3.30	3.70 Lam css	4.90	2.43	13.49
3	9J	7.02	7.27	7.14 Lam css	7.14	0.13	9.13

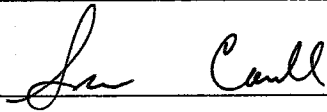
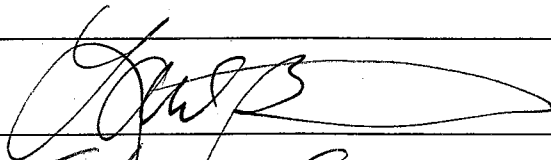
Appendix E:
Permeability Data

#meas	sample	time (s)		Description	mean	std dev	K (darcy)
3	10A	4.76	7.30	3.70 Fss	5.25	1.85	12.54
3	10B	27.39	10.86	31.73 Fss	23.33	11.01	2.75
3	10C	22.93	21.87	16.61 Fss	20.47	3.38	3.14
3	10D	7.51	9.71	3.55 Fss	6.92	3.12	9.43
3	10E	1.94	2.24	1.58 Mcss	1.92	0.33	37.94
3	10F	9.14	9.03	8.91 Mcss	9.03	0.12	7.19
3	10G	4.23	4.01	5.15 Mcss	4.46	0.60	14.87
3	10H	6.15	6.67	4.98 Mcss	5.93	0.87	11.05
3	10I	2.27	2.85	2.24 Mcss	2.45	0.34	28.49

This thesis is accepted on behalf of the
Faculty of the Institute by the following committee:

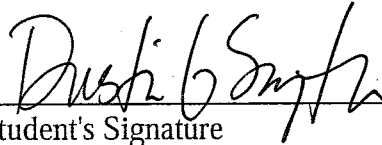


Advisor

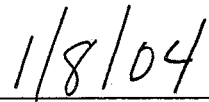


Date

I release this document to the New Mexico Institute of Mining and Technology.



Student's Signature



Date